If you have discovered material in AURA which is unlawful e.g. breaches copyright, (either yours or that of a third party) or any other law, including but not limited to those relating to patent, trademark, confidentiality, data protection, obscenity, defamation, libel, then please read our Takedown Policy and contact the service immediately

DEFECTS IN STEEL INVESTMENT CASTINGS

PHILIP NEIL WHATELEY

Doctor of Philosophy

THE UNIVERSITY OF ASTON IN BIRMINGHAM

January 1991

THE UNIVERSITY OF ASTON IN BIRMINGHAM

DEFECTS IN STEEL INVESTMENT CASTINGS

Philip Neil Whateley

Doctor of Philosophy

January 1991

SUMMARY

A general investigation was performed, in an industrial environment, of the major types of defect specific to investment castings in steel.
As a result of this work three types of metallurgical defect were selected for further study.
In the first of these, defects in austenitic stainless steel castings were found to result from deoxidation by-products.

As a result of metallographic investigation and the statistical analysis of experimental data, evidence was found to support the hypothesis that the other two classes of defects – in martensitic stainless and low alloy steels – both resulted from internal or grain boundary oxidation of the chromium alloy constituent. This was often found to be followed by reaction between the metal oxides and the ceramic mould material.

On the basis of this study, proposals are made for a more fundamental investigation of the mechanisms involved and interim suggestions are given for methods of ameliorating the effect in an industrial situation.

KEYWORDS

Investment Casting, Steel Castings, Casting Defects, Metal-Mould Reaction.

ACKNOWLEDGEMENTS

I would like to thank the members of the academic and technical staff of the University of Aston in Birmingham for their help and co-operation, especially my supervisor Mr L.W.Crane, and also Mrs H.A.Spooner of Aston Business School for her guidance with the statistical design and analysis of experiments.

I would also like to express my gratitude to the Directors, Managers and Staff of both Deritend Precision Castings and the Triplex Lloyd Group for their assistance and support. In particular I would like to thank my industrial supervisor, Mr B.Page.

The text quoted in the appendix is taken from D.C.Montgomery, 'Design and Analysis of Experiments', 2ed (New York: John Wiley and Sons, Inc.) 1984 and is used by permission of the publisher.

Finally I would like to acknowledge the Cooperative Award in Science and Engineering from The Science and Engineering Research Council, and also the financial support of Deritend Precision Castings, and the University of Aston in Birmingham.

TABLE OF CONTENTS PAGE

(cont.)

CONTENTS (*cont.*) PAGE

(*cont.*)

CONTENTS (*cont.*) PAGE

(*cont.*)

CONTENTS (*cont.*) PAGE

TABLES PAGE

(Cont.)

TABLES *(Cont.)* PAGE

FIGURES PAGE

(Cont.)

PLATES PAGE

(cont.)

PLATES *(cont.)* PAGE

(cont.)

PLATES (*cont.*) PAGE

1. INTRODUCTION.

1.1. Investment casting.

1.1.1. Historical Perspective.

Investment, or lost wax (*"Cire Perdue"*) castings are known to have been produced in Thailand as early as 4500 BC. The Mesopotamian civilisation in 4000-3000 BC produced cast artifacts of great beauty in gold, silver, copper and bronze alloys using the process which was developed by the Indians and Chinese to the east, and travelled southwards through the Levant to Egypt. The use of the process for *objets d'art* reached a peak in Renaissance Italy in the work of Benvenuto Cellini (1500-1571). The development of investment casting as an industrial process was foreshadowed by a British Patent (No. 2467) of 1875 which describes, amongst other things, the use of vulcanised rubber dies for wax pattern production, the process being widely used for dental and orthopaedic work. During the second world war, problems in the fabrication of alloys needed to develop superchargers to allow aero engines to operate at high altitudes led to greatly increased interest in precision investment casting. It was this which laid the foundation of the modern industry. (P.R.Taylor 1986)[1].

1.1.2. The Process

In classical times the process consisted of laboriously painting a hand-made wax pattern with a "refractory" slip to build up a shell of the required thickness which was then dried before the wax pattern was melted out prior to casting.

The technique used for dental and orthopaedic work, and for small items of jewellery, was to "invest" the wax pattern, or patterns attached to a sprue, into refractory material in order to form a solid block containing the wax, which was then fired to melt out the wax and harden the mould.

The use of investment casting for larger components, or for mass production techniques where many castings are fed from a single runner system, was not practical by block mould investment. This was due, amongst other factors, to the weights involved. However, the use of hydrolised ethyl-silicate binders, first devised in 1932, allowed the production of ceramic shell moulds by a dipping and stuccoing process which resulted in lightweight moulds of considerable strength.

1.1.3. The Modern Process.

The modern investment casting process has developed as a means of mass production of "near-net" castings, often in materials which are difficult or impossible to machine. The method as practised at the company associated with the research, Deritend Precision Castings Ltd, begins with the pressing of accurate wax patterns using precision machined dies (Plate 1.1), which are often of complex construction. The wax patterns are then prepared for assembly onto feeding systems by removing moulding flash and parting lines, and filling in minor surface imperfections in a process known as "frazing". After 100% inspection the waxes are assembled onto preformed feeding systems (Plate 1.2). The assembled moulds are then transferred to an environmentally controlled room for the production of the ceramic shell.

The building up of the ceramic shell involves dipping the mould by hand into a refractory slurry (Plate 1.3), usually consisting of -200 mesh zircon flour suspended in a hydrolised ethyl-silicate binder. The wet slurry coat is then dusted with stucco, (Plate 1.4) starting with fine zircon sand for the primary coat, (which determines the surface finish of the final casting), through fine molochite, to coarse molochite for the outer coats. This allows rapid build up of thickness, with adequate permeability to allow the escape of air during casting. After each coat is applied, the mould is dried in air or set in an ammoniated atmosphere to gel the ethyl-silicate.

For large moulds a robot is used to facilitate handling. The moulds are dipped by the robot and the stucco is applied by a raining machine. When the robot is used the moulds are air dried and are passed through an ammonia tunnel prior to application of the next coat. Drying is carried out using a slow moving continuous track which is controlled to introduce the required interval between a wet mould leaving the robot station and returning for the next coat. This interdip time is typically 16 to 24 hours.

The moulds are dewaxed using superheated steam in an autoclave (Plate 1.5). The use of superheated steam ensures rapid melting of the wax in contact with the shell and reduces the risk of cracking of the shell due to bulk thermal expansion of the wax. The moulds are then fired at 1000°C for one hour to burn off any adherent wax and to develop the maximum strength of the mould.

For casting air-melted alloys, the moulds are preheated (Plate 1.6) – to around 1100°C in the case of steels – to prevent the mould cracking due to thermal shock. For small moulds, of up to twenty kilogrammes metal weight, the metal is melted in a small crucible, deoxidised if appropriate, and de-slagged using granulated pearlite which absorbs and coagulates the slag as it exfoliates. The preheated mould is placed on top of the crucible (Plate 1.7), clamped in place, and the mould and crucible assembly inverted to fill the mould rapidly. Large moulds are cast using a ladle to transfer molten metal from a large induction furnace.

When the mould is cool the shell material is removed and the castings are cut away from the feeding system, fettled, ground and shot-blasted prior to inspection and heat treatment.

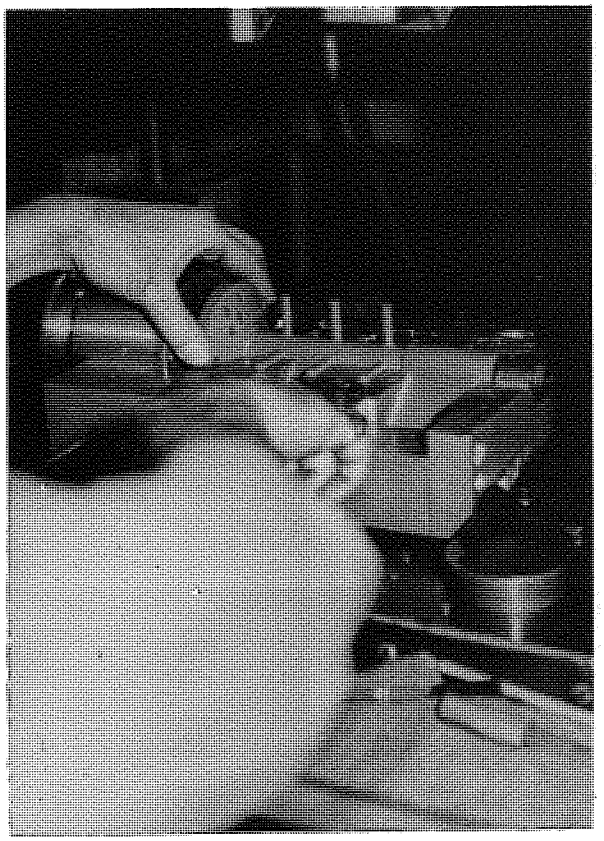

PLATE 1.1:
Removing a wax pattern from the die.

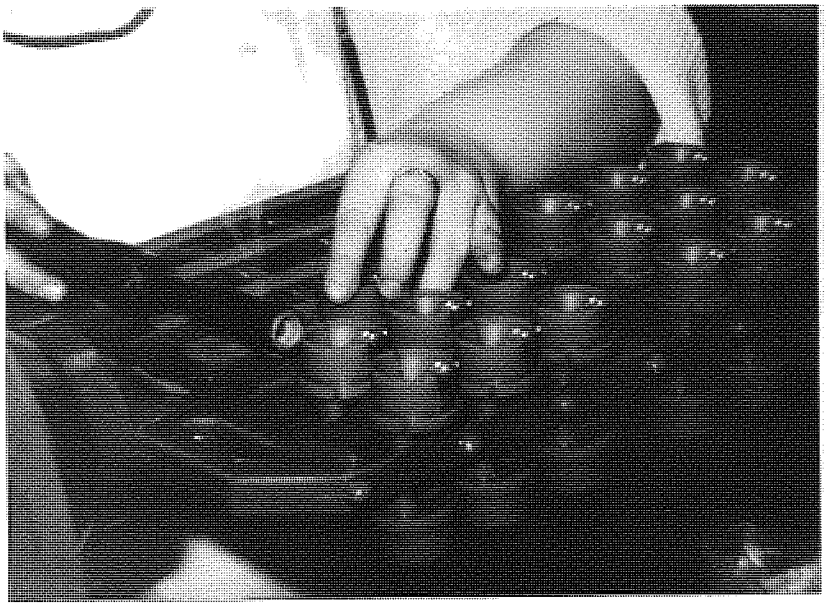

PLATE 1.2:
Assembling wax patterns onto the riser system.

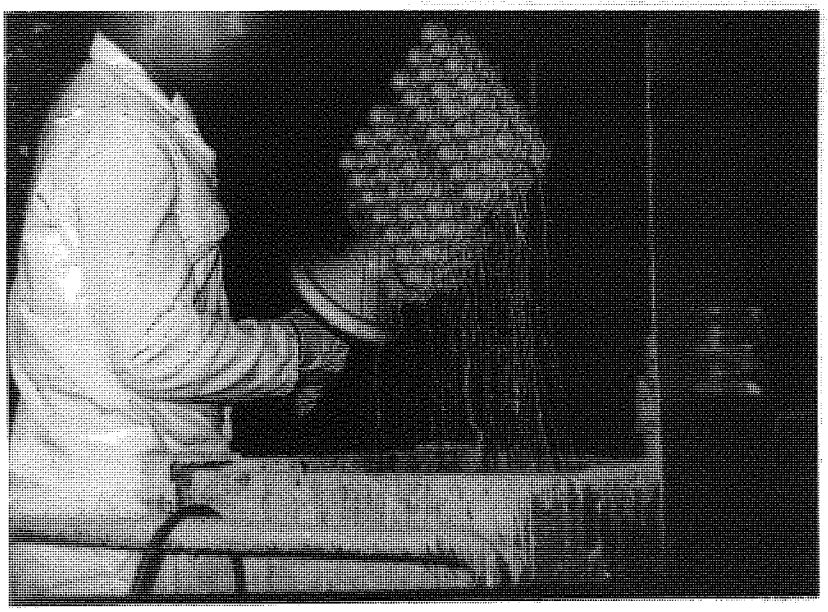

PLATE 1.3:
Dipping the assembled mould into refractory slurry.

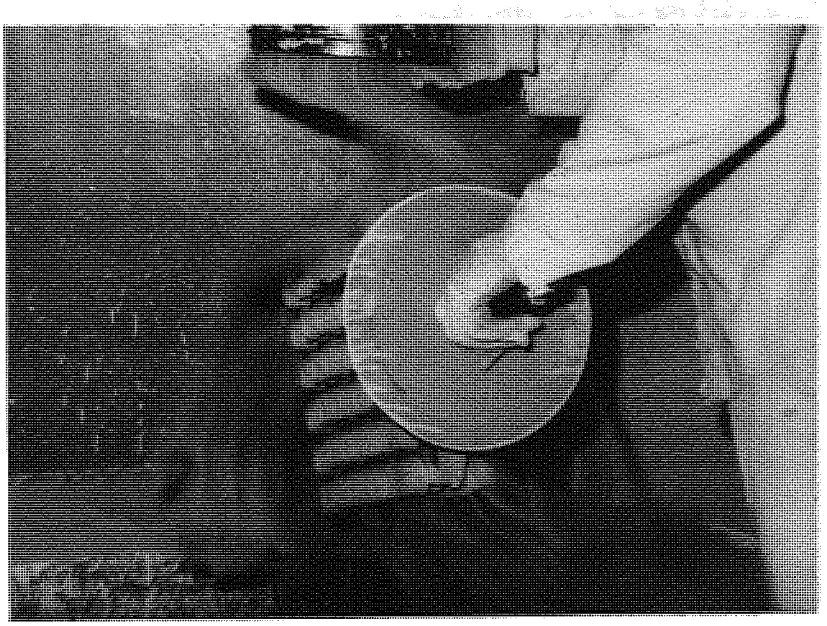

PLATE 1.4:
Dusting the dipped mould with zircon sand stucco

1.2. Quality of castings.

The production of investment castings requires stringent control of quality, especially for defence and aerospace applications. In addition to visual and dimensional examination, castings are often subject to rigorous non-destructive tests including fluorescent and magnetic-fluorescent dye penetrant inspection, and gamma and X-ray radiography.

From the casting-users point of view this is particularly important, since the main economic reason for specifying the use of investment castings is the reduction of subsequent machining operations. This means that even quite small surface flaws would often not be removed during finishing, which could lead to problems such as reduced fatigue life, for example.

For the foundry this means that castings with defects which may be quite unimportant in sand castings are unacceptable, resulting in increased overheads and reduced competitiveness .

Deritend Precision Castings were experiencing significant levels of scrap on components cast in low-alloy steels an austenitic stainless steels. The defects were usually found during dye-penetrant inspection and took the form of crack like lines and spots on the surface. As the alloy groups affected made up a major part of the company's production, the scrap incurred had a significant impact on profitability.

Because the company had been unsuccessful in determining the causes of the defects in these alloys, an approach was made to Aston University in order to establish a research project to investigate the problem and to study investment casting defects in general. As a result of this approach, an industrially based research programme was initiated, supported by the Science and Engineering Research Councils CASE award scheme (Cooperative Awards in Science and Engineering)

The objectives of the research were defined as:

1. Familiarisation with the process and methods as used at Deritend Precision Castings.

2. A general review of the major causes of scrap specific to the processing stages in the production of steel investment castings.

3. A detailed investigation of any defects which were felt to be significant in terms of their impact on overall scrap, where those defects where not properly understood. Special emphasis was to be placed on the so-called "linear" defects in low-alloy steels because of the significant amounts of scrap they were already known to cause.

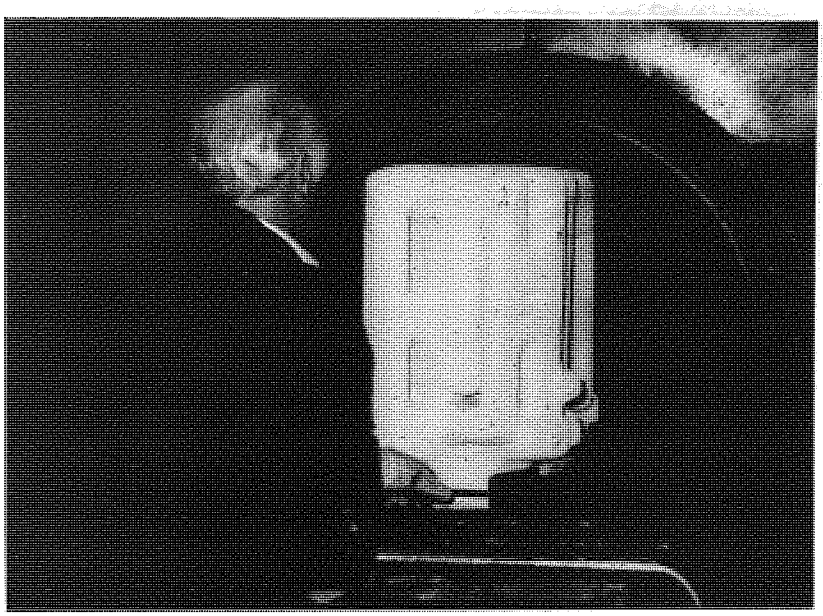

PLATE 1.5:
Removing a de-waxed mould from the autoclave.

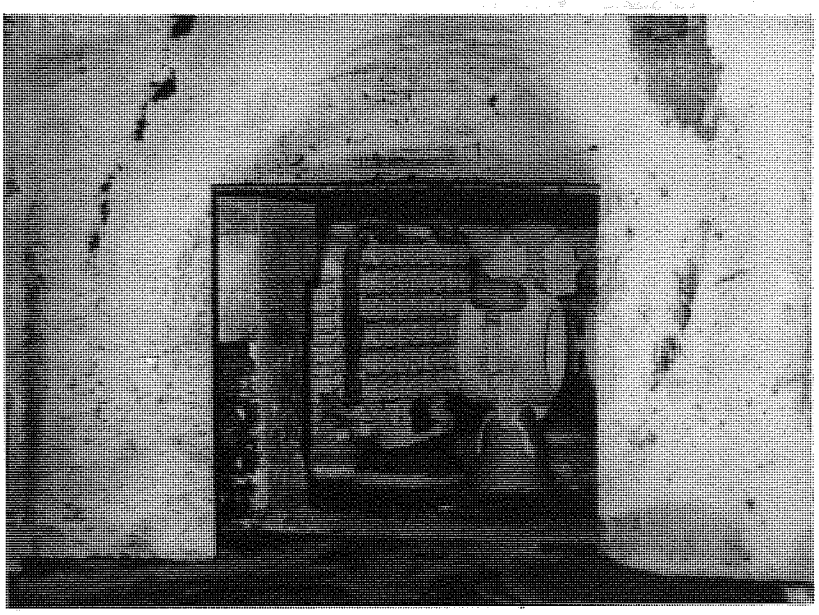

PLATE 1.6:
Moulds in the pre-heating furnace.

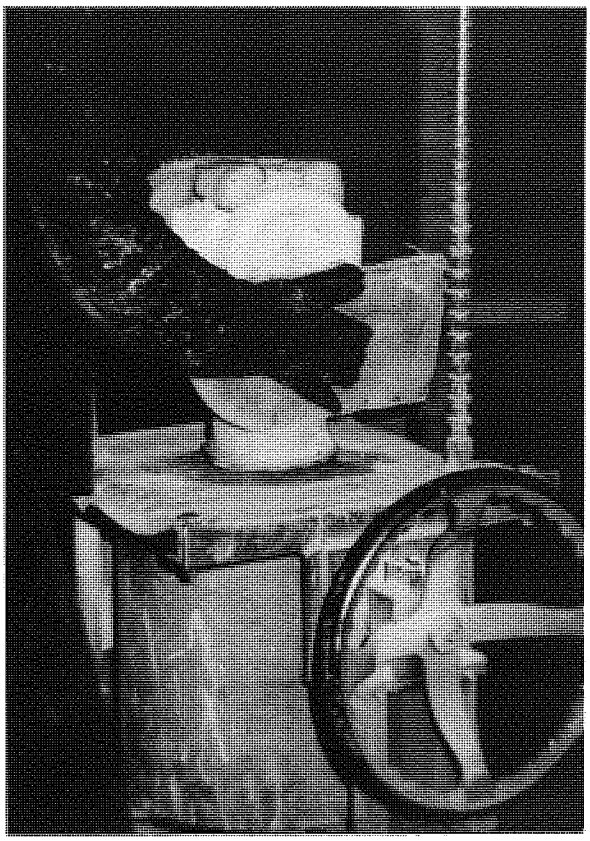

PLATE 1.7:
Mould placed on the melting furnace prior to casting.

2. PROCESS FAMILIARISATION AND PRELIMINARY INVESTIGATION.

The preliminary 'on-site' investigation was to consider and classify the major defects in investment castings in terms of the stage in the production process at which they originate.

2.1. Die Production

The dies used for the production of the wax patterns are sometimes fabricated by the customer but are more frequently produced 'in house' from the customer's component drawings. Dies for wax pattern production are usually made from aluminium alloy because of its high thermal conductivity and easy machining properties. However, where multipart dies with moving sections are required – to allow complex, single-piece waxes to be pressed – it is common practice to use brass, or even steel, for many of the die sections. This is to prevent excessive wear, which could result in a change in the die cavity dimensions.

It is obviously important that the die is machined and fabricated so as to produce dimensionally accurate castings, and allowances are routinely made for the contraction of wax patterns and the contraction of castings in the mould cavity. Mistakes in assessing the required contraction factor are rare.

2.2. Wax Pattern Pressing

Wax patterns are produced by injecting molten wax into the die cavity under pressure. The wax is then allowed to solidify with the pressure maintained until the wax is dimensionally stable. The pressure is then released, the die opened and the wax pattern removed (Plate 1.1).

There are many defects which can result in wax patterns being rejected. Amongst the most common are:-

i) Flow Lines.

These are associated with problems such as the die or wax being too cold or the injection pressure or flow rate incorrectly set. Flow lines can also result when a thick section is injected through a thin section. Flow lines are analogous to cold shuts in cast metals.

ii) Trapped Air.

Air entrapment in the wax can result from the wax temperature being too high, causing turbulence during injection. Air can also be trapped by wax flowing into the die more rapidly than the air can escape through the joints of the die. It is also possible for air to be entrapped in the wax in the machine causing air bubbles to be injected with the wax.

iii) Lubricant Marks.

Injection dies are lubricated before each pattern is pressed, to aid removal of the wax from the die. However, over-lubrication of the die can result in folds and creases in the surface of the wax pattern.

iv) Surface Finish .

The surface finish of wax patterns can also be affected by low die or wax temperature, or by insufficient injection pressure, resulting in an "orange-peel" effect.

v) Misruns.

Misruns result from incomplete filling of the mould cavity. The fault is usually caused by a cold die or cold wax, or by too low an injection rate, and is most pronounced at wax-flow restrictions such as thin walled sections in the die.

vi) Dimensional Faults.

Linear contraction of the wax is not normally a problem as it is predictable (for constant die and wax temperatures and pressures) and can be allowed for in die manufacture. However, in some cases, wax patterns may warp or twist after pressing. The most common causes of this are the removal of the wax from the die before the pattern has cooled sufficiently, or temperature fluctuations during subsequent storage.

A more serious problem is "sinkage", resulting in surface depressions, especially in thick sections. Sinkage results from die or wax temperatures which are too high, or from insufficient injection pressure or holding pressure. Other causes of sinkage are incorrectly positioned or small sprues. This results in the sprue freezing quickly and preventing sufficient application of pressure whilst the thicker section is cooling and contracting. Attempting to feed a thick section through a thin section has the same effect. A common method of avoiding sinkage is the use of "chills" which are pieces of solid, pre-injected wax, placed into the die cavity prior to injecting the pattern. The use of chills, however, can lead to other problems due to incomplete coverage of the chill or movement of the chill causing breakthrough above the surface of the wax.

vii) The Use of Cores.

Many of the wax patterns for aerospace applications involve the production of complex hollow sections. The only practical method for producing these waxes, other than assembling multipart waxes, is to use cores. There are two types of cores in common use: ceramic and water soluble.

Ceramic cores are preformed from zircon, fused silica or Molochite, and are especially useful where thin, hollow sections are to be cast into a part - for example cooling cavities within airfoil components. The ceramic core is placed into the die cavity and the molten wax is injected around it. The ceramic-wax assembly is invested in one piece and the core remains in the shell after dewaxing, to be finally removed from the metal casting. At the wax injection stage, the thin ceramic cores can be prone to distortion and breakage in the die.

Soluble wax cores are used to produce larger hollow sections, such as pipe elbow joints. Soluble wax is made from a binder, usually polyethylene glycol; a filler such as silica, mica or sodium chloride; and a breakdown agent – often a carbonate – to aid removal of the soluble wax core. A major problem with soluble wax is in the blending of a wax which is not brittle, but which at the same time is not soft or sticky due to the hygroscopic properties of the breakdown agent.

Soluble wax cores are placed in the mould cavity, in the same way as ceramic cores, but are removed by leaching in dilute acid before the wax patterns are inspected and assembled prior to dipping. Problems associated with the use of soluble wax cores include:- fracture of cores under the pressure of wax injection, (Plate 2.1), which can result in surface imperfections and "stepping" of pipe bores; poor surface finish due to moisture pickup by the water soluble core; and surface defects due to partial solution of the water soluble wax by the pattern wax, especially when the pattern wax is to hot.

2.3. Inspection and Assembly of Wax Patterns

All wax patterns are inspected and finished by hand and some waxes of particularly complex shape are assembled from more than one part if this reduces the high tooling costs associated with moving-part dies. Waxes are finished, or "frazed", to remove mould flash and parting lines, and to remove minor protruding (positive) defects. Small holes and other "negative" defects are filled using soft red wax. Wax patterns are fully inspected to reject waxes which have been damaged during or after pressing, although internal defects, such as those in the bores of pipes caused by damaged cores, can often pass unnoticed through both frazing and inspection. Waxes containing ceramic cores are sometimes X-rayed to ensure accurate location of the core and to reject patterns where the core has fractured in pressing. This radiographic inspection is performed only when the alloy cost is high enough to make such expensive scrap prevention cost effective.

The dimensional properties of wax patterns are not routinely checked, but a sample is inspected for the first use of a new die and after any die modification. An important process which takes place during finishing is the attachment of feeds, where these have not been injected "in-die". The feeds are welded onto witness pads on the injected wax patterns. The shape, cross-sectional area, and position and number of feeds are carefully determined, often by trial and error, to give castings free from shrinkage, and from inclusions due to mould erosion by the flowing metal. It is therefore crucial that feeds are correctly positioned by wax shop operatives, (Figure 2.1), as necking of feeds and misalignment can cause defects in finished castings. This has resulted in a trend towards machining the feeds into the injection die although this is not always possible as the siting of the optimum feed positions may not allow their inclusion.

2.4. Assembly onto Moulds

Wax patterns are attached by their feeds onto preformed, usually cast, wax risers using glue and heat sealing (see Plate 1.2). Placement of individual patterns on the riser affects the feeding of molten metal to each pattern cavity and is checked against photographs of an optimum assembled mould. A variety of riser designs is used, both for economy, to reduce offcuts; and to assist the feeding technique. Test bars (for the determination of mechanical properties) and chemical analysis buttons are attached to the riser as required.

2.5. Investment

The completed wax moulds are moved into a separate area for the investment of the ceramic shell mould, where the temperature is maintained at (20 ± 2)°C and the humidity at (50 ± 7)% RH in order to keep dimensional stability in the wax and to give controlled drying times.

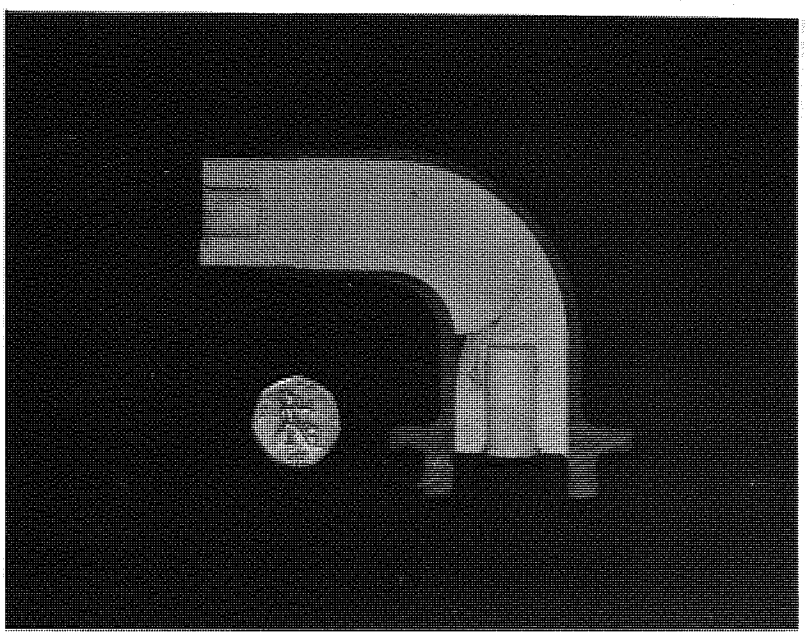

PLATE 2.1:
Section through pipe-casting wax-pattern, showing cracked water soluble core.

FIGURE 2.1 The effect of defective pattern assembly on the integrity of castings.

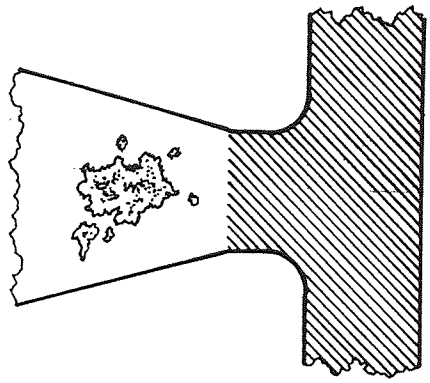

A) Feed correctly positioned. Shrinkage is restricted to the feed section, giving a sound casting.

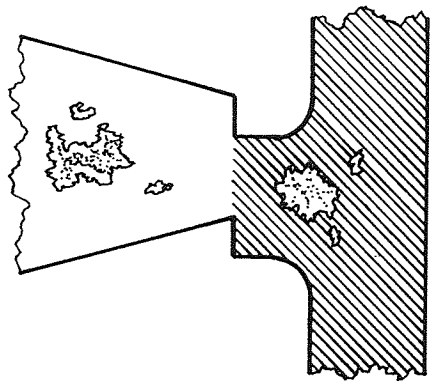

B) Feed mis-aligned during assembly. Shrinkage in both feed and casting.

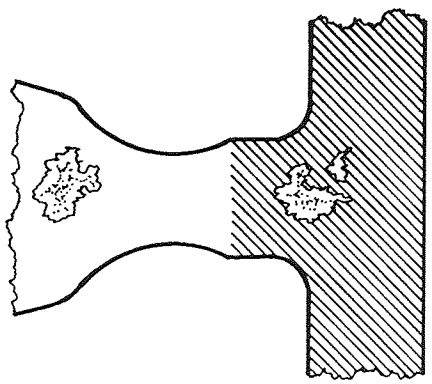

C) Feed 'necked' during assembly. Shrinkage in both feed and casting.

Small moulds are dipped by hand in refractory slurry and the wet slurry is coated with refractory stucco. The stucco is zircon sand for the primary coat, to give good surface detail, followed by increasingly coarse grades of Molochite with each coat to give a good strength to weight ratio. The binder is essentially zircon flour in a colloidal silica binder (see Table 2.1).

The moulds are dried between each coat in an ammoniated atmosphere for 40 to 60 minutes to promote gelling of the binder. The process is repeated until a ceramic shell of the required strength and thickness is built up. Larger moulds are dipped using an automated robotic system. Moulds are loaded on to hangers on a track which transports the moulds to the robot station. The robot then dips the mould in refractory slurry using a carefully programmed dipping and draining sequence. The wet mould is then coated with the appropriate stucco in a raining machine. The mould dries during the time taken to transport the hanger around the continuous track and back to the robot station, a period of from six to twelve hours. Moulds are occasionally damaged during the investment process by mechanical impact, although this is rare for the hand-dipped moulds.

TABLE 2.1. Make up of investment slurry

Syton* :- (colloidal silica binder)	1.0 litre
-200 mesh zircon flour :- (filler)	4.6 kg
Synperonic NX† :- (detergent alcohol wetting agent)	5.0 ml
Octan-1-ol :- (anti foaming agent)	3.5 ml

* Syton is a registered trademark of Monsanto
† Synperonic is an ICI trademark

Uneven drying of moulds can lead to cracking and delamination of the primary coat. Over-drying leads to defects such as cracking on flat areas of primary coat, whereas under-drying leads to spalling of primary coat from internal angles (Plate 2.2). Drying problems are frequently caused by lack of adequate control of temperature and humidity.

2.6. Dewaxing of moulds

Moulds are dewaxed in an autoclave using steam superheated to 180°C at a pressure of 7 bar for around 10 minutes (Plate 1.5). Autoclaving is used because of the rapid thermal transfer characteristics of superheated steam. This allows a layer of wax adjacent to the shell to melt before significant thermal expansion of the bulk of the solid wax causes cracking of the ceramic shell. In simple moulds the molten surface layer drains out to leave a gap between the shell and the wax. In more complex moulds the molten wax can become trapped in the mould cavity leading to cracking of the mould. This can be prevented by attaching "dewax tags" to the mould prior to dipping. The shell material can then be filed back over the tags to allow egress of the molten wax during autoclaving. Lack of control of the autoclave operation can lead to extended pressure and temperature "rise times" which can result in cracking. Moulds which do crack during dewaxing can sometimes be repaired using "Pyruma" refractory paste (Plate 2.3) which is also used to block holes left by dewax tags and to strengthen moulds. After autoclaving the moulds are fired at 1000 °C for around one hour in order to drive off any remaining wax or moisture and to develop the full strength of the ceramic shell. The moulds are then stored until required. The main source of defects during the dewaxing process is cracking of the moulds. Even when moulds are repaired the damage to the primary coat can lead to surface imperfections and to inclusions in castings due to erosion of shell material. Cracked moulds can also lead to run-out of molten metal or a burst mould either of which has obvious safety implications.

2.7. Casting.

Moulds are fired prior to casting to prevent thermal shock cracking and to aid metal flow. For steels this involves firing at 1100 °C for about one hour, although for vacuum cast alloys a mould preheat of up to 24 hours is required. For small moulds, of up to around 20 kg metal weight, the metal charge for one mould is pre-weighed; the weight being calculated from the weight of the mould in wax. The charge is melted in a crucible using a coreless induction coil operating at around 2.5 to 3.0 kHz.

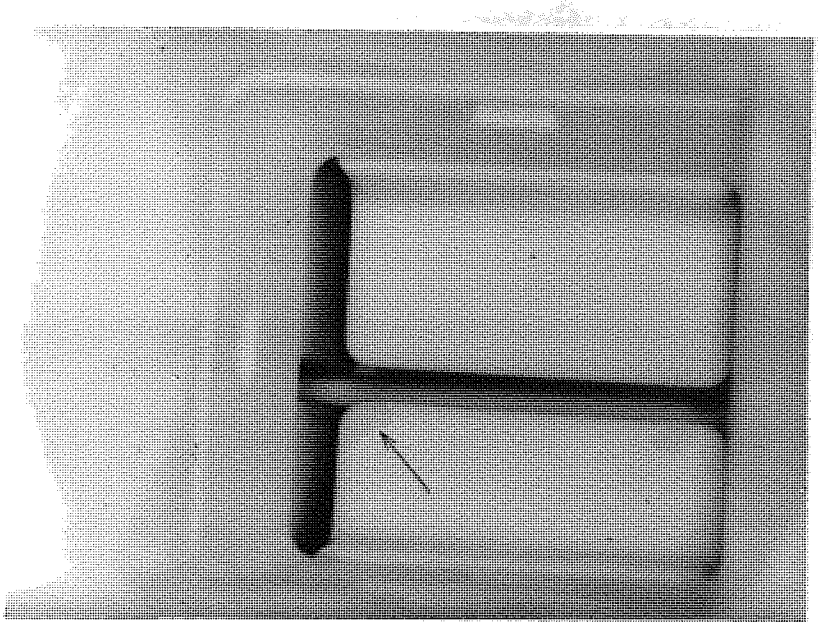

PLATE 2.2:
Spalling of the primary coat from inside a mould.

PLATE 2.3:
Repairing a cracked mould with "Pyruma" refractory paste.

When the steel is molten it is deoxidised, if required, at the casting temperature (see Table 2.2). The steel is then de-slagged using granulated pearlite to coagulate the slag. After checking the temperature of the melt, the preheated mould is inverted on top of the crucible, clamped in place, and the mould and furnace inverted to rapidly fill the mould (Plate 1.7).

TABLE 2.2. Deoxidation Practice for Steels.

Material	Deoxidation
Low alloy steels	0.1% Aluminium. Residual Aluminium should be 0.03 to 0.08%. Additions of 0.2% Ca-Si-Mn at the discretion of the works metallurgist.
Austenitic stainless steels	No Deoxidation.‡
Martensitic and precipitation hardening stainless steels.	0.1% Aluminium (NOT in precipitation hardening steels). 0.2% Ca-Si-Mn.

‡ As a result of this investigation – see § 3.3.3.

In addition to metallurgical defects, such as cracks and inclusions – which will be discussed separately – many other causes of wastage can occur at this stage. Among the most serious – although rare – is mould "run-out" or a burst mould. Large moulds, such as those which are cast by ladle rather than by "turn-over", can bulge due to the weight of molten metal, leading to dimensional problems. Defects such as mis-runs, cold shuts or castings "not-making" can result from too low a mould temperature, or from air entrapped in a mould having insufficient permeability. After casting a bag of wood shavings is placed on top of the hot mould to consume the oxygen, and the mould is placed under a metal cover to cool.

Porosity can result from gas in the metal, often due to poor deoxidation either at the casting stage or during production of the master heat at the metal suppliers. Porosity can also be caused by shrinkage resulting from poor feeding technique or incorrect placement of feeds at the wax assembly stage.

Large moulds weighing up to 160 to 200 kg "in metal" are cast using a large induction furnace and a preheated ladle to fill the mould. Metal melted in bulk tends to contain more inclusions than small melts and for the largest moulds the need to use more than one ladle to fill the mould can have a deleterious effect on casting quality.

2.8. Knock - Out

When moulds are sufficiently cool, usually after 16 to 24 hours, the ceramic shell material is removed from the mould. For most moulds this is achieved using a pneumatic hammer. However, for moulds which are susceptible to cracking – due either to the geometry of the mould or the properties of the alloy – the shell is removed by water blasting, which is performed by subcontractors. Shell residue and ceramic core material are removed by shot blasting and by leaching in 3 or 9 Molar NaOH respectively; usually after cut off (qv.).

2.9. Cut Off

Castings are parted from the moulds by cutting through the feeds using abrasive cut-off wheels. The feeds are then ground back to the casting profile and the castings grit blasted to clean off surface oxide. Castings may occasionally be damaged due to operator errors such as cutting into castings rather than feeds, but this is rare. Large castings with heavy feed sections can occasionally be damaged by the heat generated when cutting through the feeds, sometimes resulting in cracks propagating from the feeds into the casting.

2.10. Visual Inspection

All castings are inspected visually to exclude obvious defects such as misruns, broken castings, and cut off damage. Castings which are not defective can then be passed on to subsequent stages in the production process.

2.11. Heat Treatment and Setting

Castings are heat treated where necessary to give the mechanical properties required by the customer, or by the material specification. This usually involves annealing in vacuum as a preliminary operation, to soften the metal and homogenise the microstructure. It is after the castings have been softened that any setting is carried out to bring the castings within dimensional tolerances.

Small castings are usually set cold, especially if the sections to be set are fairly thin (Plate 2.4), whilst larger castings and thicker sections are heated before setting to reduce the stress required for plastic deformation.

Heat treatment can cause initiation of cracks, but the exacerbation of preexisting defects is more likely. Cold setting can certainly cause cracking at stress concentrations, and this is one of the major reasons for using hot setting. However, hot setting has been found to cause quench cracking resulting from the contact between the hot workpiece and the cold setting jig.

After setting, castings are given a final heat treatment which may involve hardening and tempering to give the required mechanical properties or aging of precipitation hardening steels or nimonic alloys.

Quenching of castings holds obvious dangers from cracking, whilst the use of barium chloride salt baths for tempering can lead to apparent increases in crack width due to leaching out of entrapped oxides.

2.12. Final Inspection

Whilst the final inspection is unlikely to cause the casting defects, it is at this stage that most of the defective castings are found. It is therefore important to discuss briefly the techniques used for final inspection, as a preliminary to discussing the main metallurgical defects which, being less easily traced to known causes than the defects discussed so far, are felt to be worthy of a more exhaustive investigation.

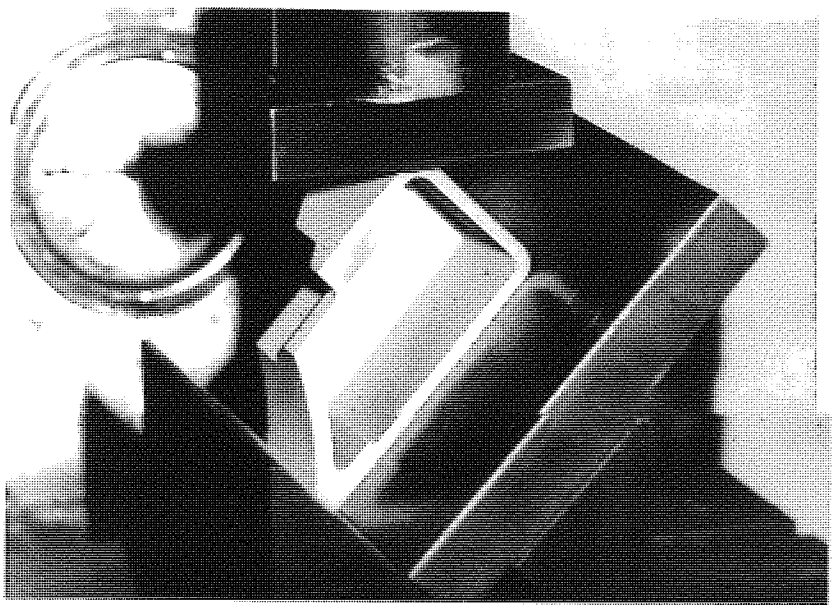

PLATE 2.4:
Cold setting of a thin-walled casting.

Prior to any non-destructive examination all castings are sand blasted to clean them and to remove oxides, scale, and grease. The method of non-destructive testing used depends mainly on the casting size and the material from which the casting is made.

a) Large castings are examined for surface defects using red dye penetrant to British Standard BSM 39, although in some cases aerosol magnetic particle penetrant is used with a portable magnetic bridge.
b) Small ferromagnetic castings are examined using fluorescent-magnetic particle testing to British Standard BSM 35.
c) Non-ferromagnetic small castings, such as those made from austenitic stainless steels, are examined using green fluorescent dye penetrant to British Standard BSM 39.

Castings may also be subject to radiographic inspection up to British Standard BSM 34 - 100% class 1; (equivalent to U.S. ASTM E192). It should be pointed out that all these inspection standards are the most stringent which may be used when requested by the customer, and lower standards may be agreed for some, commercial, components.

In addition to the assessment of metallurgical integrity given above, castings are subject to dimensional inspection and examination of microsections for porosity. These tests are usually performed as part of the approval procedure for the method of manufacture, although some customers require periodic validation inspections. The mechanical properties and chemical composition are determined – if required – from test bars cast with the mould.

The preceding general discussion of the relationship between processing stage and the incidence of defects in investment castings has covered those defects which are easily traced back to their cause. However, there are many defects which are less well understood or for which there are conflicting accounts in the literature.
As a consequence of the general investigation several categories of major defects of uncertain origin were discovered. As expected these included linear defects in both low alloy and austenitic stainless steels. One other source of significant amounts of scrap was a defect in martensitic stainless steel castings known as 'black-spot'

It was decided to investigate these sources of scrap in the following order:

i. Linear defects in austenitic stainless and low alloy steels.
ii. 'Black-spot' defects in martensitic stainless steels.

As will be seen, the problem of linear defects in austenitic stainless steel castings was rapidly solved and was, in fact, found to be unrelated to the defect of similar morphology found in low-alloy steels.
As a consequence of this, both the 'black-spot' defect and the linear defect in low-alloy steels were investigated, although more emphasis was given to the latter since, as one of the reasons for establishing the programme, it was explicitly stated in the objectives of the research.

3. SURFACE DEFECTS IN AUSTENITIC STAINLESS STEEL CASTINGS

Surface defects were regularly found during routine inspection of austenitic stainless steel castings using fluorescent green dye penetrant. The defects, which were found predominantly on pipe elbow joint castings, usually took the form of irregular speckles and lines, sometimes lunate, from which the colloquial name "half moon" defect was derived (Plate 3.1). Those defects occurring within the bore of the pipe tended to be in the form of fine speckles, whilst the other defect morphologies were more often observed on the external lugs.

The castings most prone to these defects were cast in a Rolls Royce Specification MSRR 6536 material, (Table 3.1). In addition to the defects observed by dye penetrant, shallow, flat bottomed depressions were seen in a few of these castings appearing as if an irregular prism had been pressed into the surface of the wax pattern.

3.1. Metallography

Metallographic examination of the surface defects revealed irregular beige or light grey inclusions extending from the surface. These extended inclusions often exhibited thicker "nodes" along their length with dark grey inclusions radiating from them (Plates 3.2 and 3.3).

The surface depression was also sectioned and exhibited the structure shown in plates 3.4, 3.5, and 3.6. The corners of the depression displayed clear signs of included non-metallic material.

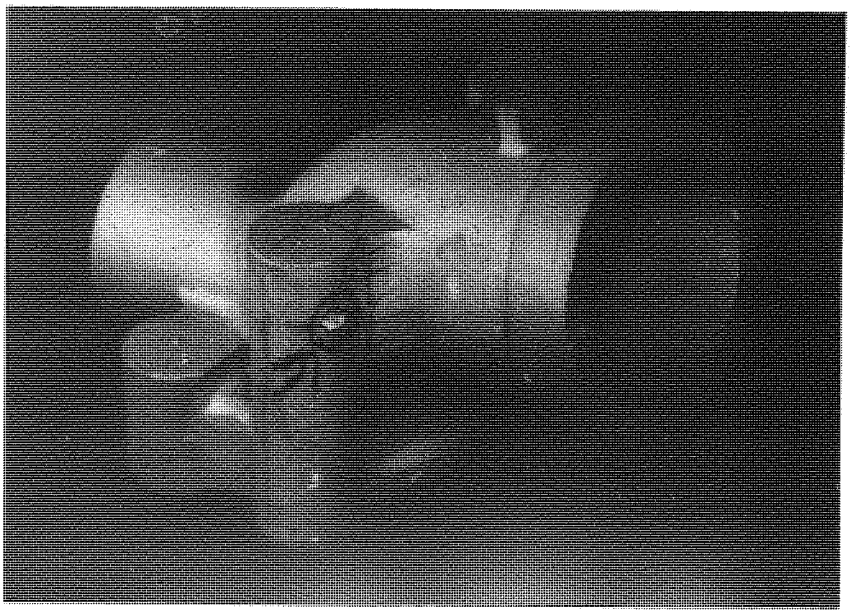

PLATE 3.1.
Stainless steel pipe casting viewed under ultra-violet light, exhibiting a characteristic "half-moon" defect by fluorescence. (Casting approx. 100mm long).

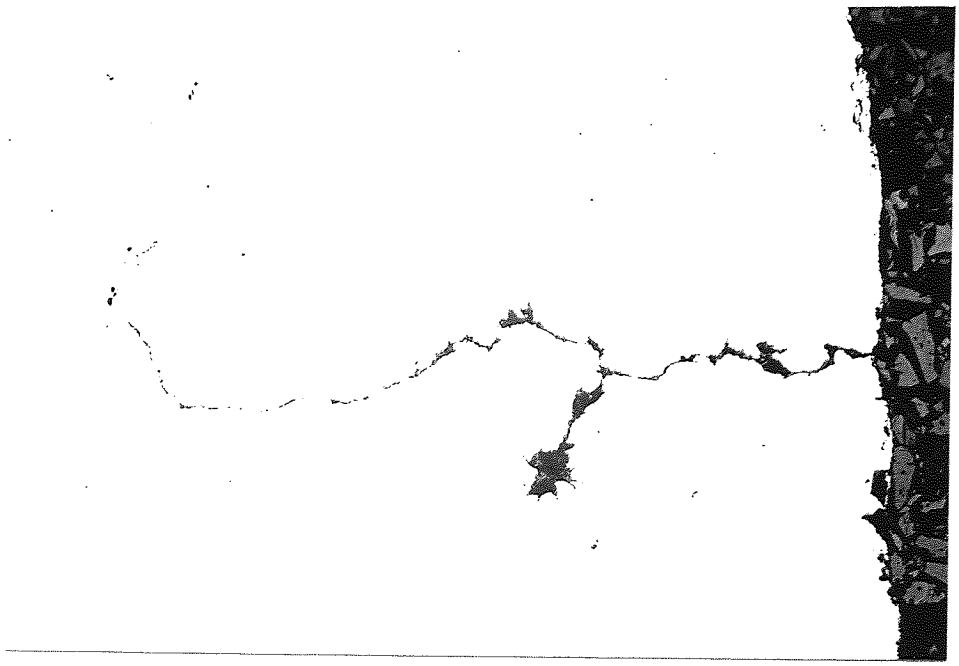

PLATE 3.2.
Section through defect shown in plate 3.1. The metal surface is at the right hand edge.
(Unetched, X 60) (Specimen No. P3C)

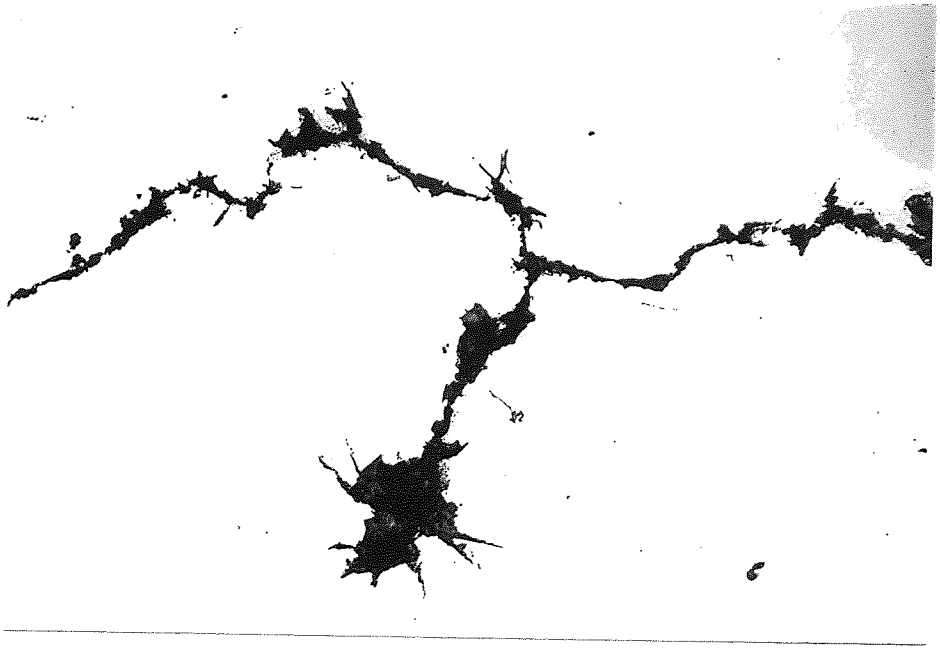

PLATE 3.3.
Enlarged portion of defect shown in plates 3.1 and 3.2.
(Unetched, X 100) (Specimen P3C)

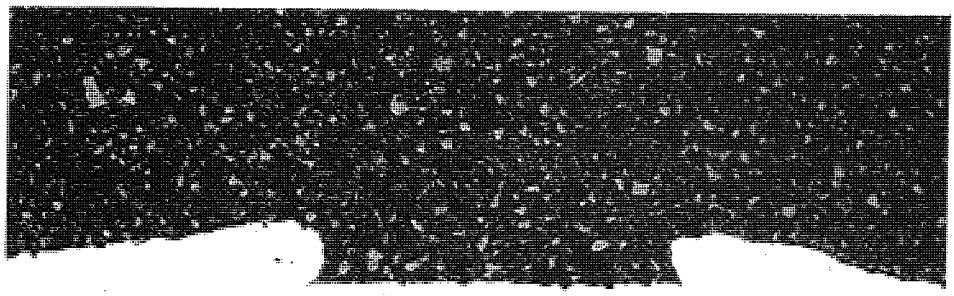

PLATE 3.4.
Section through surface depression observed on pipe casting. The metal is in the lower half of the plate.
(Unetched, X 24) (Specimen No. P4C)

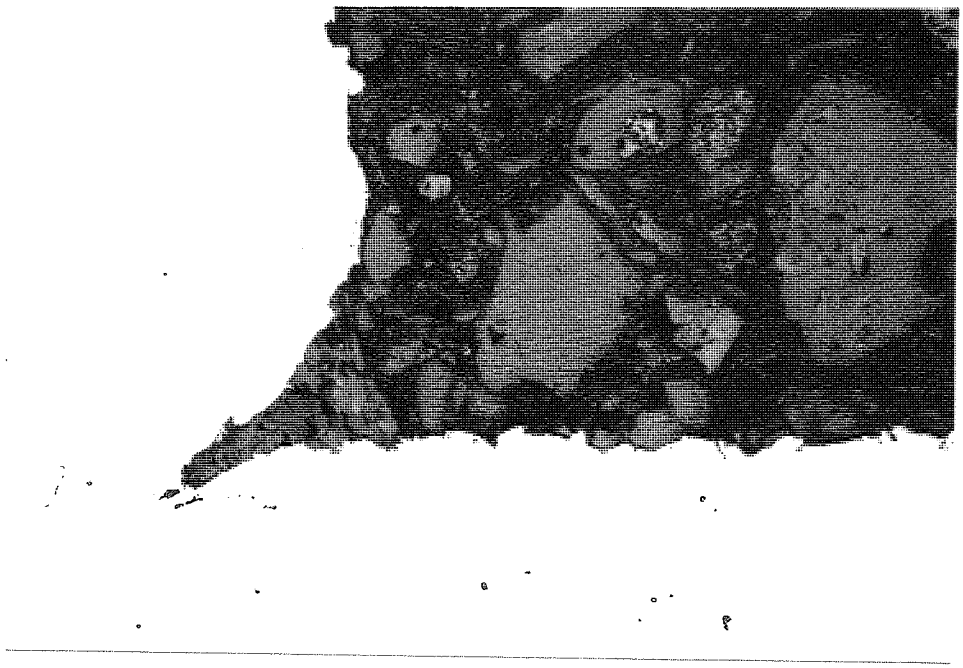

PLATE 3.5.
Enlarged section of the surface depression shown in plate 3.4.
Note the included material at the depression corner.
(Unetched, X120) (Specimen No. P4C)

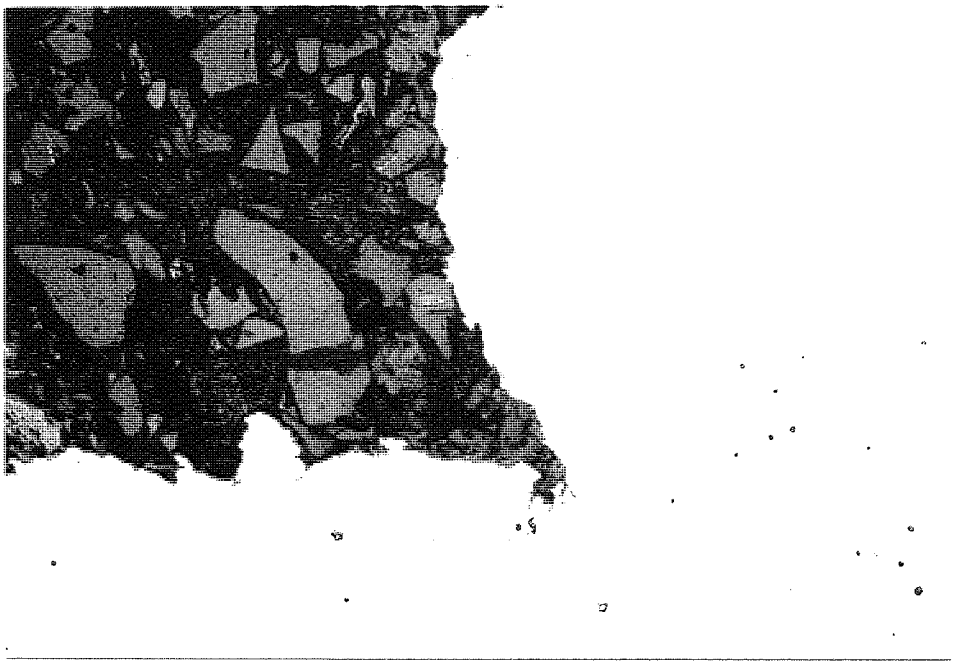

PLATE 3.6.
Enlarged section of the surface depression shown in plate 3.4.
Note the included material at the depression corner.
(Unetched, X 120) (Specimen No. P4C)

TABLE 3.1.Composition of Austenitic Stainless Steel Castings:-

Specification MSRR 6536

a) Alloying elements

Element	% Minimum	% Maximum
Carbon	0.10	0.25
Silicon	1.2	2.0
Manganese	-	1.0
Chromium	21.0	25.0
Nickel	10.0	12.0
Tungsten	2.7	3.5

b) Residual elements

Element	% Minimum	% Maximum
Phosphorus	-	0.040
Sulphur	-	0.040
Cobalt*	-	0.5
Molybdenum†	-	0.5
Niobium†	-	0.3
Vanadium†	-	0.2
Titanium	-	0.1

* Cobalt and Nickel shall not exceed 12.0 percent

† The total impurity level of these elements shall not exceed 0.5 percent

3.2. Inclusions

The complete study of non-metallic inclusions in steels covers a vast field. Comprehensive information may be found in the excellent volume by Kiessling and Lange[2]. This gives a detailed account of the formation, structure, and chemistry of inclusions, from which it is often possible to determine the origin of inclusions if their chemical composition or phase structure can be determined. Some of the common sources of inclusions in steelmaking are summarised in table 3.2. A brief outline of the field is necessary, since it has some bearing on the investigation of the defects in austenitic stainless steels.

Non-metallic inclusions fall into two groups: those of indigenous and those of exogenous origin. Indigenous inclusions occur as a result of reactions taking place in the molten or solidifying steel, whilst exogenous inclusions result from the mechanical incorporation of slags, refractories, or other materials with which the molten steel comes into contact.

Indigenous inclusions – which form by precipitation as a result of homogeneous reactions in the steel – are principally composed of oxides and sulphides, and the reactions that form them may be induced either by additions to the steel – such as during deoxidation – or simply by changes in solubility during the cooling and solidification of the steel.

The structure and composition of exogenous inclusions is very varied but they are usually easy to distinguish from indigenous inclusions. Exogenous inclusions exhibit characteristics such as larger size, sporadic occurrence, preferred location in the ingot or casting, and irregular and complex shapes and structure. In addition because they originate from slags or refractories, they are often composed of oxides.

A complicating factor, however, is that indigenous precipitation is most likely to occur on preexisting exogenous nuclei. This means that the composition and structure of these inclusions is continuously changing as they cool down to the temperature below which no significant diffusion can occur.

TABLE 3.2. Possible inclusion sources in steelmaking

Inclusion source		Key elements
Furnace	Furnace slags	Ca
	Furnace refractories	Ca
	Ferro-alloys	Cr, Al, Si
Tapping	Launder refractories	Mg, Ti, K
	Oxidation	FeO
Ladle	Deoxidation	Dependent on deoxidant
	Ladle slag	Ca, Mg
	Ladle refractories	Mg, Ti, K
Teeming	Stopper and nozzle refractories	Mg, Ti, K
	Oxidation	FeO
	Deoxidation	Dependent on deoxidant
Ingot mould	Refractories	Mg, Ti, K
	Deoxidation	Dependent on deoxidant
Heat treatment and rolling	Surface oxidation	FeO
	Surface sulphurisation	FeS
	Inner oxidation	SiO_2
	Hot-shortness	FeS
Welding	Welding slags	Ca, Ti
	Electrode coatings	Ti, V
	Steel inclusions	
	Hot tearing	S

After Kiessling and Lange (1978)[2]

3.3. Investigation of Inclusions

As a first step in determining the possible sources of both types of inclusions found in these castings, it was decided to perform semi-quantitative energy-dispersive X-ray analysis on inclusions in microsections.

3.3.1. Equipment and specimen preparation.

Semi-quantitative analysis was carried out using a Cambridge S150 scanning electron microscope fitted with a Link Systems energy dispersive spectrometer and analyser.

Specimens to be analysed were mounted in conducting bakelite and polished to 1μm diamond grit and were, in most cases, left unetched.

3.3.2. Experimental and results.

Semi-quantitative energy dispersive analysis was carried out on inclusions within the defect in plate 3.2. The results of these analyses are given in table 3.3.

Similar defects in two other castings were analysed and these results are given in tables 3.4 and 3.5. In addition to the point analyses, given in tables 3.3 to 3.5, X-ray maps were produced of the defect in specimen P3C in order to show the distribution of calcium and aluminium within the defect (Plates 3.7, 3.8, and 3.9).

TABLE 3.3. Semi-quantitative analyses of defects in an Austenitic stainless steel casting. (Specimen No. P3C)

a) Bulk material, away from the defect.

Fe	Ni	Cr	Si	
63.84	6.84	24.97	2.57	(%)

b) Light grey inclusion, within defect.

Fe	Mn	Ni	Cr	Ti	Si	Al	Ca	Zr	
5.11	0.38	0.16	3.18	1.37	8.08	**51.67**	**29.83**	0.24	(%)

c) Dark grey inclusion

Fe	Mn	Cr	Ti	Si	Al	Ca	Zr	
1.34	0.43	0.98	1.02	12.75	**54.12**	**27.84**	1.51	(%)

TABLE 3.4. Semi-quantitative analyses of defects in an Austenitic stainless steel casting. (Specimen No. P13C)

a) Bulk material, away from the defect.

Fe	Ni	Cr	Si	
61.94	8.10	26.51	3.45	(%)

b) Inclusion in defect.

Fe	Cr	Al	Zr	
0.44	1.62	94.14	3.80	(%)

c) Inclusion in defect.

Cr	Al	Zr	
1.72	97.97	0.32	(%)

d) Defect side branch.

Fe	Mn	Ni	Cr	Si	Al	Ca	Zr	
3.56	0.67	0.37	2.08	0.18	83.0	7.67	2.47	(%)

e) Inclusion away from main defect

Fe	Mn	Cr	S	Al	Ca	Zr	
1.60	1.26	1.08	0.31	94.83	0.68	0.24	(%)

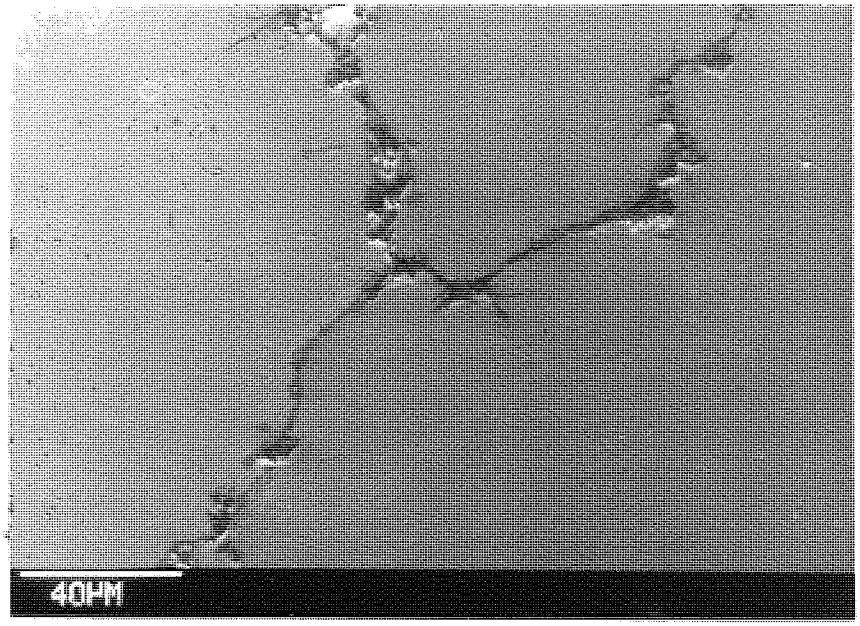

PLATE 3.7.
Scanning electron image of section through 'half-moon' defect in pipe casting.
(Unetched, magnification as shown) (Specimen No. P3C)

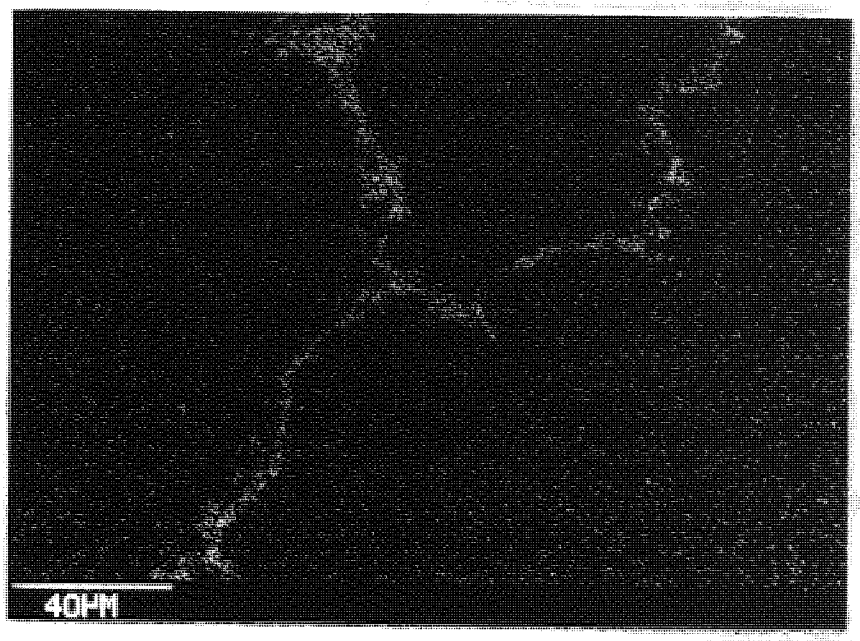

PLATE 3.8.
Calcium X-ray map for the area shown in plate 3.7.
(Unetched, magnification as shown) (Specimen No. P3C)

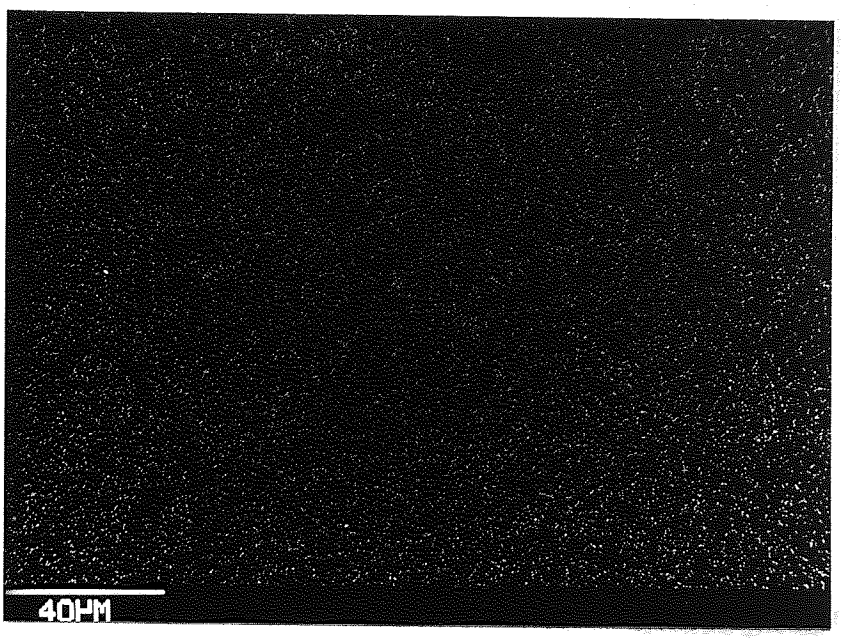

PLATE 3.9.
Aluminium X-ray map for the area shown in plate 3.7.
(Unetched, magnification as shown) (Specimen No. P3C)

TABLE 3.5. Semi-quantitative analyses of inclusions associated with defects in an Austenitic stainless steel casting. (Specimen No. P14C)

a) Inclusion in defect.‡

Fe	Mn	Cr	Ti	Si	Al	Ca	
6.01	44.25	16.84	0.55	4.27	27.57	0.52	(%)

b) Inclusion in defect.

Fe	Mn	Cr	Si	Al	Zr	
1.49	7.6	5.36	3.6	21.34	60.62	(%)

c) Defect material

Fe	Mn	Cr	Si	Al	Zr	
1.76	7.39	8.04	3.5	78.42	0.9	(%)

d) "Spur" inclusion.

Fe	Mn	Ni	Cr	Si	Al	Ca	Zr	
13.77	7.82	2.03	11.21	4.04	50.94	2.36	7.82	(%)

‡ Low count rate for this analysis, suggesting high levels of light elements such as oxygen.

Analyses were also performed on the residual material left in the corners of the surface depression shown in plate 3.4. The results of this analysis are given in table 3.6.

TABLE 3.6. Semi-quantitative analyses of residual material in a surface defect on an austenitic stainless steel casting. (Specimen No. P4C)

a) Bulk material, away from the defect.

Fe	Ni	Cr	Si	
61.46	8.42	26.61	3.51	(%)

b) Included material (i)

Fe	Mn	Cr	Si	Zr	
1.39	0.47	0.86	35.69	61.6	(%)

c) Included material (ii)

Si	Zr	
38.21	61.79	(%)

The analyses of the irregular surface defects strongly suggests that the defects are associated with the deoxidation practice for these alloys, which involves the use of calcium-aluminium. Calcium-aluminium alloys have been widely used for the deoxidation of austenitic stainless steels used for investment casting, although the reasons for this are by no means clear.

Calcium is regarded as a metal which is all but insoluble in liquid iron (Kiessling and Lange, 1978)[3], and although Sponseller and Flinn[4] found small amounts of calcium dissolved in iron at 1600 °C, the primary source of calcium bearing inclusions must be exogenous. Calcium has the highest affinity for oxygen of any of the elements used for deoxidation of steels and so ought to be the best deoxidant. However, Simms and Briggs[5] have reported that calcium has no apparent deoxidising effect in steel. Calcium is also reported to be difficult to add to steel (Simms and Briggs[5], and Keissling and Lange[3]) due to its low melting and boiling points, (847 °C and 1487 °C), and high vapour pressure, which cause

violent agitation in the molten steel, thus reducing the contact time between the calcium and the metal. Simms and Briggs[5] report that the agitation of the melt increases the oxygen content of the steel in some cases. However, Shortsleeve and Hilty[6] report that "*...several investigators have shown that calcium added along with aluminium, markedly improves the ductility of steel castings by minimising intergranular sulfide inclusions.*"(sic).

Kiessling and Lange (op. cit.) observe that the very high vapour pressure of calcium-silicon alloys aids deoxidation by increasing the vapour pressure of the silicon.

On further investigation at Deritend Precision Castings, it was found that deoxidation of these alloys was carried out, in practice, by adding coarse (5 to 10 mm) granules of calcium-aluminium to the surface of the melt at the liquidus temperature, and not at the casting temperature. It seems likely, therefore, that the deoxidant is oxidising in air at the surface of the melt and the remaining coarse oxides – predominantly $CaO\text{-}Al_2O_3$ – are incorporated into the steel either by sinking into the melt or adhering to the crucible wall before being washed into the mould cavity on casting. Discussion with the deoxidant suppliers confirmed that the correct procedure for deoxidation with calcium-aluminium is to plunge finely-powdered deoxidant to the bottom of the crucible when the casting temperature has been reached, which allows the maximum time of contact between the deoxidant and the melt.

High alloy steels, especially when the re-melting stock was produced under vacuum, should have an oxygen content below the specification maximum, especially when melted in small quantities. Trial moulds were therefore cast omitting any deoxidation and it was found that, whilst there was a significant

reduction in the frequency of castings with surface defects or inclusions, there was no concomitant increase in the incidence of gas porosity, nor impairment of mechanical properties.

The analyses of the residual material in the surface depression (Table 3.6) clearly show that – because of the presence of zirconium – the material originated from the ceramic shell. From its shape it is apparent that the defect is a result of a flake of refractory adhering to the mould wall – rather than a depression in the surface of the wax pattern – since there is evidence of metal flowing around the edges of the flake in plate 3.4.

The adherence of the flake to the mould wall implies the presence of moisture. This suggests that the most likely place for the shell fragment to have entered the mould cavity is between autoclaving (when the wax is removed) and firing (when the mould is dried) although it is possible for the flake alone to have been sufficiently moist if it originated outside the mould. Incomplete sealing of wax patterns onto the riser, or of the feed head onto the riser could, however, result in thin flakes of shell protruding into the mould cavity which could easily become detached during handling of the mould after dewaxing.

It is felt that standards of "housekeeping" were sufficiently high, at the time the investigation was performed, to prevent the ingress of extraneous fragments of shell into the mould. Poor sealing of waxes is, therefore, the most likely source of these defects.

4. SURFACE IMPERFECTIONS IN MARTENSITIC STAINLESS STEELS

"Black Spot", "Spotted-Dick" or "Fusion" defect.

Surface defects in the form of discrete, raised black spots have often been found on stainless steel castings, (Plate 4.1). In some cases these defects have been so severe as to merge to form a continuous layer on the surface of the casting. Removal of the defect by shot blasting – which is not easily accomplished – results in pits or depressions in the surface of the casting, suggesting that the discrete defects are lenticular in form. The steels most prone to this defect are the martensitic stainless steels – such as BS 3146 part II ANC1, and ANC2, among others, see table 4.1 – although it has occasionally been observed in 18-8 austenitic stainless steels as well.

TABLE 4.1. Chemical compositions of some martensitic stainless alloys.

i) BS 3146 : Part 2 : 1975 Type ANC1

	Grade A		Grade B		Grade C	
Element	% min.	% max.	% min.	% max.	% min.	% max.
Carbon	-	0.15	0.12	0.20	0.20	0.30
Silicon	0.2	1.2	0.2	1.2	0.2	1.2
Manganese	0.2	1.0	0.2	1.0	0.2	1.0
Phosphorous	-	0.035	-	0.035	-	0.035
Sulphur	-	0.035*	-	0.035*	-	0.035*
Chromium	11.5	13.5	11.5	13.5	11.5	13.5
Nickel	-	1.0	-	1.0	-	1.0

* Where a free machining grade is specified the sulphur content may be as high as 0.3% and / or other suitable elements may be present.

TABLE 4.1. (*cont.*)

ii) BS 3146 : Part 2 : 1975 Type ANC2

Element	% min.	% max.
Carbon	0.12	0.25
Silicon	0.2	1.0
Manganese	0.2	1.0
Phosphorous	-	0.035
Sulphur	-	0.035
Chromium	15.5	20.0
Nickel	1.5	3.0

The location of the defects was variable. However, the defect appeared particularly severe on feeds – which are intended to remain hot to prevent shrinkage – although the defects also appeared on thin sections such as the blades of a small shrouded impeller.

4.1. Literature on the "fusion" defect.

Taylor[7] has reported that the fusion defects are caused by slag reacting with the casting surface to cause pits in the metal surface.This paper appears to be one of the earliest references to this defect and is little more than a review of the several methods for reducing or preventing the problem on a commercial basis, without attempting to propose a hypothesis for the mechanism involved. In general the main principle behind most of the methods studied in the paper involve the exclusion of oxygen or the provision of a reducing atmosphere after casting.

With regard to the exclusion of oxygen from the mould, the critical factor seems to be the provision of a high vacuum – 1 μm Hg (1.333×10^{-3} mbar) – both during and after casting. An additional factor was extended mould firing time – of the

order of 20 hours – which prevented fusion defects forming even at the moderately low pressure of 1 mm Hg (1.333 mbar).

The provision of reducing atmospheres had varying degrees of success in preventing the defect. Methods used involved mixing graphite powder into the slurry for shell dipping; provision of carbonaceous backing to moulds either before or after casting; casting and cooling in a coal gas atmosphere; and injecting hydrocarbons into the mould cavity immediately prior to casting. In general these methods are reported as having only limited success, the two best being the use of carbonaceous backing both before and after casting, or the use of graphite loaded shell with reduced firing time.

The silicon-to-manganese ratio, which affects high temperature scaling in stainless steels, is reported as having no effect on the formation of fusion defects – high silicon steels were as badly affected as high manganese steels.

V. S. Larin and V. A. Vasil'ev [8], working in the Soviet Union, have studied these defects in a type Kh17N2L (17% Cr, 2% Ni) steel. (U.S.S.R. specification GOST 5632-72) They reported the following observations in their paper:–

A. The corrosion resistance of castings with the defect is reduced, especially within the defect recesses.
B. The defect material contains iron (in oxide form and as the free metal), chromium, silicon, and small amounts of nickel and manganese.

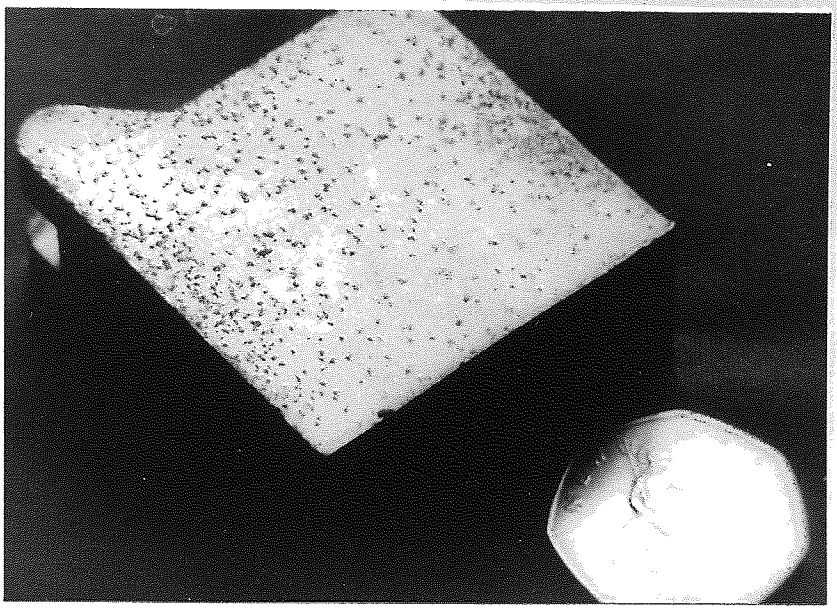

PLATE 4.1.
Martensitic stainless steel electrical component casting showing severe "spotted-dick" attack.

Larin *et al.* (op. cit.)[8] then investigated the effects of heating specimens of the steel in quartz ampoules with synthetic oxide mixtures consisting of a refractory oxide – such as SiO_2, $ZrSiO_4$, or α-Al_2O_3 – with a combination of metal oxides such as iron, manganese, and vanadium oxides. They report that metal heated in sealed ampoules with oxide powders exhibited no defect formation, although a greenish scale was observed. However, metal samples heated to 1100°C in open ampoules exhibited defects in almost every case. Samples heated to lower temperatures in open ampoules, or heated at very slow heating rates (20 to 30 °C min^{-1}), exhibited varying degrees of defects and scaling. Larin *et al.* state that the defects may be eliminated by adjusting the silicon-to-manganese ratio to higher silicon contents (cf. Taylor[7]); introducing reducing agents or neutral atmospheres; evacuating the moulds; increasing the cooling rate; or adopting highly refractory materials. In addition they mention the use of carbonaceous back-up or the use of α-alumina refractories to prevent the defect.

The only recent paper on this type of defect (Matsuno and Ohama, 1981)[9] was unfortunately not available to the author in an English translation. However, from the abstract and illustrations it appears that the authors believe that the defect is due to localised oxidation resulting either from oxygen trapped in pores in the shell, or oxygen entering the mould through micro-cracks in the shell.

The method they proposed for preventing the formation of defects involved placing 30 mm discs of metallic silicon, or Fe-Si, flush in the mould wall. The discs appeared to be sited in the riser so as to provide reducing conditions within the mould cavity, although this was difficult to ascertain from the limited amount of information given in English in the paper.

4.2. Experimental Procedures and Observations

Metallographic sections of an impeller blade exhibiting this defect were prepared, mounted in conducting bakelite and polished to 1 μm diamond finish. The material from which the casting was made was an 18% Cr, 2% Ni martensitic steel, specification BS 3146 : Part 2 : 1975, type ANC2 (see Table 4.1 b). A photomicrograph of the complete defect is shown in plate 4.2 with the central portion enlarged in plate 4.3. The structure of the defect appears to be an accretion of metal (the white phase) with multiphase oxides and porosity. There appears to be a dark grey oxide matrix with lighter grey oxides dispersed within it. However, the larger areas of light grey oxide – for example at the top right in plate 4.3 – appear to consist of two distinct phases.

The observation of the interpenetration of metal and oxides is important, since it suggests that the defect was formed whilst the metal was still molten, or that internal oxidation had taken place. There is, therefore, possible inconsistency between the mechanism by which defects are formed on castings, and attempts to model the formation of defects at lower temperatures by Larin *et al.* (op. cit.)[8].

Higher magnification images were obtained using a Cambridge S150 scanning electron microscope (Plate 4.4). In order to attempt to identify some of the phases present in the defects, X-ray maps were produced for the area shown in plate 4.4. These were produced for zirconium (Plate 4.5), silicon (Plate 4.6), chromium (Plate 4.7), iron (Plate 4.8), and nickel (Plate 4.9). The low count rates for these elements (whilst indicating that they are present as oxides) makes interpretation difficult, but it appears that at least some of the light areas are richer in zirconium and silicon than the darker matrix, whilst the matrix appears to be slightly richer in chromium and iron. Nickel is, in general, very low, but it appears slightly more concentrated in the lighter particles, *except* where these are enriched with zirconium.

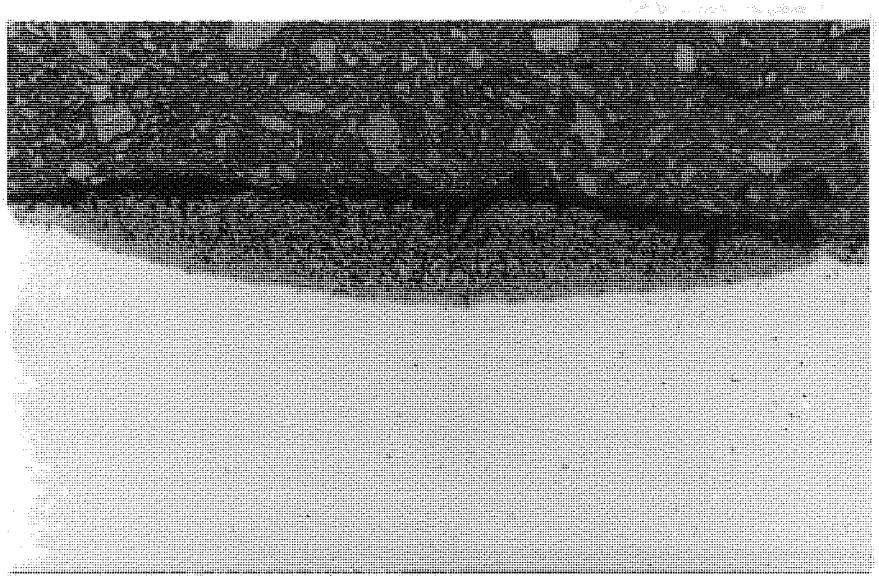

PLATE 4.2.
Section through "spotted-dick" defect on ANC2 rotor blade. The metal is at the bottom of the plate, and the dark material in the top half above the defect is bakalite.
(Unetched, X 84) (Specimen No. P46C)

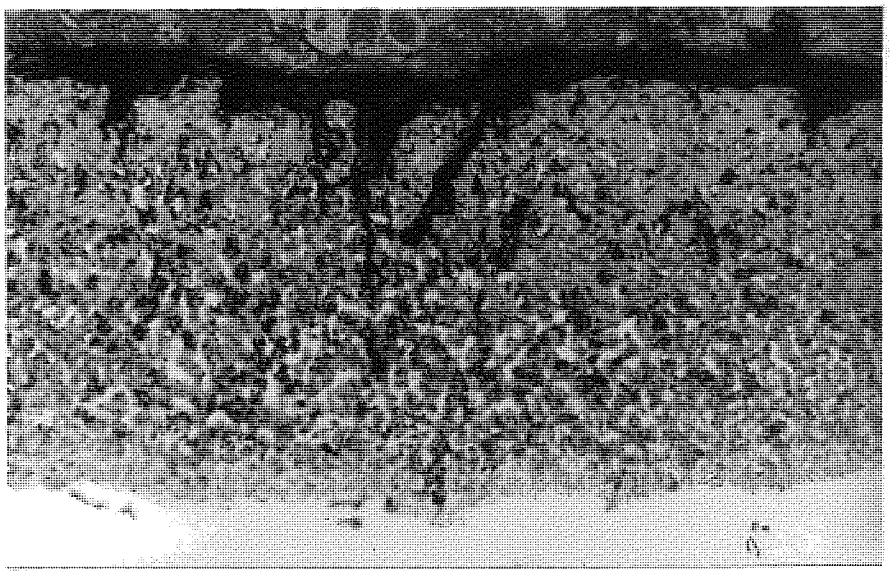

PLATE 4.3.
Enlarged section through "spotted-dick" defect on ANC2 rotor blade, as plate 4.2.
(Unetched, X 336) (Specimen No. P46C)

An attempt was made to perform X-ray diffraction on another part of the casting where the black spots had coalesced to form a continuous film (some 15 to 20 mm across), so that the phases present could be determined crystallographically. However the diffraction trace showed no significant peaks, suggesting that any phases present were predominantly amorphous. Any crystalline material which may have been present produced so weak a diffraction, that the peak was lost in the background noise. It may be that removal of some of the material for powder diffraction would give an indication of any crystalline phases present. Quantitative chemical analysis of the phases present using the scanning electron microscope may also be of help, although the absence of crystalline material suggests that the composition may be non-stoechiometric.

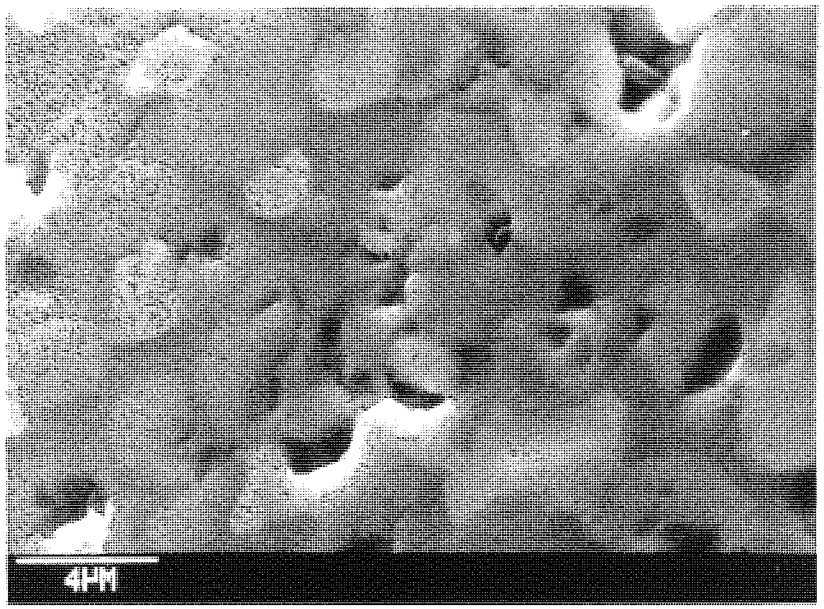

PLATE 4.4.
High magnification scanning-electron image of part of the defect shown in plate 4.2.
(Unetched, magnification as shown)
(Specimen No. P46C)

PLATE 4.5.
Zirconium X-ray map of the area shown in plate 4.4.
(Unetched, magnification as shown)
(Specimen No. P46C)

PLATE 4.6.
Silicon X-ray map of the area shown in plate 4.4.
(Unetched, magnification as shown)
(Specimen No. P46C)

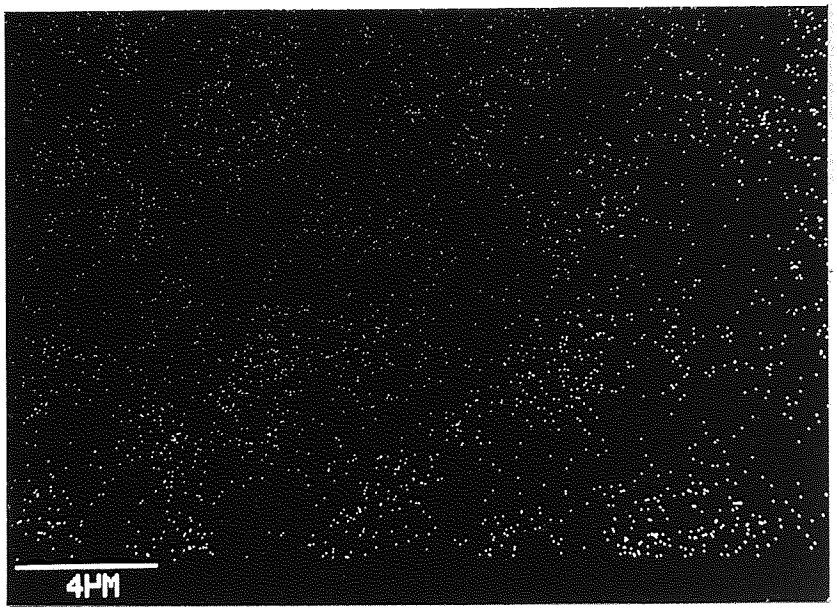

PLATE 4.7.
Chromium X-ray map of the area shown in plate 4.4.
(Unetched, magnification as shown)
(Specimen No. P46C)

PLATE 4.8.
Iron X-ray map of the area shown in plate 4.4.
(Unetched, magnification as shown)
(Specimen No. P46C)

PLATE 4.9.
Nickel X-ray map of the area shown in plate 4.4.
(Unetched, magnification as shown)
(Specimen No. P46C)

4.3. Experimental Investigation

In order to test the assumption made by Larin *et al.* (op.cit.)[8], that scaling (produced at temperatures below the solidus of the material), is identical in both structure and causal mechanism, with the "black spot" defect found on castings, it was decided to repeat some of their tests. It was decided to concentrate on the worst case, that of heating the metal – in contact with refractory oxides – in air. In order to test the effect of the manganese-to-silicon ratio on defect formation, test bars were cast in ANC2 (qv.); one batch with high manganese and the other with high silicon. The chemical compositions were determined from analysis coupons included on each mould, (Table 4.2).

The test bars were machined to remove approximately 1 mm from the surface and were then cut into 10 mm lengths using spark erosion to minimise mechanical work and heating. This gave small test buttons approximately 10 mm in diameter by 10 mm long. One face of each button was ground to 600 grit using silicon carbide paper to give a standard surface finish.

Samples of each material – high-silicon and high-manganese – were buried in refractory powder so that the ground face was uppermost and roughly 2 mm beneath the top surface. The powders used were –200 mesh zircon flour and –200 mesh fused silica – of the same grade used in the casting process – and they were contained in platinum crucibles to exclude any possible effect due to the silica ampoules used by Larin *et al.*

The crucibles were then placed in a laboratory muffle furnace at 1100°C for 90 minutes. At the end of this period the crucibles were removed from the furnace and allowed to cool to room temperature before examination

4.4. Observations and Results

The first important observation was made in the as cast condition, before the test bars were machined. It was evident that both sets of test bars were equally covered, on approximately one quarter of their surface area, by the "black-spot" defect. This demonstrates that the manganese-to-silicon ratio has had no effect on the severity of the defect as formed during casting.

TABLE 4.2 Analyses of ANC2 test bars

Element	High Silicon (code 'S') %	High Manganese (code 'M') %
Carbon	0.18	0.19
Silicon	**1.11**	**0.66**
Manganese	**0.55**	**1.01**
Sulpher	0.010	0.011
Phosphorous	0.032	0.034
Nickel	2.39	2.35
Chromium	16.0	16.1
Molybdenum	0.11	0.12
Copper	0.08	0.09
Aluminium	<0.05	<0.05
Cobalt	0.07	0.07
Nitrogen	387.ppm	387.ppm

The results of heating the test buttons in refractory oxide powders are shown in plates 4.10 to 4.13. It is evident from these photographs that the worst affected specimen was the high-silicon steel in zircon ($ZrSiO_4$) whilst the high-manganese

steel in fused silica showed hardly any attack at all. The high-manganese steel in zircon and the high-silicon steel in fused silica were also affected, although in the latter case the spalling of the oxide layers makes it difficult to determine the severity of the attack. This last sample also shows evidence of preferential attack on the dendritic – as-cast – structure, which implies that coring may have an effect on the severity of the reaction – at least in the model proposed by Larin.

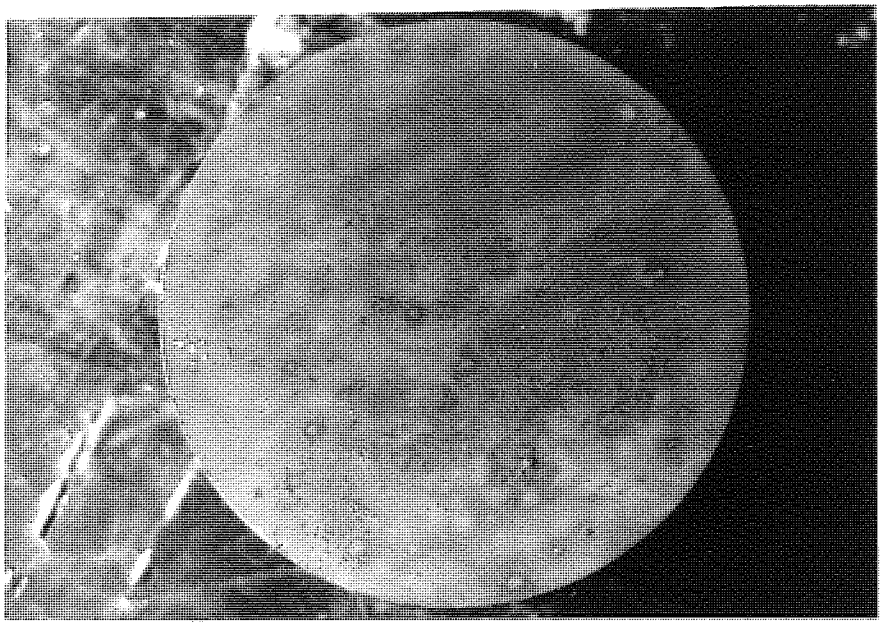

PLATE 4.10:
The results of heating a high manganese steel sample in fused silica. 90 minutes at 1100°C.
(X 8 approx.)

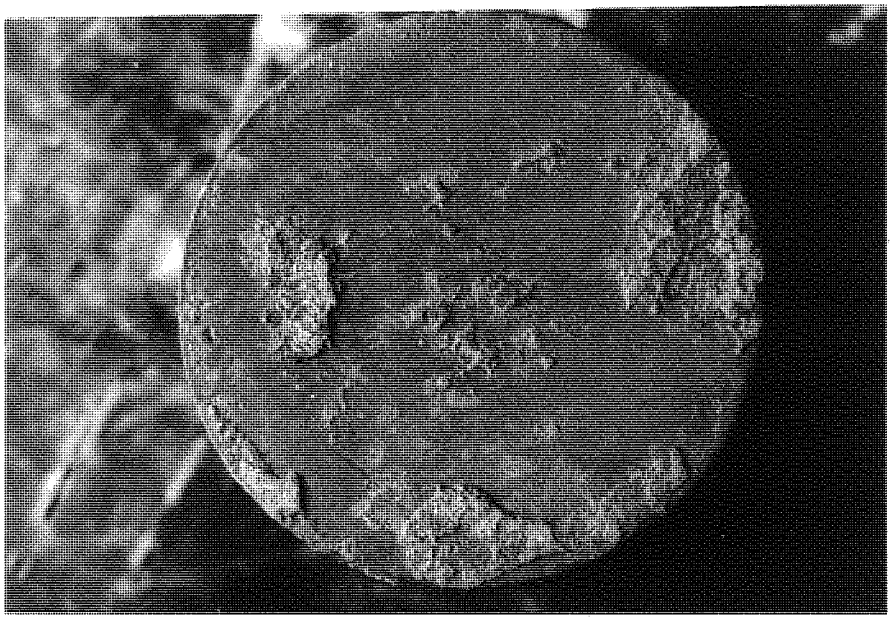

PLATE 4.11:
The results of heating a high manganese steel sample in zircon flour. 90 minutes at 1100°C.
(X 8 approx.)

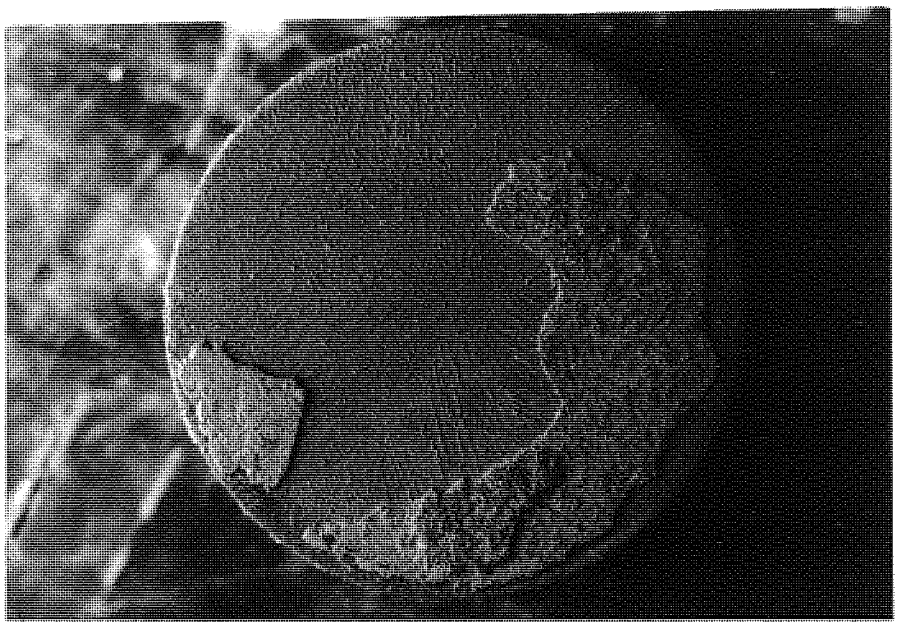

PLATE 4.12:
The results of heating a high silicon steel sample in fused silica.
90 minutes at 1100°C.
(X 8 approx.)

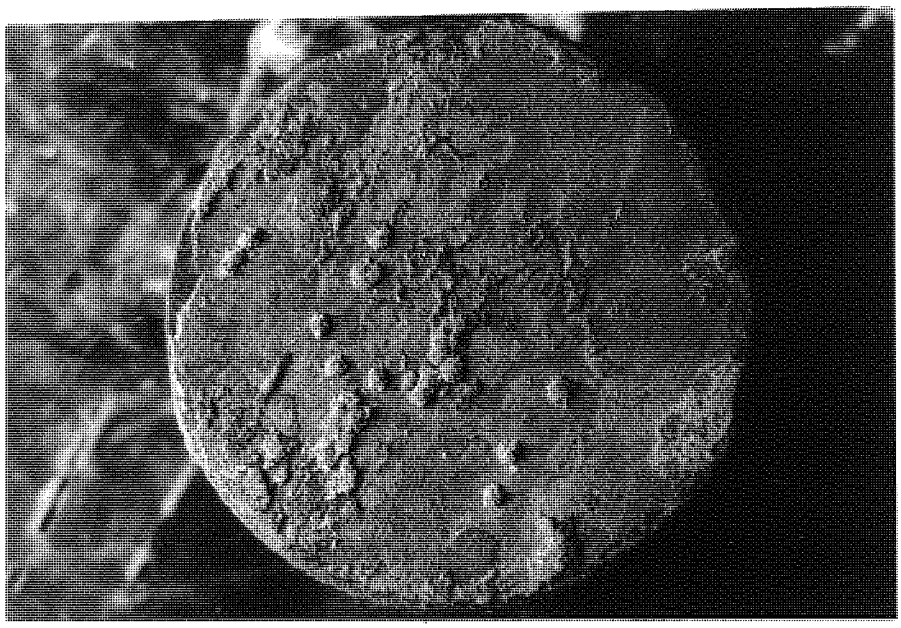

PLATE 4.13:
The results of heating a high silicon steel sample in zircon flour.
90 minutes at 1100°C.
(X 8 approx.)

The difference in attack between the samples which were affected is probably less significant than the differences between the high-manganese steel in silica and the high-manganese steel in zircon, and the differences between the high-manganese steel and high-silicon steel in silica.

In summary, as far as reactions with martensitic steel at temperatures below the solidus are concerned, zircon refractory is more reactive than silica and the effect is exacerbated by high levels of silicon in the steel.

4.5. Discussion

P.W.Wright[10] has studied the reactions of zircon refractories with molten steel. The main mechanism reported by Wright is the reduction of silica by manganese and carbon in the steel according to the reactions:

$$2[Mn] + SiO_2 = 2(MnO) + [Si] \ \dagger, \text{ and}$$

$$2[C] + SiO_2 = 2CO + [Si] .$$

The manganese oxide then promotes the formation of glassy phases by the subsequent reaction:

$$(MnO) + SiO_2 = (MnO{\cdot}SiO_2).$$

In addition, Wright proposes the following reaction for the decomposition of zircon refractories:

$$3ZrO_2{\cdot}SiO_2 + 2[Mn] = 2(MnO{\cdot}SiO_2) + 3ZrO_2 + [Si].$$

It should be noted that the work by Wright was carried out using low alloy steels (typically 0.4% C, 1% to 1.5% Mn, and 0.3% Si). However, the following factors were reported as being important in exacerbating the reaction with zircon refractories:

i) High manganese in the steel,

ii) Low silicon in the steel, and

iii) High carbon in the steel.

† where [ ] indicates solution in metal and ( ) indicates solution in oxide phases.

In addition the presence of aluminium in the steel is reported as lowering the zircon dissociation temperature to 1550°C.

Wright also reports work by Shultz and Muan[11], who found that liquid oxide forms at 1245°C in the system $MnO - ZrO_2 - SiO_2$. In addition to observing that the silicon-to-manganese ratio has no effect on the formation of "black-spot", except in the tests performed by Larin *et al.* (op.cit.)[8] – which are felt by this author to be a possibly inadequate model – further observations on castings have shown that a material similar to ANC2 (qv.) but with an increased carbon content (see Table 4.3) is almost invariably free from defects. It must be pointed out that, whilst ANC1 has a lower nickel content than ANC2, the same steel with a normal carbon content (ANC1, approx. 0.15% C) is prone to these defects.

TABLE 4.3. Typical analysis of ANC1 .8C high carbon martensitic stainless steel

	%		%
Carbon	0.74	Molybdenum	0.04
Silicon	0.53	Vanadium	0.04
Manganese	0.49	Copper	0.033
Sulphur	0.004	Tin	0.005
Phosphorous	0.020	Aluminium	0.04
Nickel	0.31	Cobalt	0.02
Chromium	12.84	Titanium	0.017

Muzyka *et al.* [12] have studied reactions between iron-chromium alloys and silica refractories in some considerable depth. They report that a very low-carbon, low-manganese, low-chromium steel, (<0.005% C, <0.003% Mn, <0.01% Cr), reacted strongly with a fused silica test tube within which it was heated, and that

increasing the chromium content of the steel inhibited the reaction in proportion to the amount of chromium added. However, even when sufficient chromium had been added to almost eliminate the reaction (8.8% Cr), the addition of quite small amounts of manganese promoted rapid reaction (Muzyka *et al.*, 1968)[13]. The mechanism suggested by Muzyka *et al.* [12],[13] , in both of these papers, involves the solution of silica by iron oxide. This may explain the previously mentioned effect of reducing atmospheres in ameliorating the incidence of "black-spot" defects, since the formation of iron oxide will be suppressed. The presence of chromium in the iron is believed by Muzyka *et al.*[12] to reduce the effect of reaction due to the precipitation of solid, chromium-rich $(Fe,Cr)_2O_3$-sesquioxide which rapidly increases the viscosity of the oxide melt.

The mechanism by which manganese promotes a reaction with a steel which would otherwise be protected by chromium, is not developed by Muzyka *et al.* ; neither do they make it clear whether the oxygen required to oxidise the melt is provided by diffusion through the silica, or through the surface of the melt.

There is an obvious anomaly between the work of Muzyka *et al.* and the formation of defects on high chromium martensitic stainless castings, since Muzyka reports that reactions occur most rapidly in the lowest chromium steels. However, the prevention of reactions by the use of reducing atmospheres is one area of agreement.

No work has been reported in the literature on the reactions of high chromium steels with zircon refractories, nor has there been any attempt – leaving aside the paper by Matsuno and Ohama[9] – to develop a mechanistic theory for the formation of "black-spot" defects. Since no totally reliable method of preventing this defect has been found, it may well be that a more detailed investigation will lead to a satisfactory solution.

5. "LINEAR" SURFACE IMPERFECTIONS IN LOW ALLOY STEELS

Low alloy steel castings, usually containing between 1.5% and 3.0% chromium, are prone to a "linear" surface defect, which is observed when castings are inspected using magnetic-fluorescent dye penetrant. The defect commonly appears on inside or reentrant angles – even those of quite large radius – but it is also often observed on flat surfaces adjacent to these angles. One of the steels on which this defect is common is a 3% Cr - Mo alloy, which for the purpose of "in-house" scrap analysis and reclamation is known as "Group 9", and the defect is thus known colloquially as the "Group 9 defect".

Most of the steels which exhibit this defect are supplied to customers in the form of fully heat treated castings – often for ordnance or aerospace applications – and it is fully heat treated castings which are routinely inspected for defects. No published literature has been found by the author relating to the problem. However, a report on defects found in a 3% Cr-Mo nozzle assembly was commissioned by the company in 1983.

The consultants concerned found defects consisting of narrow fissures lying at right angles to the metal surface. They were bordered by bands of material showing oxide penetration and occurred in characteristic positions, such as the radii between the four nozzles and the base plate on which they are mounted. They further reported that energy dispersive X-ray analysis showed no moulding material trapped in the defect, and only matrix material in the oxidised band.

The consultants concluded that the degree of oxidation along the "crack-like" defects implies formation at high temperature, which could only occur in one of two ways: either by hot-tearing or cold-shutting. The preferred location of these defects suggested – in their opinion – a mechanism of hot-tearing caused by excessive mould restraint.

5.1. Initial Examination and Observations

Metallographic sections were prepared from defective components cast in several low alloy steels. Photomicrographs of a representative defect area from a casting (Fig 5.1) in steel GS15 Cr Ni 6 – a German specification casting steel of nominal composition as given in table 5.1.– are shown in plates 5.2, 5.3, and 5.4.

TABLE 5.1. Chemical composition of GS15 Cr Ni 6 specification steel.

Carbon	0.12 – 0.17 %	Silicon	0.30 – 0.50 %
Manganese	0.40 – 0.60 %	Phosphorous	< 0.035 %
Sulphur	< 0.035 %	Chromium	1.4 – 1.7 %
Nickel	1.4 – 1.7 %		

The morphology of the crack is indicative of hot tearing, with evidence of inclusions around the mouth of the defect. Energy dispersive X-ray analysis was performed on the large inclusion at the mouth of the defect; on a smaller, isolated inclusion; and on the bulk material away from the defect. The results of these analyses are given in table 5.2. The large inclusion is almost certainly a deoxidation product because of the high aluminium content. However, what is not clear is why the smaller inclusions are so rich in chromium. The levels of chromium and nickel in the bulk analysis are not representative of the nominal specification but are probably within the limits of error of semi-quantitative analysis.

Further investigations of inclusions associated with defects in other – similar – castings, gave broadly similar chemical analyses, containing iron, chromium, nickel, manganese, and silicon. In some cases chlorine was also found, in quantities of between two and ten percent. It was assumed that the chlorine originated in the barium-chloride salt baths used in heat-treatment.

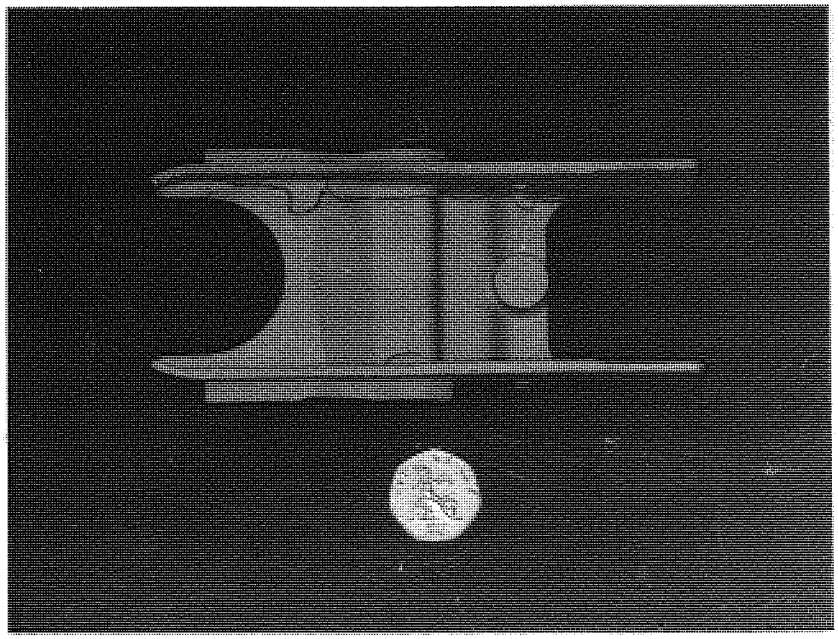

PLATE 5.1:
A typical GS 15 Cr Ni 6 casting showing areas prone to 'group 9' defects outlined.

PLATE 5.2:
A section through a defect found in a GS 15 Cr Ni 6 casting after heat treatment. The metal is the light coloured area with the metal surface at the extreme right hand edge.
(Un-etched, X 48) (Specimen No. P5C)

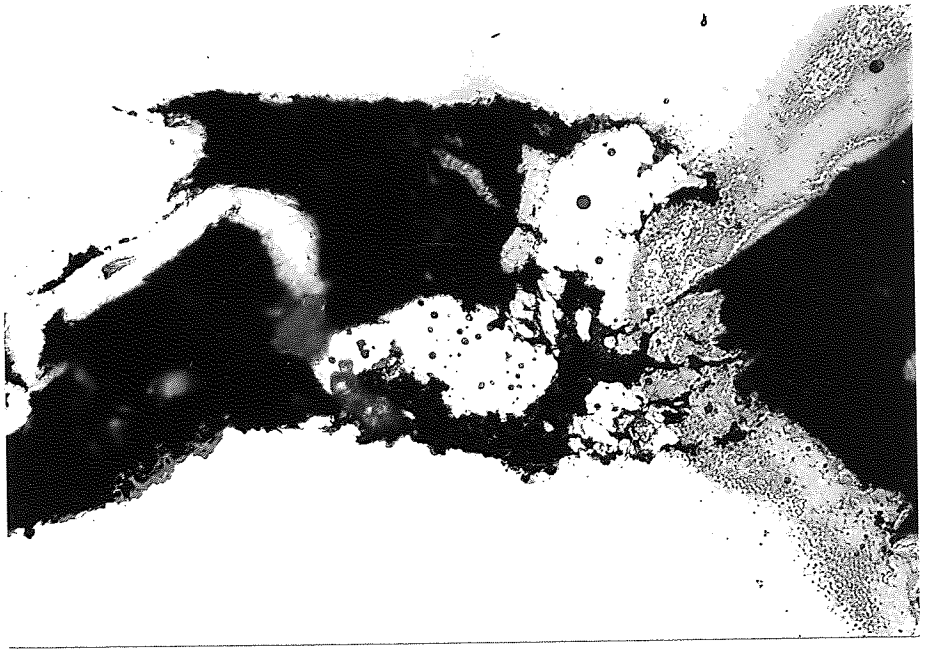

PLATE 5.3:
A section through a defect found in a GS 15 Cr Ni 6 casting after heat treatment. Note the large number of inclusions at the defect mouth, and the large inclusion at centre.
(Un-etched, X 188) (Specimen No. P5C)

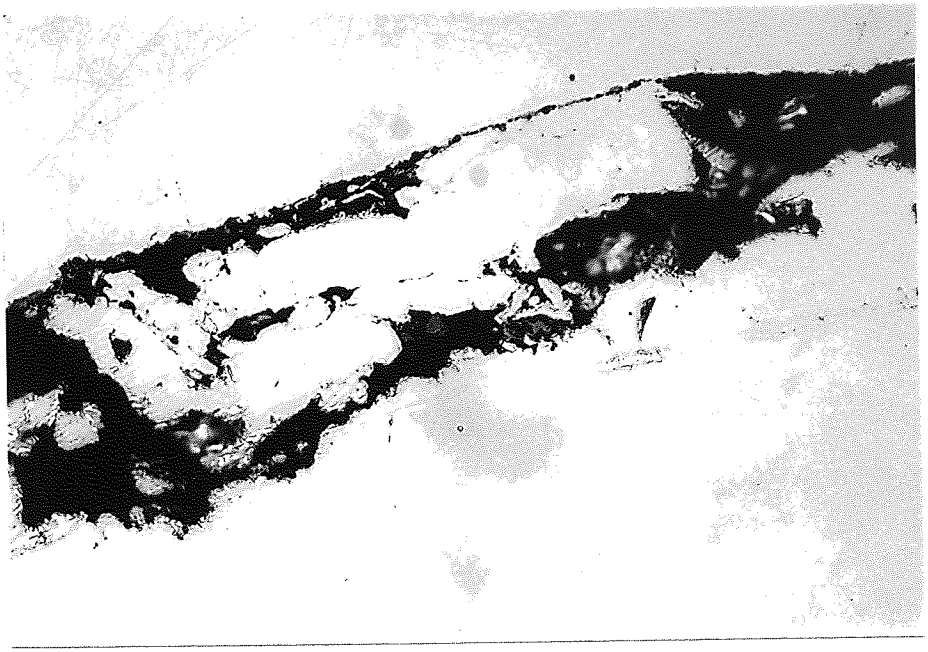

PLATE 5.4:
A section through a defect found in a GS 15 Cr Ni 6 casting after heat treatment showing a line of residual oxide at top.
(Un-etched, X 188) (Specimen No. P5C)

It seemed possible that the defects resulted from inclusions of oxides, and slag, which caused cracks to initiate and propagate on heat treatment, and it was decided to test this hypothesis by looking for defects or inclusions in castings prior to heat treatment. Magnetic-fluorescent particle inspection of castings prior to heat treatment revealed a considerable number to be defective, although the proportion was less than were usually defective after heat treatment. The defective castings were removed for further investigation and the satisfactory castings were passed forward to heat-treatment.

TABLE 5.2. EDAX analyses (semi-quantitative) on inclusions and bulk of a GS15 Cr Ni 6 casting

a) Large inclusion

Fe	Ti	Al	
0.92	0.43	98.65	(%)

b) Small isolated inclusion

Fe	Cr	Si	
64.31	16.50	19.19	(%)

c) Bulk material

Fe	Ni	Cr	Si	
96.01	0.86	2.06	1.08	(%)

After the good castings had been heat treated, they were inspected again, and an additional number were found to have developed defects, showing that the heat-treatment used exacerbates defects occurring in this material. In the worst case, the proportion of defective castings increased from 25% or 30% before heat-treatment, to a total of 50% or 60% afterwards.

Metallographic examination of defects found in castings prior to heat-treatment revealed a markedly different morphology to the cracks originally observed after heat treatment. Plates 5.5, 5.6, and 5.7 show a typical defect found in a GS15 Cr Ni 6 casting prior to heat-treatment. Another defect in a similar ~1% Cr-Mo steel – casting is shown in plates 5.8 and 5.9. There is a noticeable difference between those defects examined before heat-treatment and defects previously examined in the heat-treated condition.

All the defects examined in the as-cast condition contained grey material – probably oxide. In the etched specimen there appears to be some association between the defect and the nucleation of a second phase in the metal formed either within or at the boundaries of the prior-austenite grains. It is of course possible that this phase has nucleated onto the defect itself, although it appears more likely, on the evidence so far, that it was formed before the defect as some of the grains appear to be divided either side of the defect.

In addition to the main defects, which were detected by magnetic particle inspection, inclusions – of varying morphology – were found beneath the casting surface. These inclusions usually appeared in the form of round globules which were often in the form of "strings of beads" (i.e. moniliform inclusions), which were sometimes coalesced to form continuous inclusions (see plates 5.10 and 5.11). In an attempt to identify the oxide material observed in the main defect, the micro-sections were examined using a Cambridge S150 scanning electron microscope, with a view to performing semi-quantitative X-ray analysis. Analyses were performed on an unetched specimen exhibiting a defect similar to the etched specimen and from the same mould. The semi-quantitative results for the material in the linear defect, and for one of the small globular inclusions, are given in table 5.3. The analysis for the small inclusion is unlikely to be very accurate due to the penetration of the electron beam through the back of the included material, resulting in excitation of the surrounding material.

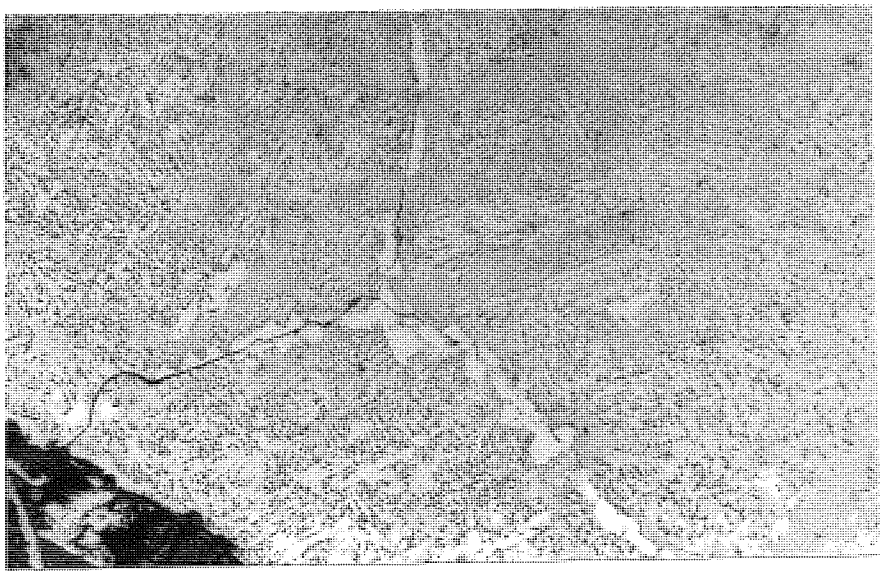

PLATE 5.5:
A section through a defect found in a GS 15 Cr Ni 6 casting prior to heat treatment. The metal surface is in the lower left-hand corner. (Etched in 1.0% Nital, X 84) (Specimen No. P40C)

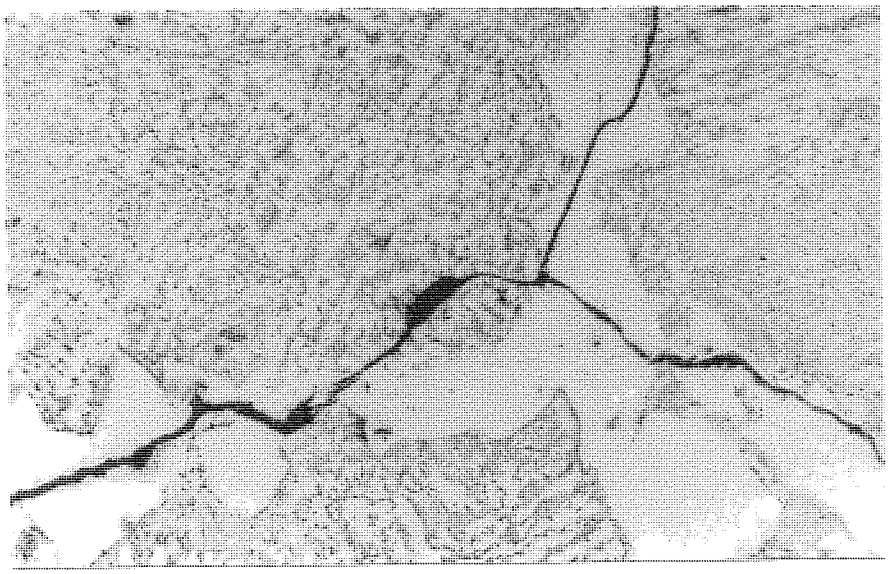

PLATE 5.6:
A section through a defect found in a GS 15 Cr Ni 6 casting prior to heat treatment (as plate 5.4.) This shows the included oxide phase running through the light phase on the prior austenite grain boundaries
(Etched in 1.0% Nital, X 420) (Specimen No. P40C)

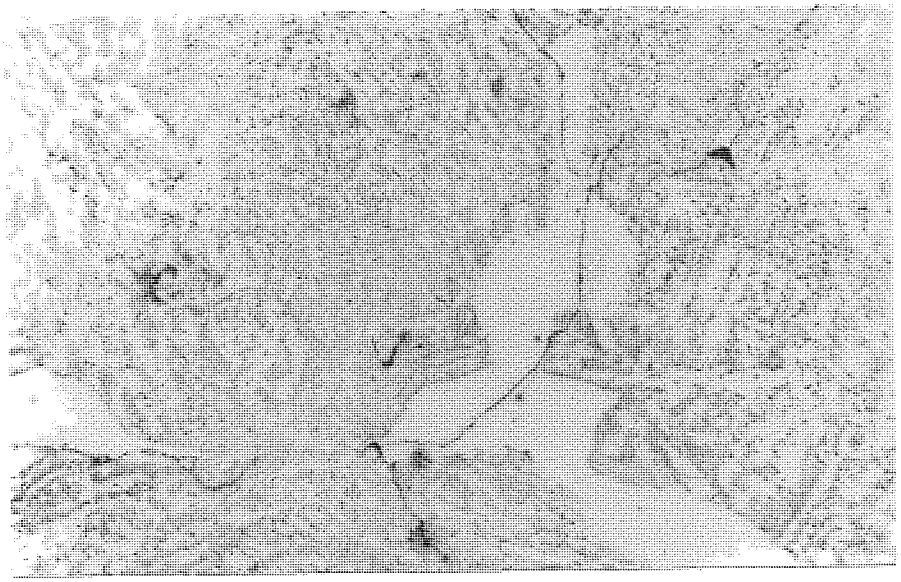

PLATE 5.7:
A section through a defect found in a GS 15 Cr Ni 6 casting prior to heat treatment as plate 5.4.
(Etched in 1.0% Nital, X 420) (Specimen No. P40C)

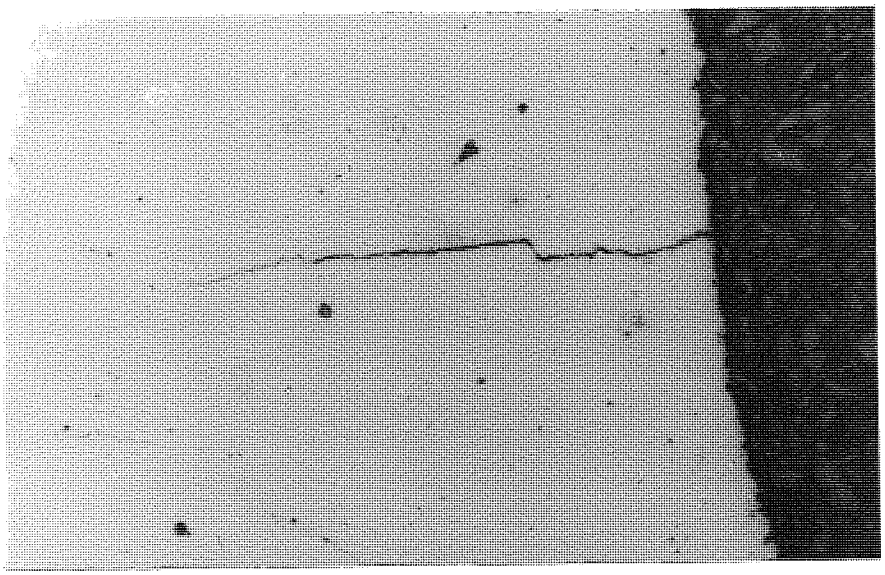

PLATE 5.8:
A section through a defect found in a 1% Cr-Mo steel casting (prior to heat treatment). The dark area adjacent to the metal surface (right) is the bakalite mount.
(Un-etched, X 84) (Specimen No. P44C)

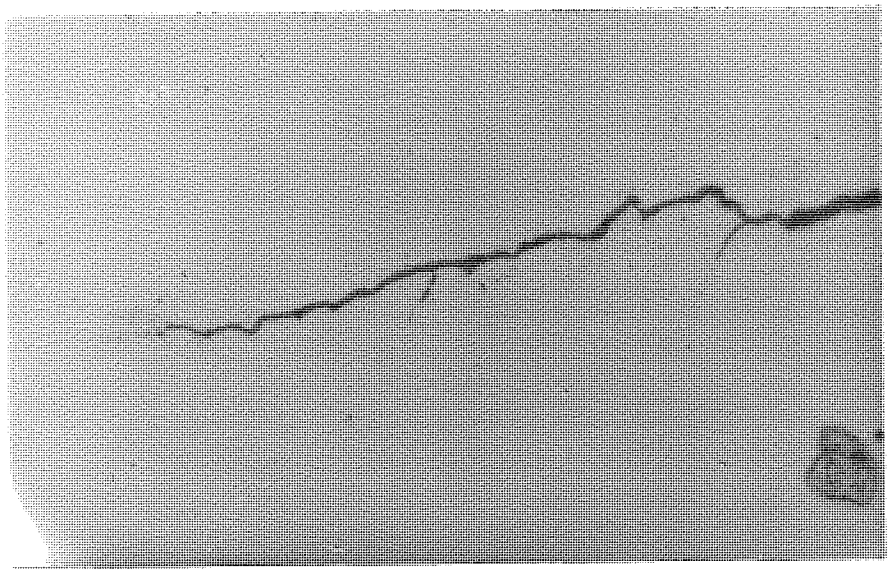

PLATE 5.9:
A section through a defect found in a 1 % Cr-Mo steel casting prior to heat treatment, as plate 5.7.
(Un-etched, X 420) (Specimen No. P44C)

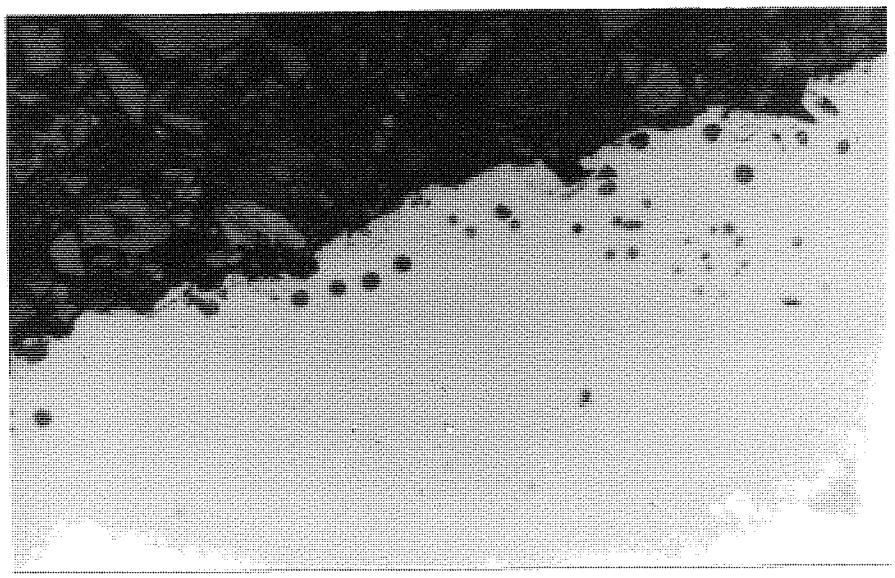

PLATE 5.10:
A section through a GS 15 Cr Ni 6 steel casting, prior to heat treatment, showing sub surface inclusions.
(Un-etched, X 420) (Specimen No. P41C)

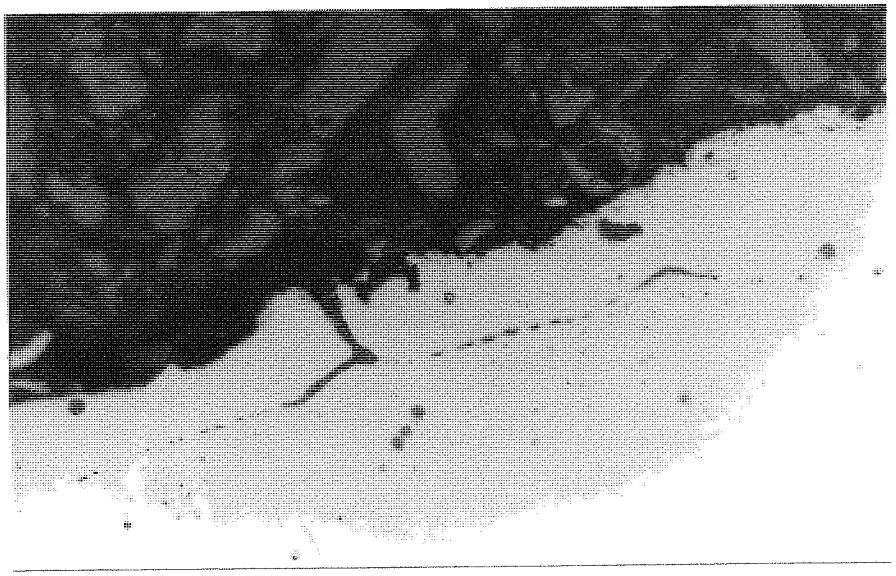

PLATE 5.11:
A section through a GS 15 Cr Ni 6 steel casting, prior to heat treatment, showing sub-surface inclusions, some of which have partially coalesced to form moniliform inclusions.
(Un-etched, X 420) (Specimen No. P41C)

X-ray maps were also produced of the defect shown in plates 5.5 to 5.7, for the elements silicon, zirconium, and aluminium (plates 5.12, 5.13, 5.14, and 5.15). These plates clearly show the presence of silicon and zirconium, and the absence of aluminium, in the defect.

TABLE 5.3.Semi-quantitative analysis on defects and included material in a GS15 Cr Ni 6 casting.

i) Material in "linear defect" *

Fe	Si	Zr	
4.6	37.77	57.63	(%)

ii) Material in globular defect near surface

Fe	Mn	Cr	Ti	Si	Al	
32.18	21.12	23.80	1.32	7.57	14.02	(%)

* Low count rate, suggesting oxides.

5.2. Summary of observations

The analyses and the X-ray maps reveal that the defects found in low alloy steels contain high levels of silicon and zirconium which almost certainly originate in the shell. It is noticeable however, that the 'moniliform' included material has not been found to contain shell material but appears to have a higher Cr content, in proportion, than was present as an alloying element in the steel.

It can be assumed that, during subsequent heat-treatment, the included shell material is lost, probably by dissolution into the barium-chloride salt bath.

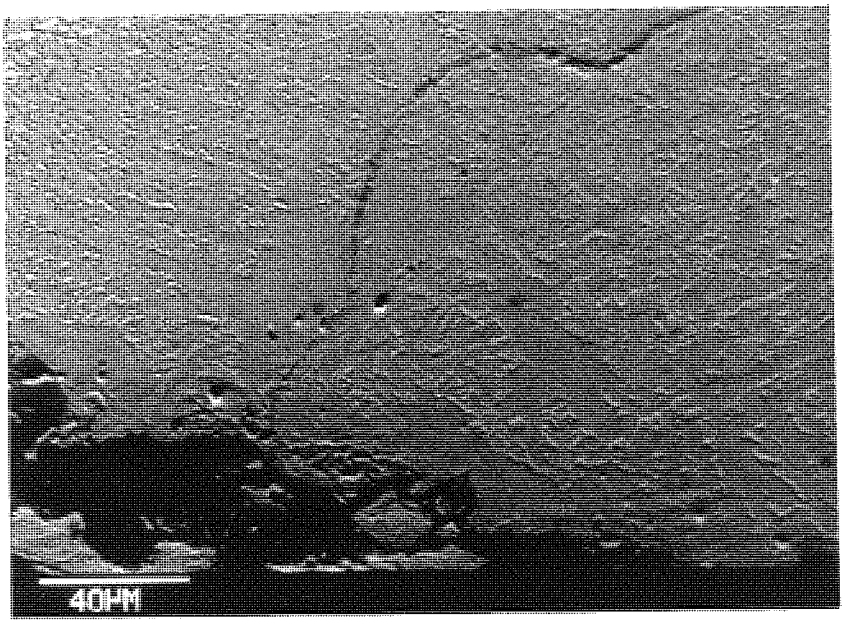

PLATE 5.12:
Scanning electron image of the defect shown in plates 5.5 to 5.7.
(Etched in 1% Nital, magnification as marked)
(Specimen No. P40C)

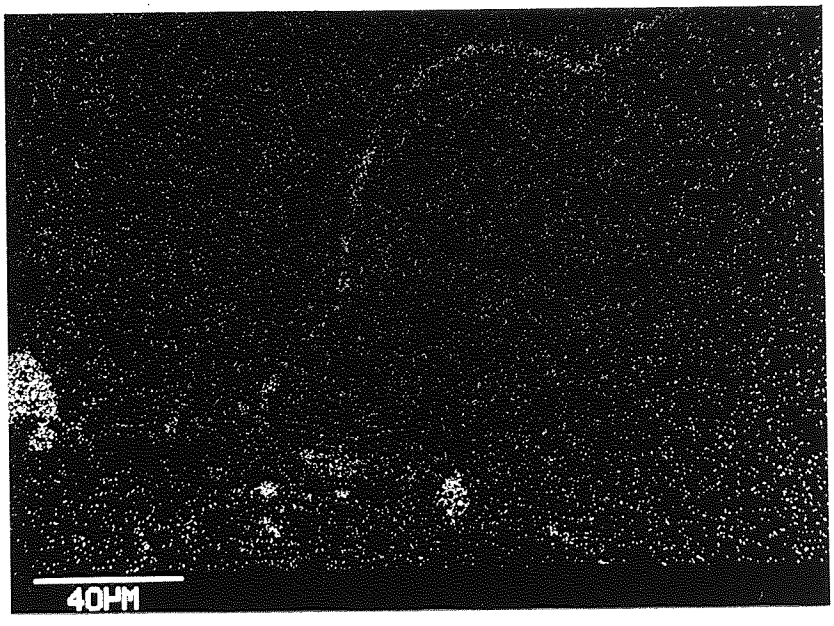

PLATE 5.13:
Silicon X-ray map of the area shown in plate 5.12.
Note the presence of silicon compounds in the defect
(Etched in 1% Nital, magnification as marked)
(Specimen No. P40C)

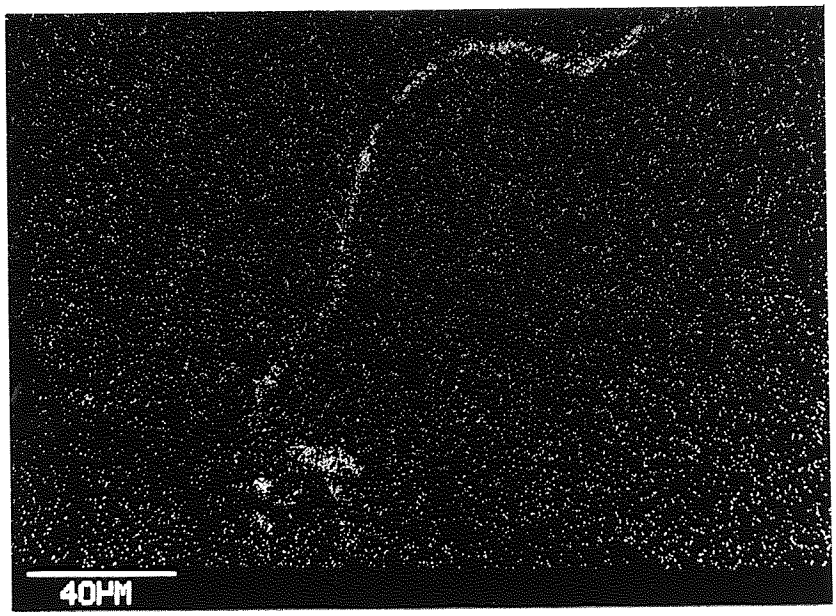

PLATE 5.14: Zirconium X-ray map of the area shown in plate 5.12. Note the presence of zirconium compounds in the defect. (Etched in 1% Nital, magnification as marked) (Specimen No. P40C)

PLATE 5.15: Aluminium X-ray map of the area shown in plate 5.12. Note the absence of aluminium compounds in the defect.
(Etched in 1% Nital, magnification as marked)
(Specimen No. P40C)

5.3. Alternative Hypotheses for the formation of "Group 9" Defects.

Given the deep penetration of the shell material into the defect, several main mechanisms may be proposed for the formation of "Group 9" defects, although each has many areas in common with the others. The mechanisms may, however, be divided into those based on the incorporation of slag from the surface and those where the defects are formed within the solid metal.

5.3.1. Mechanism A:– Entrapment

This mechanism is dependent on the entrapment of liquid oxides by the solidifying metal. From the observed shape of the globular and moniliform inclusions below the surface of these castings, a mechanism similar to that proposed by Myers and Flemings[14], for the formation of multi-membered silica inclusions in partially solidified steels, seems possible. Myers *et al.* (op. cit.)[14], investigating the behaviour of silica inclusions in a partially solidified iron base alloy, found that inclusions were pushed ahead of the dendrite arms as they grew by coarsening (see also Davies[15]). They also found that inclusions moved within the liquid of the liquid-solid zone, colliding with one another and partially coalescing to form extended, multi-membered inclusions (Plates 5.10 and 5.11).

This mechanism would adequately explain the preferred location of the observed defects in low alloy steel castings, since the reentrant angles and surfaces of castings are the last to solidify. Thus inclusions would tend to be "swept" towards the last part to solidify by the advancing solidification front.

The major objection to this hypothesis, however, is that the material in the defect appears to have a significantly different composition to that found in the sub-surface inclusions

5.3.2. Mechanism B:– Cracking

The second mechanism is dependent on the metal cracking or hot tearing. Obviously this must happen at temperatures high enough for oxides – containing zirconium and silicon – to still be liquid, since they must either be sucked into the crack as it opens or enter the crack by capillarity. There is, of course, a considerable body of literature on hot tearing. However, no literature was found relating to the mechanisms by which oxide slags subsequently become entrapped in the cracks. This hypothesis is also subject to the objection that all the defects, whether surface connected or not, would be expected to have similar chemical composition if they all arose from the same cause.

5.3.3 Mechanism C:- Shrinkage

For alloys having a wide freezing range compared with the temperature gradient across the metal mould interface, solidification can occur by extensive rather than by progressive freezing. This means that, rather than a layer of solid metal forming at the mould interface and then progressing inward preceded by a "mushy" zone, a mushy or semi-solid region forms at the interface and then grows inward without a fully solid region being formed until late in the solidification. When shrinkage then occurs within the casting liquid metal can be pulled from the surface in order to "feed" the centre of the casting. Liquid slags formed at the surface can then be sucked into the surface of the casting. This mechanism is analogous to "tin sweat" in bronze castings where hydrogen evolution on solidification pushes tin rich liquid out to the surface of a casting. Again, a major objection to this hypothesis is the different composition of the surface connected and sub-surface included material.

5.3.4 Mechanism D:- Oxidation

The fourth mechanism is one of oxidation, probably due to grain boundary diffusion of oxygen, which results in the formation of moniliform inclusions along grain boundaries. As these inclusions increase in size by a mechanism of nucleation and growth, they eventually coalesce and break through to the surface. At this stage the oxides dissolve the shell material, allowing zirconium and silicon to diffuse into the defects. After solidification the oxides may act as "wedges" causing cracks to propagate as the metal contracts.

5.4. Discussion of the Hypotheses

Zircon does not form any liquid below 1687 °C [11], whilst silica (residual from the ethyl-silicate binder) does not melt until 1723 °C [16]. Both of these temperatures are above the temperature at which the alloy steels are cast (1580°C). However, as was discussed in section 4, many refractory oxides react with the oxides of iron and the other alloying elements to form solutions having considerably lower melting points. A selection of these pseudo-binary eutectics is given in table 5.4.

Reactions with zircon refractories are more complex, but Jones, Kimura, and Muan (1967)[17], investigating the system $FeO–Fe_2O_3–ZrO_2–SiO_2$, report minimum solidus temperatures of 1140°C in excess oxygen and 1157°C to 1180°C when oxide mixtures are in equilibrium with metallic iron. However they report solidus temperatures of 1425°C to 1438°C in air (Po_2 = 0.2 atm. = 202.65 mbar) at equilibrium. Shultz and Muan [11], studying the system MnO–"FeO"–ZrO_2–SiO_2, report the formation of liquids in the system MnO– ZrO_2–SiO_2 at 1245°C, although the amount of liquid formed is small for a given amount of MnO. However, they also report that increases in temperature above the FeO–MnO–SiO_2–ZrO_2 quaternary liquidus invariant point (1173°C) cause rapid increases in the liquid

volume for "FeO" rich mixtures, as compared with MnO rich mixtures which have higher liquid contents at high temperatures (≈ 1670°C). To assess the time available for reactions to occur it is necessary to consider the cooling rates of the casting surface.

R. McCallum, of the National Engineering Laboratory, has performed considerable work on the assessment of ceramic shell systems under casting thermal conditions [18]. Cooling curves were obtained by placing thermocouples between the coats of a ceramic shell . The curves obtained are for simple ingot type moulds with a seven coat shell system, and do not represent the complexities of heat transfer in a normal casting. However, even for a mould of such simple geometry, the interface between the metal and the ceramic shell remains above the minimum equilibrium oxide liquation temperatures for some nine to ten minutes after casting.

For castings of more complex geometry, some areas are likely to have retarded cooling rates allowing even longer for oxidation of the metal and dissolution of the refractory to occur. There is also the possibility that super-cooling may depress the zircon / metal-oxide eutectic temperature and hence increase the reaction time still further.

In general the only practical ways to determine the precise mechanism are either; to attempt to model the defect formation mechanism using techniques such as casting simulation, or; to attempt to modify factors which are likely to be critical to only one of the hypotheses, and assess the effect of the modification using statistical techniques.

The first of these methods was felt likely to involve considerable time to build apparatus which, whilst realistic for a purely academic research programme, would not be achievable within the constraints of a project having such a large commitment to industrial cooperation.

TABLE 5.4.Some pseudo-binary eutectics between steel alloying element oxides and silica or alumina

---

SILICA REFRACTORIES

SiO_2 with Cr_2O_3

Eutectic formed between Christabolite (tetragonol SiO_2) and chromic-oxide at around 2.4 % by weight Cr_2O_3. Minimum equilibrium melting temperature of 1720°C.

SiO_2 with "FeO"

i) Eutectic formed between Tridymite (orthorhombic SiO_2) and Fayalite (Fe_2SiO_4) at 62 % by weight "FeO". Minimum equilibrium melting temperature of 1180°C.

ii) Eutectic formed between Fayalite (Fe_2SiO_4) and Wüstite ("FeO") at 78 % by weight "FeO". Minimum equilibrium melting temperature of 1180°C.

SiO_2 with MnO

Eutectic formed between Rhodonite ($MnSiO_3$) and Tephroite (Mn_2SiO_4) at 38 % by weight SiO_2. Minimum equilibrium melting temperature of 1251°C.

(*cont.*)

TABLE 5.4. (*cont.*)

ALUMINA REFRACTORIES

Al_2O_3 with Cr_2O_3

Continuous solid solution between alumina (Al_2O_3) and chromic oxide (Cr_2O_3). Minimum melting temperature is that of alumina (2045°C). Cr_2O_3 melts at 2275°C.

Al_2O_3 with "FeO"

Eutectic between "FeO"-rich solid solution and Hercynite ($FeO{\cdot}Al_2O_3$) at around 94.9 % by weight "FeO". Minimum equilibrium melting temperature of 1330°C.

Al_2O_3 with MnO

Eutectic between MnO and Galaxite ($MnO{\cdot}Al_2O_3$) at 24 % by weight Al_2O_3. Minimum equilibrium melting temperature 1520°C.

It was noted that the mechanisms were all differently dependent on thermal effects – due to cooling rates etc. – and on chemical effects involving both the oxidation of the metal and reactions to form a low melting point slag. In particular, the mechanism based on internal oxidation should be almost independent of physical factors such as temperature distribution and cooling rates except insofar as these alter the times available for reaction. Mechanisms based upon hot tearing, on the other hand, should be almost wholly a function of thermal factors, since hot tears should develop whether or not there is surface slag present to be sucked into them. After some consideration it was decided to attempt to devise a statistical experiment to separate the dependence of the actual mechanism between physical effects and chemical effects such as reaction thermodynamics and kinetics.

6. DESIGN OF EXPERIMENTS AND STATISTICAL ANALYSIS

The evidence from initial metallographic examination of 'group 9' defects suggests that the defect formation mechanism may be:

1. Incorporation of oxide slags into the solidifying metal;
2. Suction of slags, formed at the surface of the casting, into surface connected interdendritic spaces;
3. A combination of hot tearing, together with penetration of the grain boundaries by low melting point oxide slags; or
4. Internal grain boundary oxidation.

In order to test these hypotheses and reduce the incidence of these defects to a minimum it is necessary to isolate the critical part of the mechanism.

In essence the mechanisms are dependent upon either oxidation and slag formation (chemical effects) or upon cracking or tearing (physical effects). It is vital to be able to determine which of these effects is fundamental to the mechanism and, hence, which must be controlled to reduce the formation of defects.

The need to distinguish between chemical and physical effects in the mechanism led to an experimental design using different mould back-up materials to give different combinations of chill and reducing (or inert) atmospheres.

6.1 EXPERIMENTAL CONSTRAINTS

The ideal experiment would involve investigating each combination of chill and reducing atmosphere as follows:

1. Moulds with normal atmosphere and no chill – The normal (Control) method.
2. Moulds with normal atmosphere and chill.
3. Moulds with reducing atmosphere and no chill.
4. Moulds with reducing atmosphere and chill.

The following approximations to the ideal experimental regime were selected as being achieveable in practice.

i.) The standard method of casting without backup would remain as the control.

ii.) Moulds with chill only could be approximated in practice by the use of cold Molochite grit poured around the mould immediately after casting.

iii.) No practical way was found to produce a reducing atmosphere with the resources available. However, it was possible to cast moulds on a special casting unit which would allow flushing with (inert) argon immediately after casting. This would at least produce a non-oxidising atmosphere.

iv.) Moulds with reducing atmosphere and initial chill could be approximated by backing up the mould with cold charcoal grit immediately after casting.

On discussion it was decided that, because argon flushing would involve the use of a smaller mould, additional factors would be introduced into the experimental design. For example, the cooling rate of the mould is fundamentally related to the surface area to volume ratio of the mould, as well as the geometry of the mould surface. The cooling rate is probably fundamental to the formation of the defects by whatever mechanism.

It was therefore decided that a suitable experimental model would involve testing the effect of charcoal back-up or Molochite back-up against a control using no back-up. The statistical model chosen was a three stage nested design with replicates. This involved studying treatments (control, charcoal, or Molochite) nested under days, with individual moulds of four castings nested under treatments. This design allows the analysis of day to day variation and variation between crucibles.

6.2 THE STATISTICAL MODEL

In general, the data obtained from a statistical experiment may be represented as an equation relating the measured value (the 'response variable') to the sum of the overall mean, any treatment or other effects, and an error term. A mean derived from a single population would be defined by the equation:

$$y_i = \mu + \varepsilon_i \qquad \text{.....[6.1]}$$

for example, where μ is the mean, y_i is the ith measurement, and ε_i is the error associated with the i^{th} measurement. In this case there is no treatment effect, of course.

For models where effects are 'crossed', in factorial designs for example, there are also terms representing the interaction between the crossed factors.

The linear statistical model for the design in question is as follows:-

$$y_{ijkl} = \mu + \alpha_i + T_{j(i)} + \gamma_{k(ij)} + \varepsilon_{l(ijk)} \qquad \text{.....[6.2]}$$

where y_{ijkl} is the response variable, μ is the overall mean, α_i is effect of the i^{th} day about the overall mean, $T_{j(i)}$ is the effect of the j^{th} treatment about the i^{th} day, $\gamma_{k(ij)}$ is the effect of the k^{th} mould about the j^{th} treatment, and $\varepsilon_{l(ijk)}$ is the experimental error. By convention Greek letters are used for random components of the model and Latin letters for fixed effects. The hierarchical or nested model assumes that there is no interaction between the components of the model.

The repetition of the experiment over several days is important since it increases the sensitivity of the test, and at the same time reveals the effect of factors such as variation between crucibles.

The name *analysis of variance* is derived from a partitioning of total variability into its component parts. The total corrected sum of squares

$$SS_{Total} = \sum_{i=1,a} \sum_{j=1,b} \sum_{k=1,c} \sum_{l=1,n} (Y_{ijkl} - \bar{Y}_{....})^2 \qquad \text{.....[6.3]}$$

is used as a measure of overall variability in the data. (The "dot" subscript notation implies summation over the subscript it replaces, so Y.... is the grand total of all observations, for example.) Intuitively, this is reasonable since if we divide the total sum of squares by the appropriate degrees of freedom, we obtain the sample variance of the response variables.

The total sum of square (SS_{Total}) is partitioned symbolically as:-

$$SS_{Total} = SS_{Mean} + SS_{Days} + SS_{Treatments} + SS_{Moulds} + SS_{Errors} \quad \cdots\cdots[6.4]$$

For the various sources of variation, the degrees of freedom and calculation formulae for the sums of squares are given in table 6.1:

TABLE 6.1: Degrees of Freedom (DF) and calculation formulae for the Sums of Squares (SS) for the sources of variation (SV)

SV	DF	SS
Mean, μ	1	$(Y....)^2$ / abcn
Days, α	a - 1	$[\Sigma (Y_i...)^2 / bcn] - [(Y....)^2 / abcn]$
Treatments, T	a(b - 1)	$[\Sigma (Y_{ij}..)^2 / cn] - [\Sigma (Y_i...)^2 / bcn]$
Moulds, γ	ab(c - 1)	$[\Sigma (Y_{ijk}.)^2 / n] - [\Sigma (Y_{ij}..)^2 / cn]$
Castings (or error), ε	abc(n - 1)	$[\Sigma (Y_{ijkl})^2] - [\Sigma (Y_{ijk}.)^2 / n]$

Where i = (1...a) days, j = (1...b) treatments per day, k = (1...c) moulds per treatment and l = (1...n) castings (or replicates) per mould.

The degrees of freedom and the calculation formulae for the sums of squares are deduced using the method given by Montgomery [19].

The mean squares for each source of variation are calculated by dividing the sum of squares by the degrees of freedom for that source of variation. The expected mean squares are also derived using the method proposed by D.C.Montgomery .

Since the treatment is a fixed effect with all other effects random, we find that the expected mean squares, E(MS), are:-

For α_i (Random effect) $E(MS_\alpha) = \sigma_\varepsilon^2 + n\,\sigma_\gamma^2 + b\,c\,n\,\sigma_\alpha^2$ .....[6.5a]

For $T_{j(i)}$ (Fixed effect) $E(MS_T) = \sigma_\varepsilon^2 + n\,\sigma_\gamma^2 + c\,n\left[\sum\sum T_{j(i)}^2 / a\,(b-1)\right]$ .....[6.5b]

For $\gamma_{k(ij)}$ (Random effect) $E(MS_\gamma) = \sigma_\varepsilon^2 + n\,\sigma_\gamma^2$ .....[6.5c]

For $\varepsilon_{l(ijk)}$ (Random effect) $E(MS_\varepsilon) = \sigma_\varepsilon^2$ .....[6.5d]

The test hypotheses and the related test statistics for the F distribution are:-

$H_0: \sigma_\alpha^2 = 0$ $\therefore$ $F_0 = MS_\alpha / MS_\gamma$ Random effect .....[6.6a]

$H_0: T_{j(i)} = 0$ $\therefore$ $F_0 = MS_{T(\alpha)} / MS_\gamma$ Fixed effect .....[6.6b]

$H_0: \sigma_\gamma^2 = 0$ $\therefore$ $F_0 = MS_\gamma / MS_\varepsilon$ Random effect .....[6.6c]

where the F_0 test statistics are derived from the expected mean squares on the basis that, if the null hypothesis is true, we expect $F_0 = 1$. (If all the null hypotheses are true, then the statistical model simplifies to that given in equation [6.1].)

The results of an analysis of variance are usually presented in the form of an analysis of variance table. For the statistical model in question the analysis of variance (ANOVA) table, in symbolic form, is given in table 6.2.

TABLE 6.2: Symbolic analysis of variance table for the statistical model given in equation 6.2

SV	DF	SS	MS	F_0
μ	1	SS_μ	SS_μ	
α	a - 1	SS_α	$SS_\alpha / (a - 1)$	MS_α / MS_γ
T	a(b - 1)	SS_T	$SS_T / a(b - 1)$	MS_T / MS_γ
γ	ab(c - 1)	$SS\gamma$	$SS\gamma / ab(c - 1)$	$MS_\gamma / MS_\varepsilon$

6.3 EXPERIMENTAL METHOD

6.3.1. Statistical Conditions

For the purpose of the experiment the order in which the moulds were dipped and dewaxed was randomised with respect to the order in which the original wax moulds were assembled. The order in which the treatments were assigned to the daily batch of six moulds was also randomised.

In order to minimize the day to day and melt to melt variability the following working conditions were adhered to:-

1. The same foundry operators and techniques were used each day.
2. Whilst different crucibles had to be used each day, they were taken from the same suppliers batch.
3. Each crucible was given an identical pre-run 'wash-out' melt with mild steel to minimise variability within the day's run due to unrepresentative conditions from a new crucible. This mild steel was taken from the same suppliers cast number.
4. The preparation of each mould was kept as consistent as possible. Each mould was given the same length of pre-heat at the same temperature.
5. The method of melting was carefully monitored to reduce (and quantify) variations due to foundry practice.

In addition, other process parameters were monitored. Residuals can thus be studied not only to verify the statistical model used, but also to analyse the effect of any variation in uncontrolled parameters.

6.3.2. Mould Preparation

Enough wax patterns were produced in one run from the same batch of wax, to produce sufficient moulds for the entire experiment.

Moulds 'in wax' were prepared using the standard method for the component being studied. Four wax patterns were assembled, two on each side of a flat, vertical riser. Each wax assembly was weighed before being dipped. A total of thirty-five moulds was produced for the experiment. This allowed five spare moulds to be processed in the same batch to allow for breakage.

A ceramic shell was produced by a standard method, with the order of dipping randomised with respect to the order of wax assembly.

Moulds were de-waxed and fired in the order of dipping, in batches of six.

After the fired moulds had cooled they were weighed, the shell thickness was measured, and the moulds were inspected for damage. Two faulty moulds were rejected at this stage.

The first thirty remaining moulds (in the original order of assembly) were assigned in blocks of six to each of the five daily runs.

The order of the six moulds within the daily run was randomized, as was the allocation of the three treatments to the six moulds.

6.3.3. Casting

Moulds were preheated for a known time (nominally one hour) prior to casting, at a temperature of 1100°C.

A new crucible was used each day in order to guarantee near identical conditions for each experimental run. The new crucible was given a 'wash-out' melt of mild steel to condition the crucible before the experiment began.

The metal stock was melted and cast following a standard procedure:

1. Begin melting
2. Add deoxident when metal has fully melted.
3. Increase temperature to peak and hold during deslag.
4. Adjust temperature to pouring temperature and hold.
5. Place preheated mould and tin over crucible and clamp in place.
6. Turn off power and invert crucible to cast.
7. Remove cast mould in tin, add back-up if required and cover till cool.

The melting stages were carefully timed for each mould. The following information was collected during each melt.

---

a. Pre-heat time.

b. Time from start of melting to:-
   - i) deoxidant added
   - ii) maximum temperature reached
   - iii) deslag started
   - iv) casting temperature reached
   - v) mould cast
   - vi) mould covered

c. Peak temperature

d. Casting temperature

6.3.4. Preparation for inspection

After cooling, the moulds were despatched to a subcontractor for removal of the ceramic shell by water blast.

After removal of the ceramic shell, every casting was etched with a unique identifying code before removal from the riser. The purpose of this was twofold; firstly to ensure that castings were not mixed; and secondly, by using codes without overt significance, to reduce the likelihood of bias during examination of the castings.

The castings were then cut off the mould, retaining the test bars and runners, risers and the head for examination. The feed pads were ground flush and the castings sand-blasted to remove surface scale and oxide.

The castings were then examined using fluorescent magnetic dye penetrant. The area of the casting affected by 'group 9' defects was measured using vernier calipers to give a quantitative assessment of the severity of the defects on a particular casting.

At the same time, the analysis buttons from each mould were submitted for spectroscopic chemical analysis.

7. ANALYSIS OF RESULTS

After the collection of the data the first stage of the investigation is to perform an analysis of variance. Then diagnostic tests must be carried out to test the validity of the statistical model.

7.1 The analysis of variance

The analysis of variance (ANOVA) table for the data obtained is as follows:

TABLE 7.1 Analysis of variance table for Original Data

Source of Variation	DF	SS	MS	F_0
Days	4	42106.4	10526.61	9.3202×10^{-2}
Treatments	10	2794317.2	279431.72	2.4741*
Moulds	15	1694145.9	112943.06	5.7489†
Error	90	1768155.4	19646.17	

* Significant at 5.51 % † Significant at < 1.00 %

This analysis suggests that there is a statistically significant difference between moulds nested within treatments. A significance level is also given for the difference between treatments nested within days. However, the different magnitudes of the $(100 \cdot \alpha)\%$ significance-levels given are not to be taken as implying that either effect is "more significant" or "less significant" than the other. For any analysis, differences are either "significant" or "not significant" at a particular level of test [20]. No significant difference was found between the days and crucibles.

7.2 Model diagnostics

The next stage in the analysis is to perform diagnostic checks on the distribution of the response variables and residuals. This is important since the validity of the model used depends upon the independence of the response variables and the normality of the random errors.

The residuals are given by:

$$e_{ijkl} = Y_{ijkl} - \hat{Y}_{ijkl} \qquad \text{.....[7.1]}$$

where $\hat{Y}_{ijkl}$ is the expected value of Y_{ijkl}

However, as $\hat{Y}_{ijkl} = \hat{\mu} + \hat{\alpha}_i + \hat{\tau}_{j(i)} + \hat{\gamma}_{k(ij)}$;

and since $\hat{\mu} = \bar{Y}_{....}$, $\hat{\alpha} = (\bar{Y}_{i...} - \bar{Y}_{....})$, $\hat{\tau} = (\bar{Y}_{ij..} - \bar{Y}_{i...})$, and $\hat{\gamma} = (\bar{Y}_{ijk.} - \bar{Y}_{ij..})$;

then $\hat{Y}_{ijkl} = \bar{Y}_{....} + (\bar{Y}_{i...} - \bar{Y}_{....}) + (\bar{Y}_{ij..} - \bar{Y}_{i...}) + (\bar{Y}_{ijk.} - \bar{Y}_{ij..})$

$= \bar{Y}_{ijk.}$ .....[7.2]

Hence $e_{ijkl} = Y_{ijkl} - \bar{Y}_{ijk.}$ .....[7.3]

The residuals are thus the deviations, for each individual casting on a mould, from the average for the four castings on each mould.

The first diagnostic procedure is a plot of the residuals on normal probability paper to test the assumption that the errors are normally distributed.(Fig. 7.1). This plot is often known as an "empirical cumulative distribution" or ECD plot (Daniel)[21]. It is clear from this plot that the assumption of normality is not justified. The plot appears to show positive kurtosis (see R.G.Miller 1986)[22], in other words excessive weight in the tails of the distribution.

Further diagnostic tests involve plotting residuals against any variables of interest,

in particular against time and against the fitted values $\bar{Y}_{ijkl}$.

Residuals were plotted against dip sequence (1 - 35), casting sequence (1 - 30) and also against the sequence of casting within each day (1 - 6).

The plots of the residuals against dip sequence (Fig 7.2) and against cast sequence (Fig. 7.3) are unstructured and show nothing unusual. The plot of residuals against cast sequence within each day, however, does show some slight trend towards increased variance for the last three moulds cast each day.

Figure 7.1

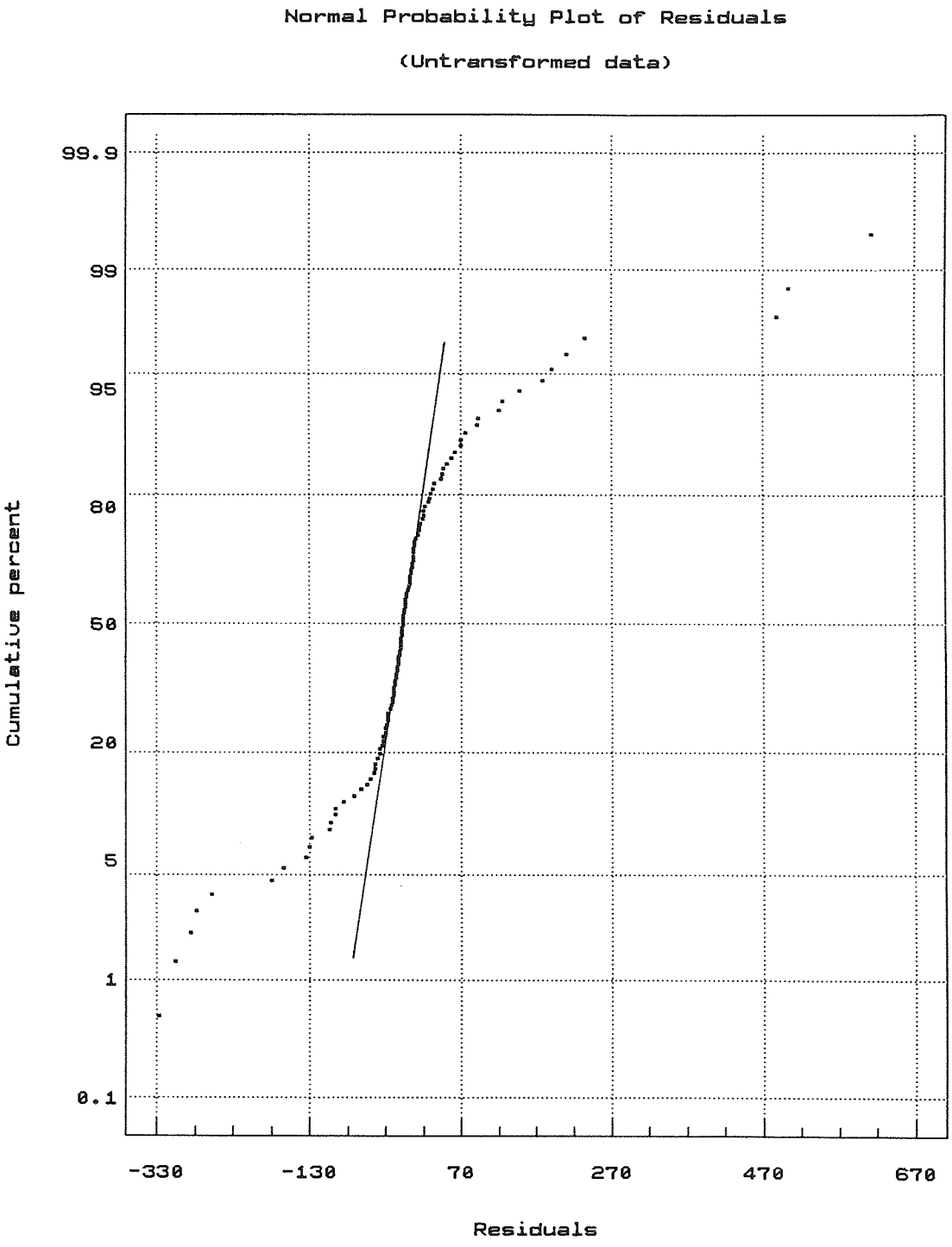
Normal Probability Plot of Residuals
(Untransformed data)
99.9
99
95
80
50
20
5
1
0.1
Cumulative percent
-330
-130
70
270
470
670
Residuals

Figure 7.2

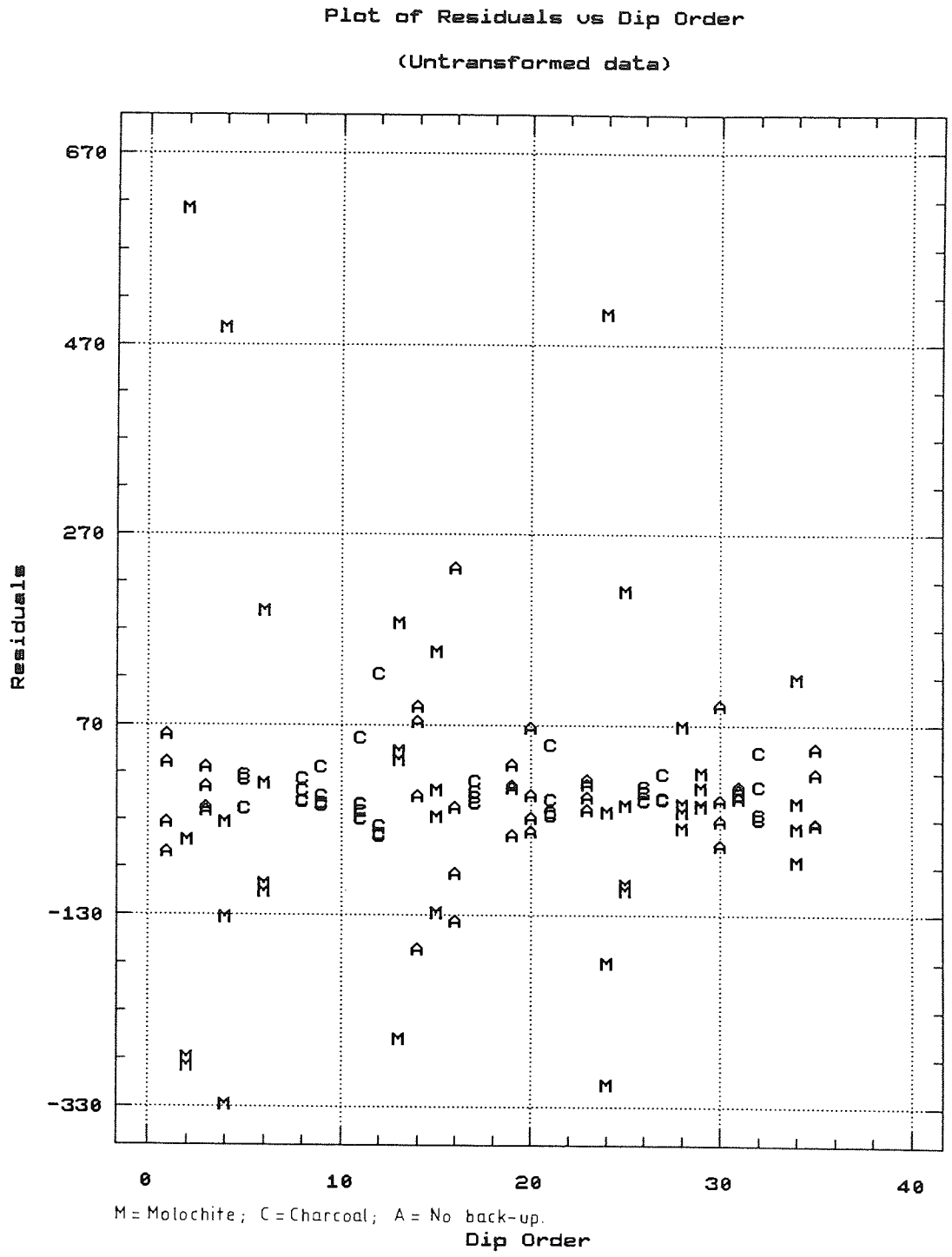
Plot of Residuals vs Dip Order
(Untransformed data)
Residuals
670
470
270
70
-130
-330
0
10
20
30
40
M = Molochite ; C = Charcoal ; A = No back-up.
Dip Order

FIGURE 7.3

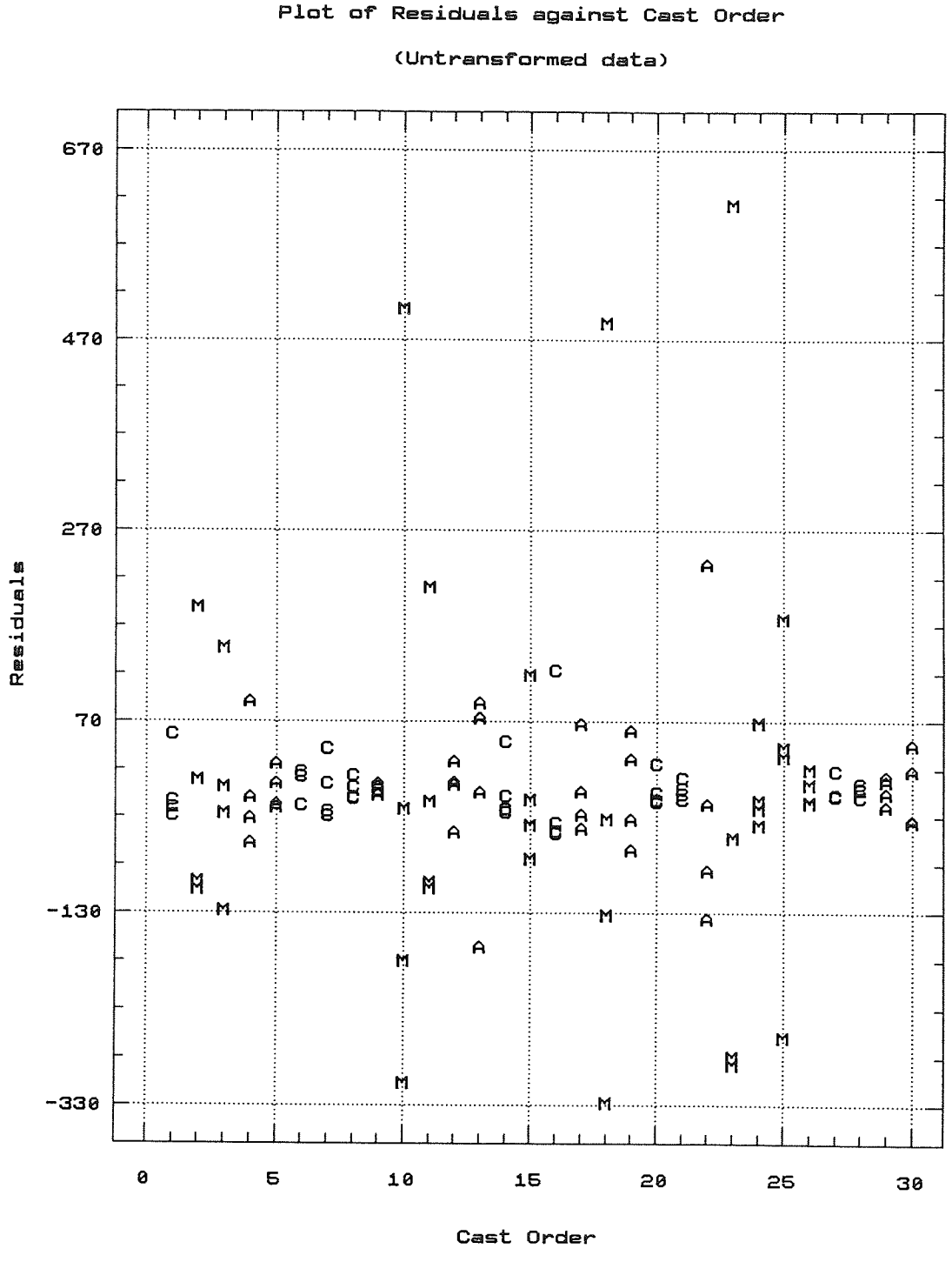
Plot of Residuals against Cast Order
(Untransformed data)
Residuals
670
470
270
70
-130
-330
0
5
10
15
20
25
30
Cast Order

FIGURE 7.4

Plot of Residuals against Cast order within the day.

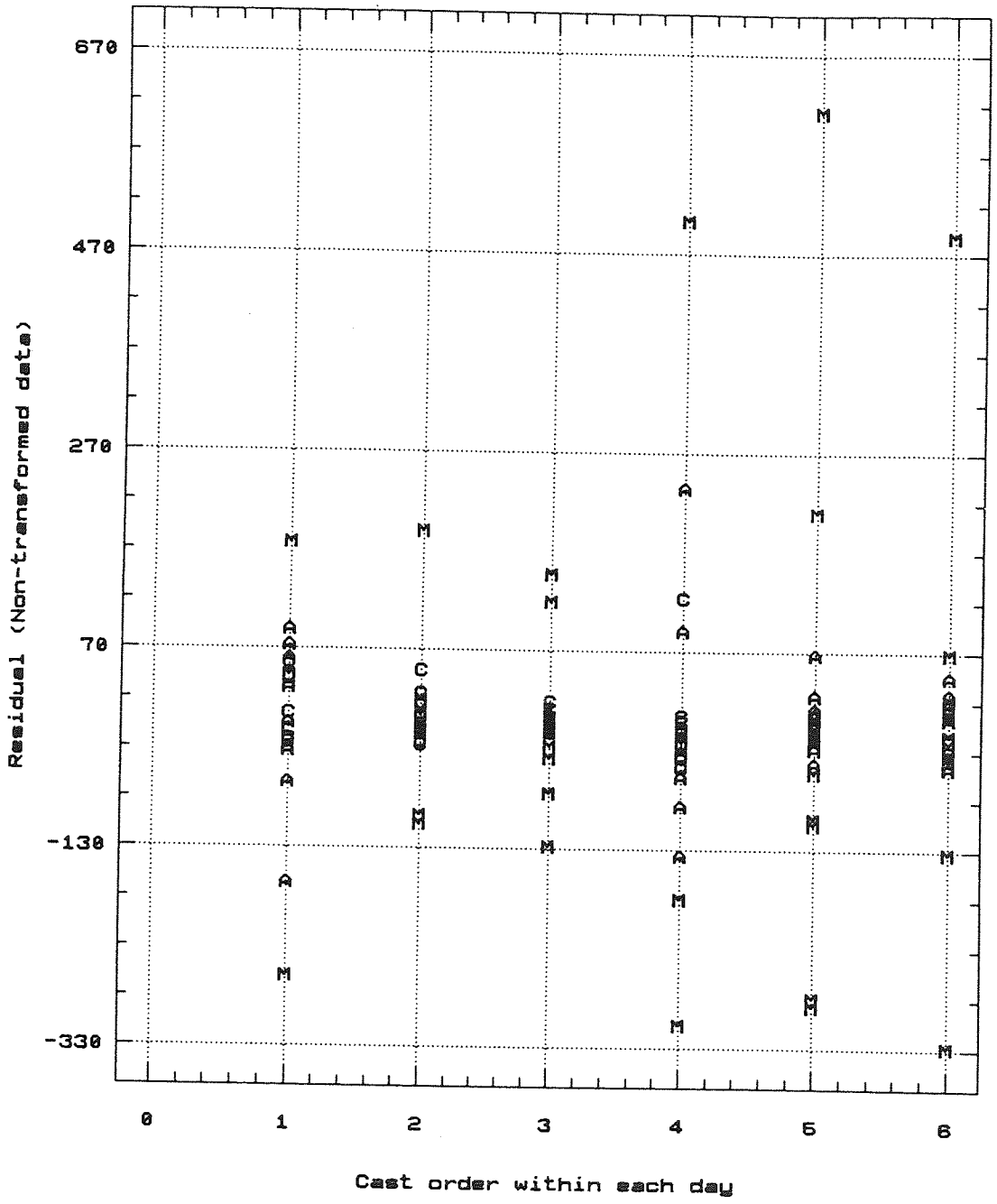

A = Air, M = Molochite, C = Charcoal.

The plot of the residuals against fitted values is given in figure 7.5. It is immediately apparent that the residuals are tightly grouped around zero for low fitted values, but open up in a "trumpet" shape as the fitted values get larger. This indicates that the variance is non-constant and is dependent on the size of the fitted values. This is a serious violation, since, for models where the effects are random or mixed, non-constant variance severely disturbs the F test. In addition, it appears that the variance for the Molochite treated moulds, in particular, is large compared with the other treatments. In other words the variance appears to be related to the treatment.

The usual approach to dealing with nonconstant variance is to apply a *variance stabilising transformation*, and then perform the analysis of variance on the transformed data; noting that the conclusions of the analysis of variance apply to the *transformed* data. The selection of an appropriate transformation is often empirical. A transformation is sought which will equalize the value of the variance regardless of the value of the mean. In this case both square root and logarithmic transformations were investigated, since they are the most common.

Prior to repeating the ANOVA on the transformed data, residual plots were produced.

7.2.1. Square root transformation i.e. $y^*_{ijkl} = \sqrt{\{y_{ijkl}\}}$

Plots of residuals against cast and dip sequence (Figs.7.6 and 7.7) for square root transformed data show no significant structure. The plot of residuals against fitted values is an improvement over the untransformed data (Fig 7.8) but there is still evidence of non constant variance. The ECD plot of the residuals (Fig 7.9) shows less deviation than the untransformed data but there is still considerable non-normality.

FIGURE 7.5

Plot of Residuals against Fitted values

(Untransformed data)

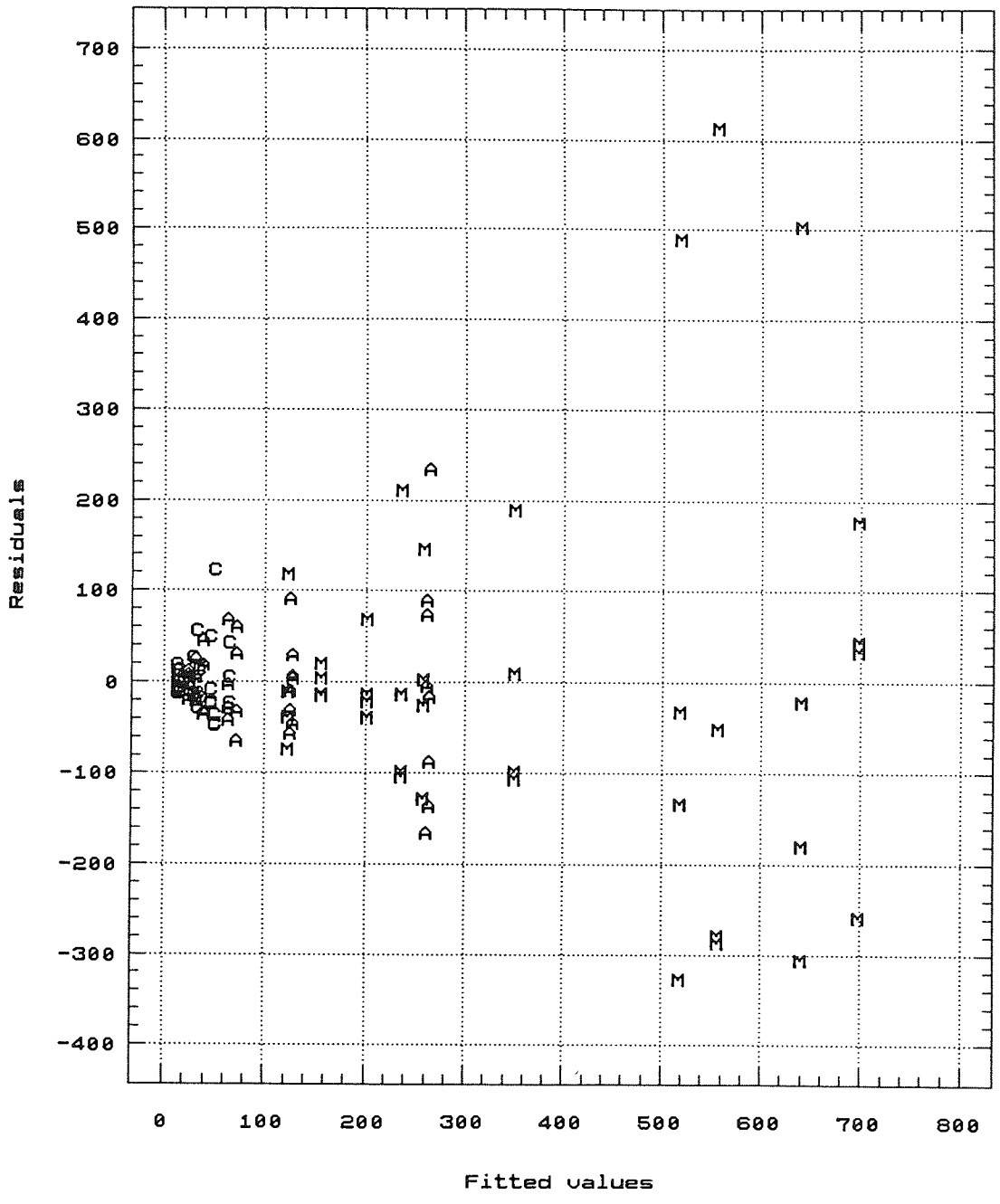

A=air, M=molochite, C=charcoal

FIGURE 7.6

Plot of Residuals v Cast Order

(Square Root Transformed data)

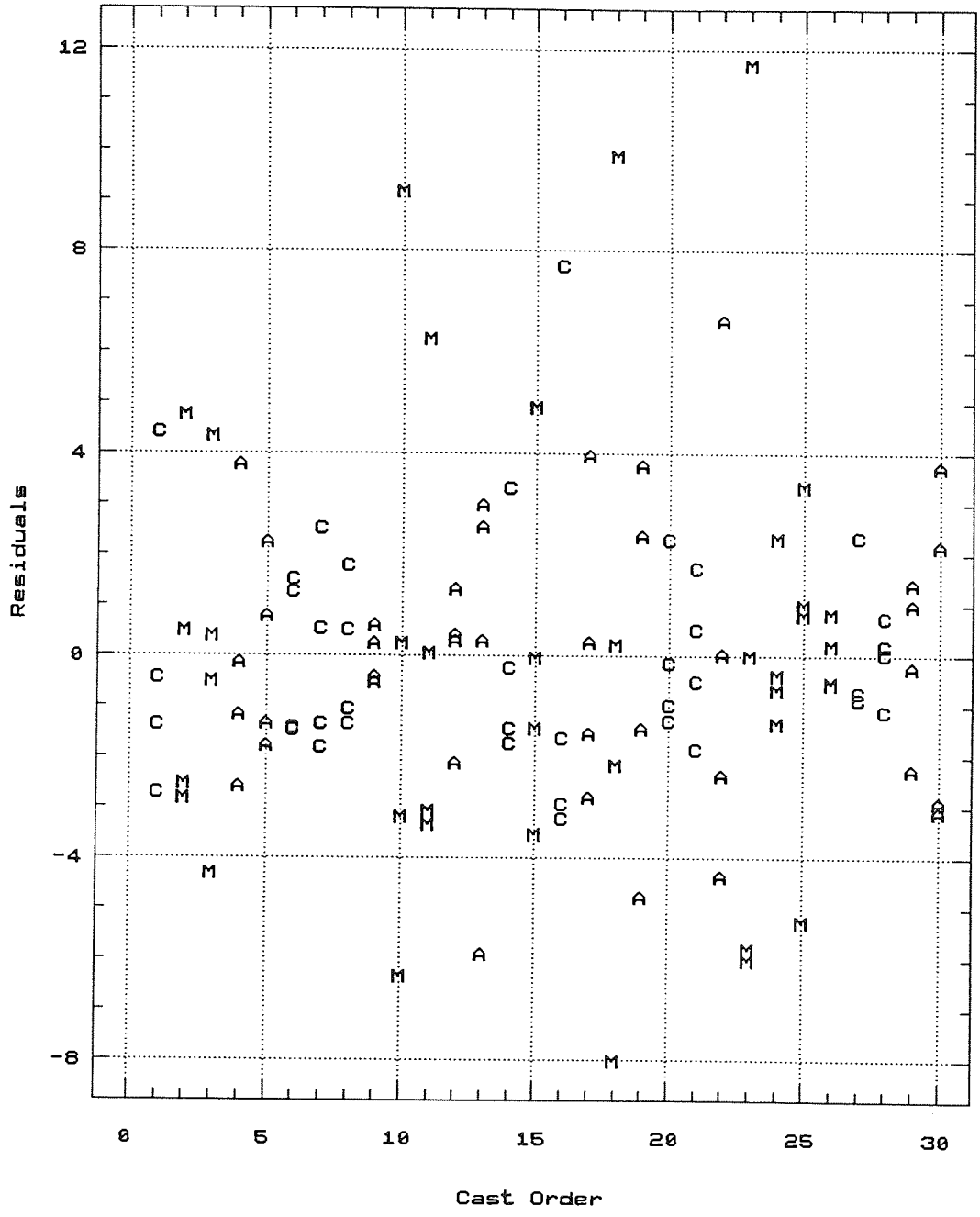

FIGURE 7.7

Plot of Resduals v Dip Order

(Square Root Transformed Data)

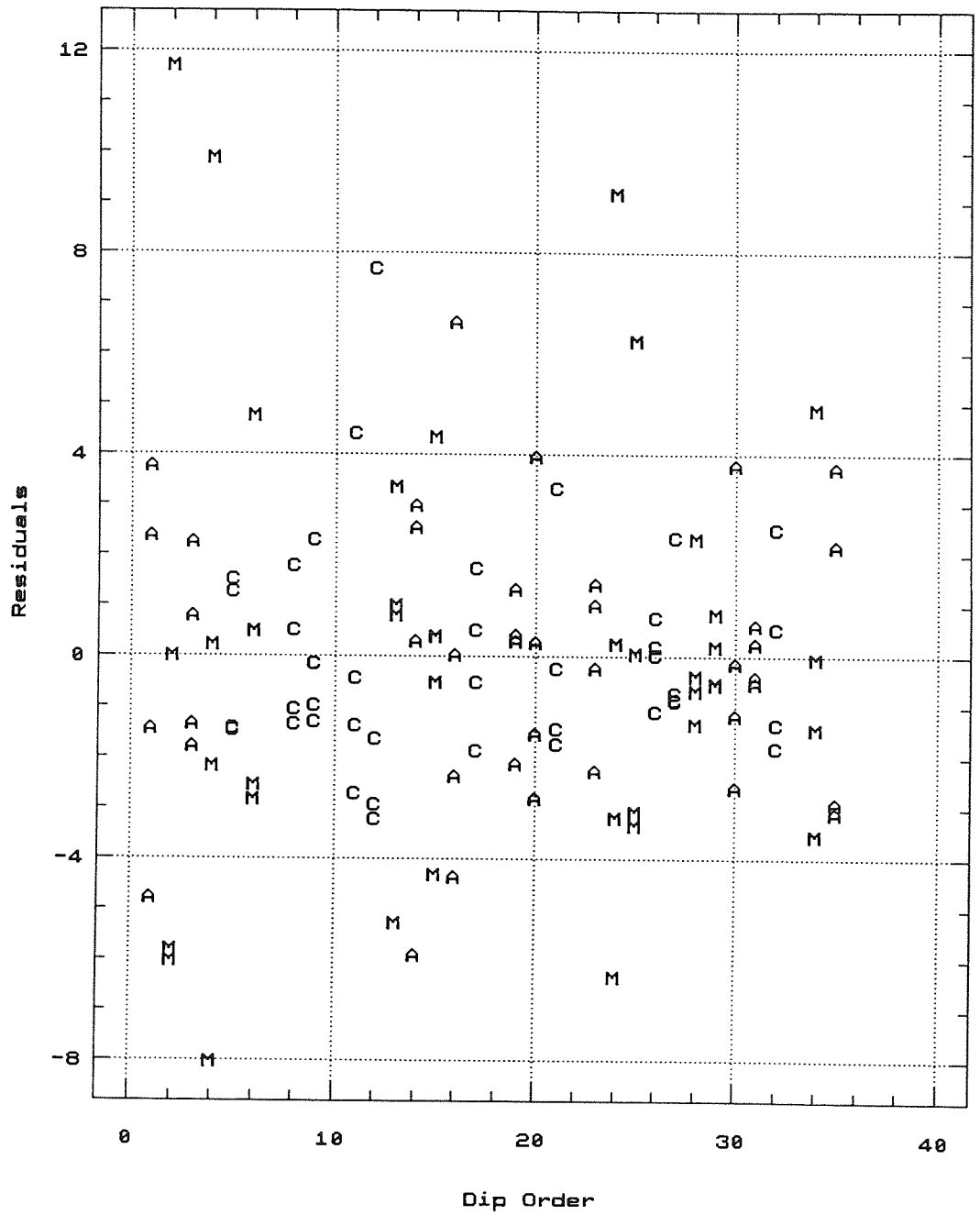

FIGURE 7.8

Plot of Residuals vs Fitted values

(Square root transformation)

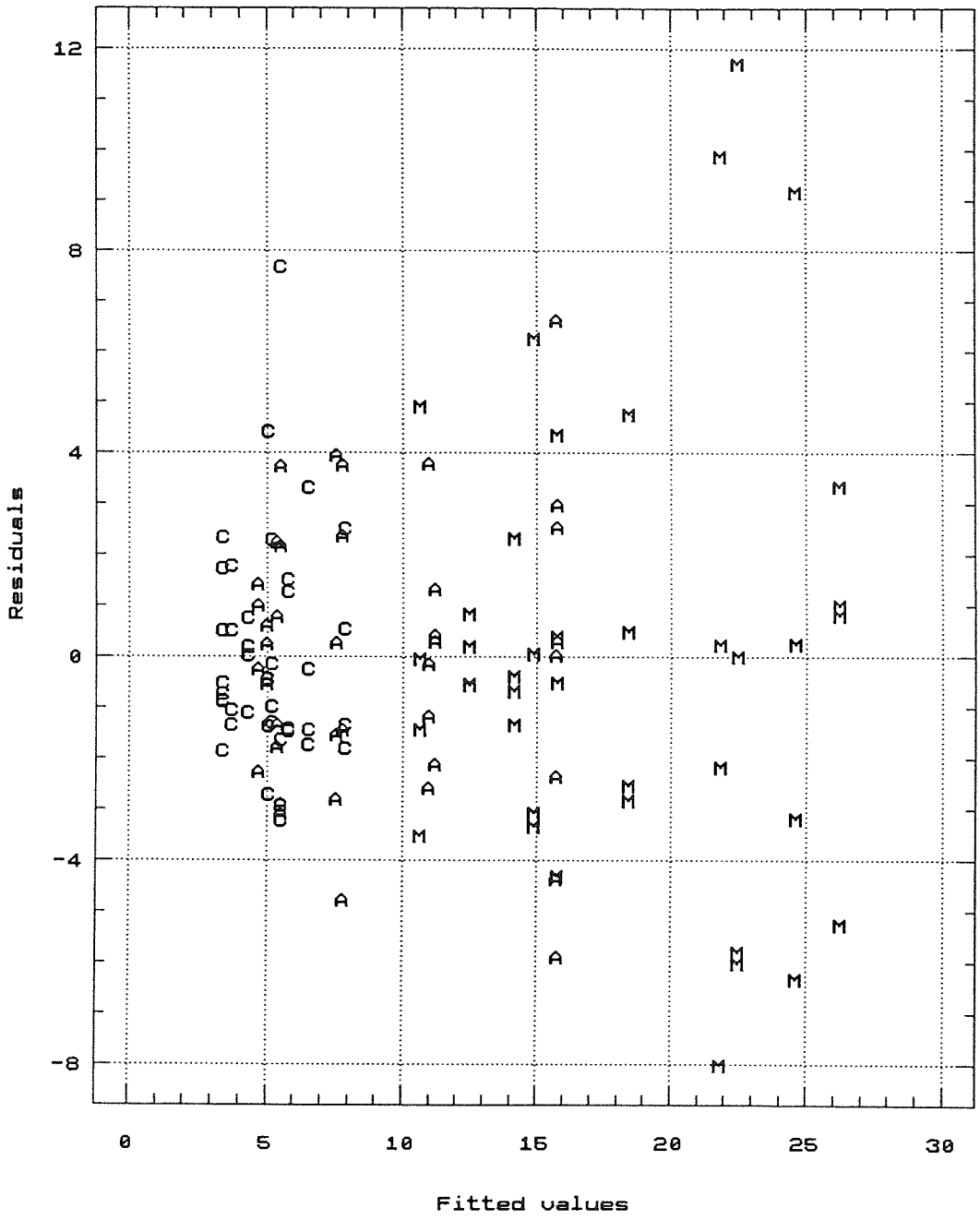

A=air, M=molochite, C=charcoal

FIGURE 7.9

Normal Probability Plot of Residuals

(Square root transformed data)

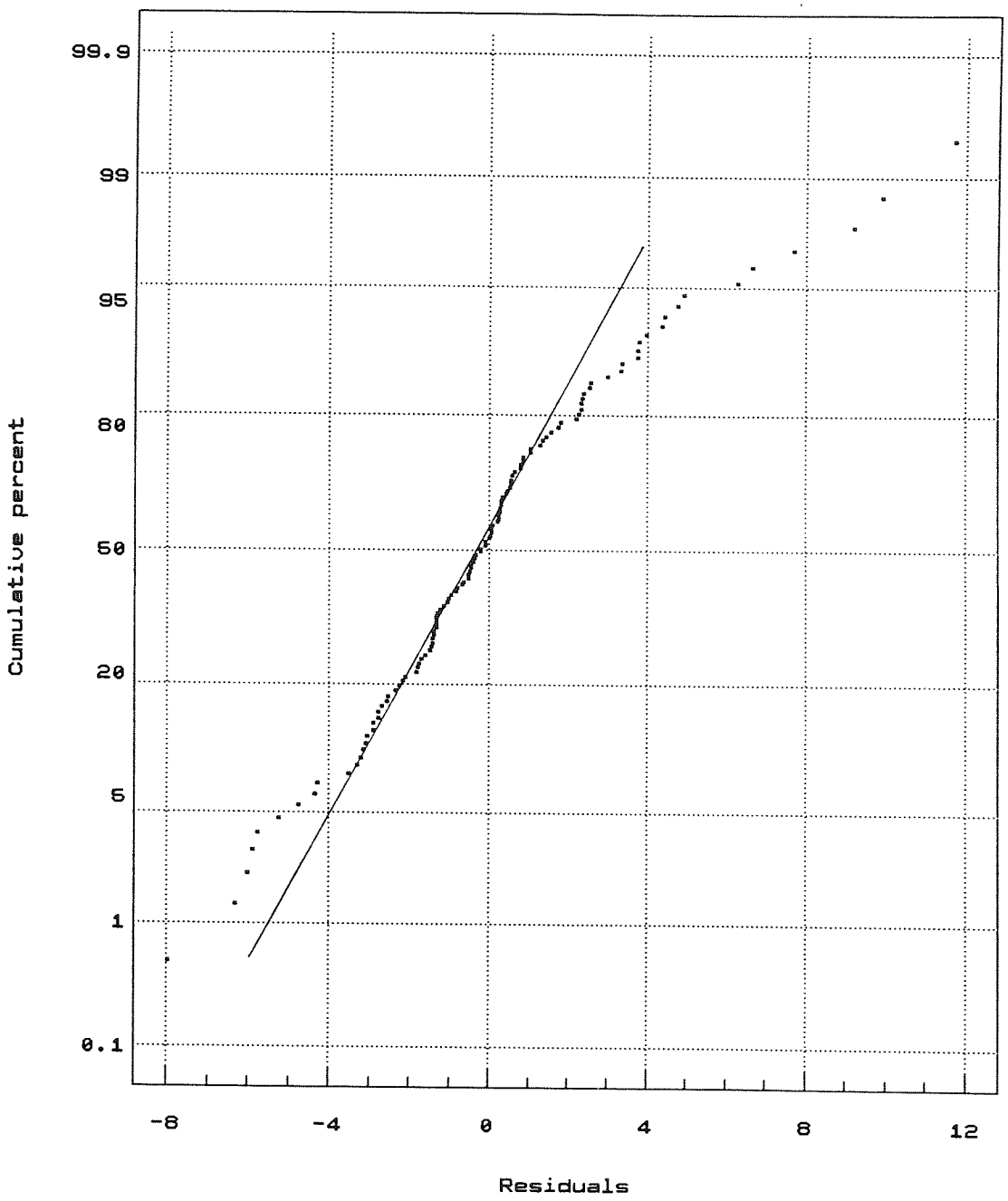

7.2.2. Logarithmic transformation i.e. $y^*_{ijkl} = \ln\{y_{ijkl}\}$

Plots of residuals against cast and dip sequence for logarithmically transformed data (Figs. 7.10 and 7.11) show no significant structure. The plot of residuals against fitted values (Fig 7.12) shows no evidence of structure.

At first sight then, it seems likely that the log transformation will have a beneficial effect on the analysis. The ECD plot for the log transformed data is a little "stepped" but there is no serious deviation at the ends of the plot which correspond to the tails of the normal curve (Fig 7.13).

The validity of the logarithmic transformation suggests that the original data was distributed lognormally. As can be seen in figure 7.14 a fitted lognormal curve corresponds closely to the distribution of the original, untransformed data. For the data to be distributed lognormally suggests that the linear model is multiplicative rather than additive. i.e:-

$$y_{ijkl} = \mu \cdot \alpha_i \cdot T_{j(i)} \cdot \gamma_{k(ij)} \cdot \varepsilon_{l(ijk)} \; ; \quad \text{(cf. equation [7.2])} \quad .....[7.4]$$

so that, with the log transformation, this becomes:-

$$\ln(y_{ijkl}) = \ln(\mu) + \ln(\alpha_i) + \ln(T_{j(i)}) + \ln(\gamma_{k(ij)}) + \ln(\varepsilon_{l(ijk)}) \; ; \quad .....[7.5a]$$

or, if y* is used to represent the transform f(y) = ln(y),

$$y^*_{ijkl} = \mu^* + \alpha^*_i + T^*_{j(i)} + \gamma^*_{k(ij)} + \varepsilon^*_{l(ijk)} \quad .....[7.5b]$$

The logarithmic transformation has thus been used to remove "transformable non-additivity" (Box, Hunter and Hunter)[23]. The analysis of variance can then be performed on the transformed data. The analysis of variance table for the log transformed data is given as Table 7.2.

TABLE 7.2 Analysis of variance table for Log Transformed Data

Source of Variation	DF	SS	MS	F_0
Days	4	6.5746	1.6437	0.6119
Treatments	10	153.7865	15.378	5.7249 †
Moulds	15	40.2943	2.6863	4.9636 †
Error	90	48.7109	0.5412	

† Significant at < 1.00 %

FIGURE 7.10

Plot of Residuals against Cast Sequence

(Log transformed data)

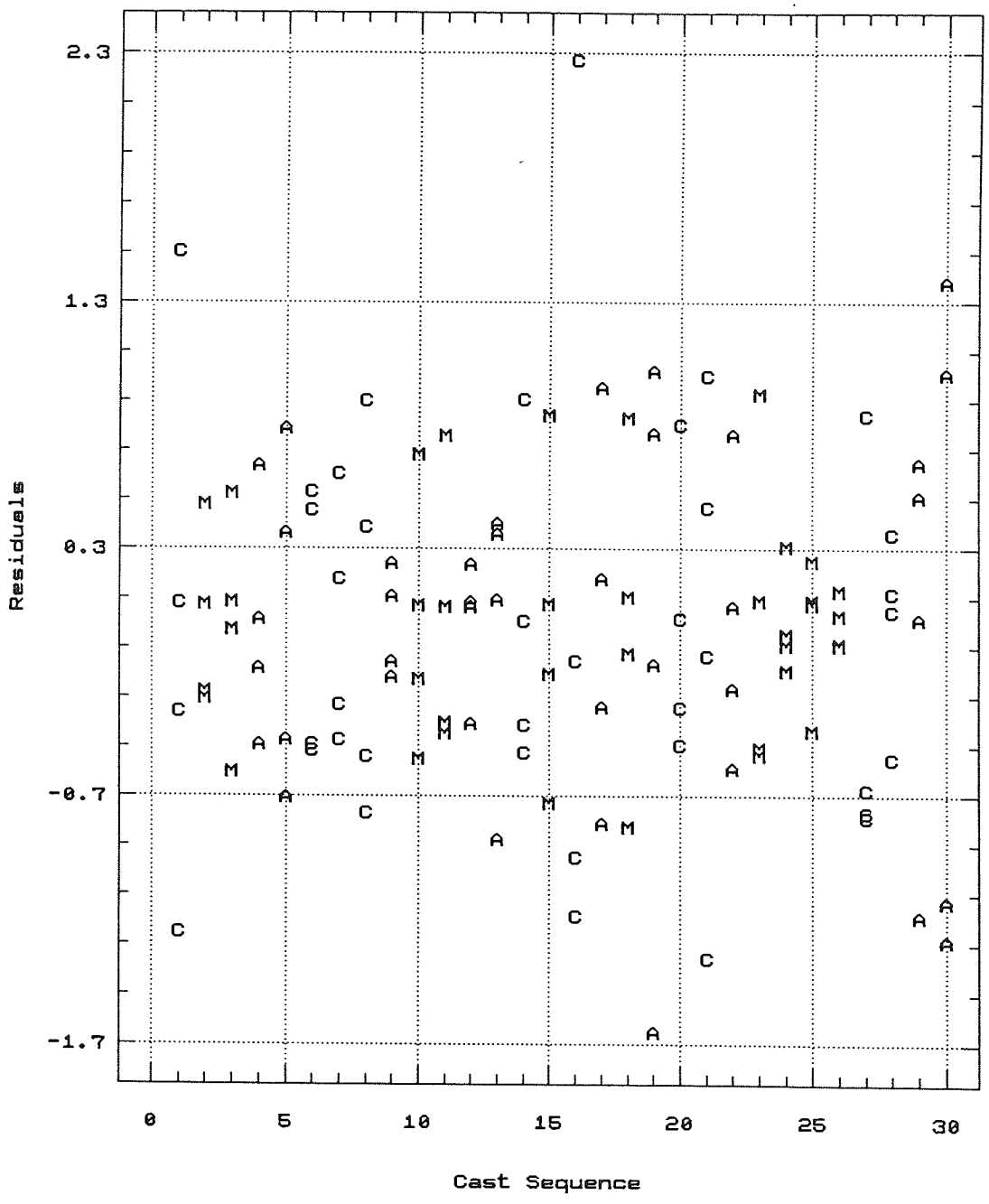

FIGURE 7.11

Plot of Residuals against Dip Sequence

(Log transformed data)

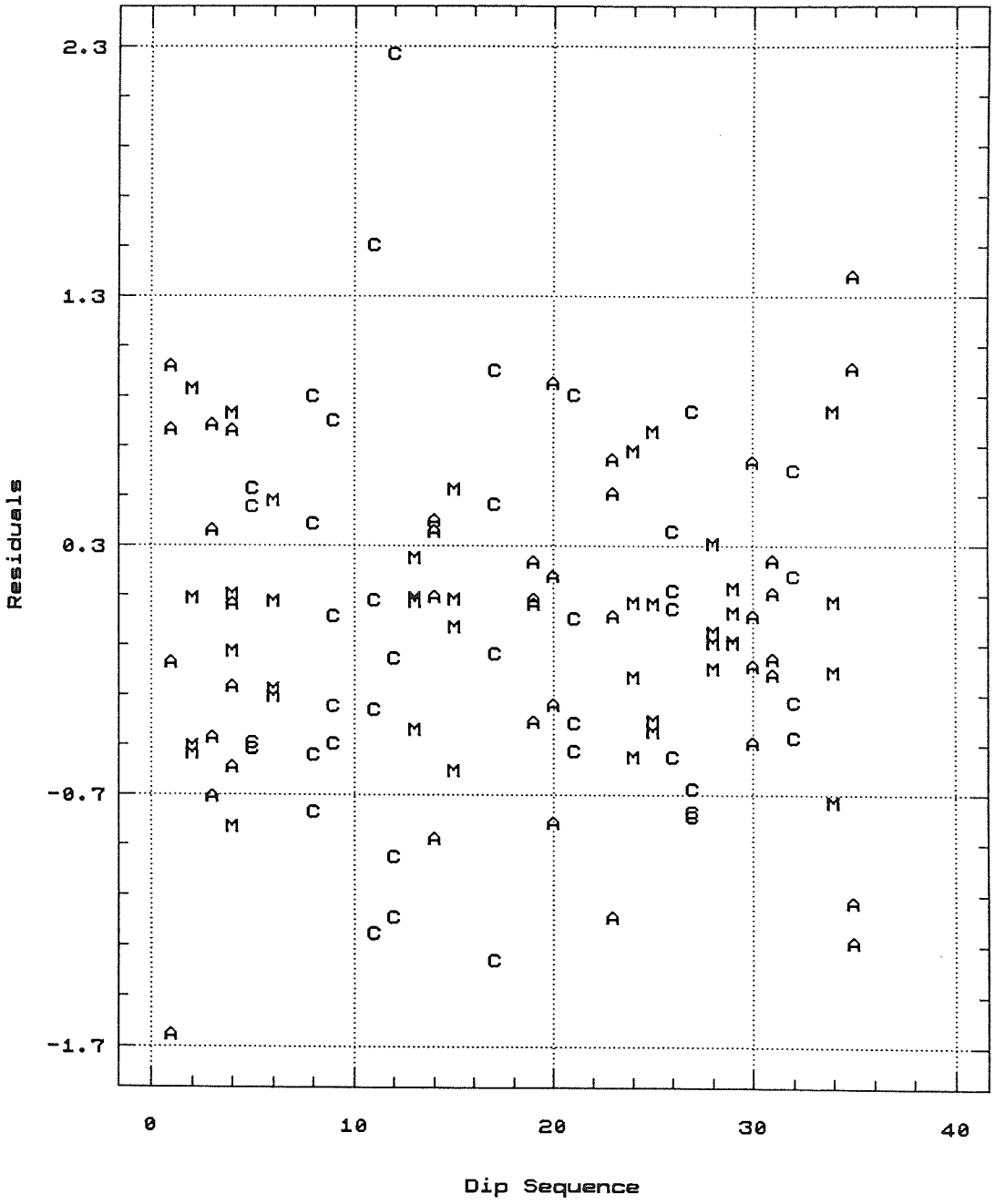

FIGURE 7.12

Plot of residuals against fitted values

(Log transformed data)

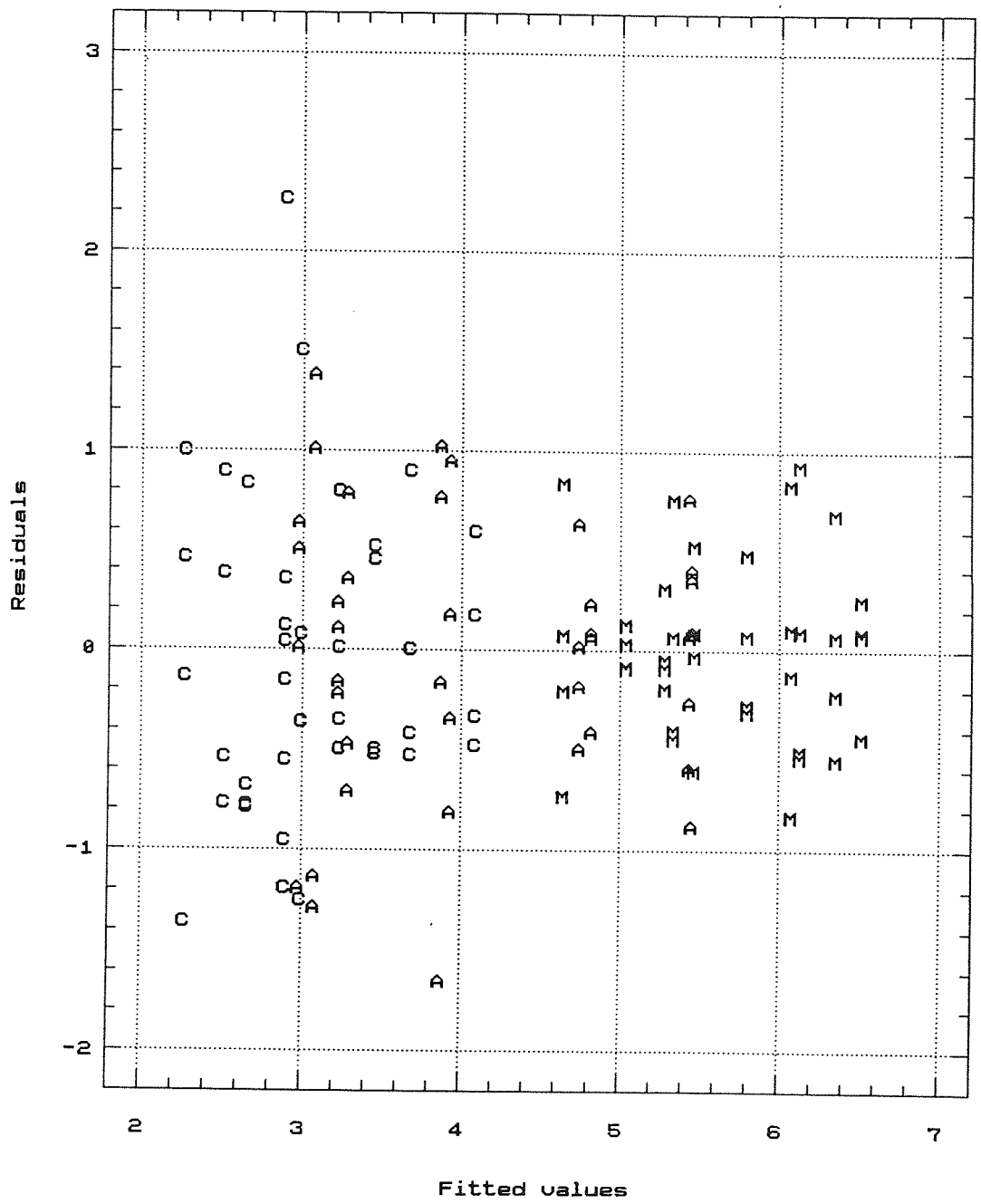

A=air, M=molochite, C=charcoal

FIGURE 7.13

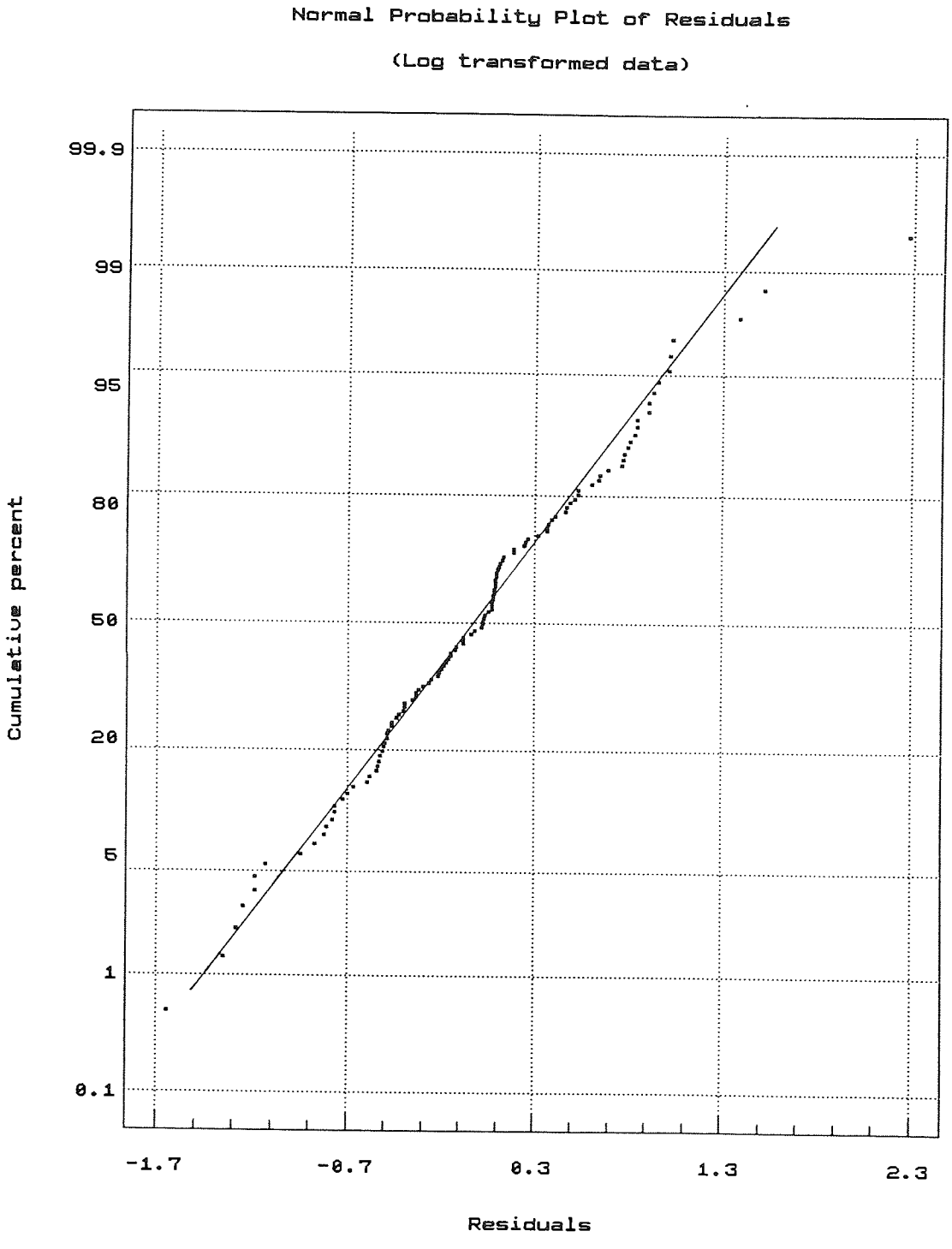
Normal Probability Plot of Residuals
(Log transformed data)
99.9
99
95
80
50
20
5
1
0.1
Cumulative percent
-1.7
-0.7
0.3
1.3
2.3
Residuals

FIGURE 7.14

Frequency Histogram for untransformed data. Fitted Lognormal distribution

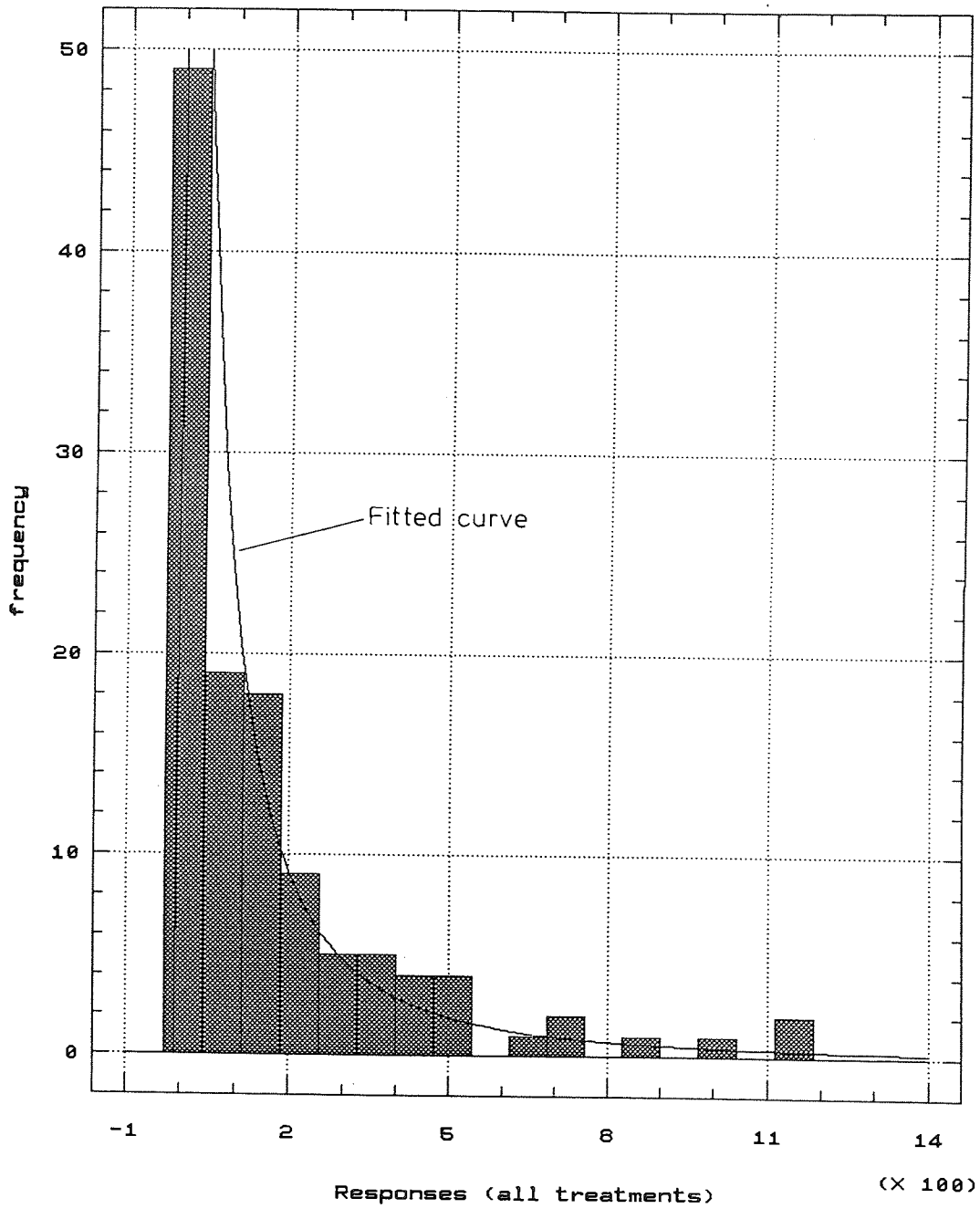

7.2.3 Non-parametric verification – The 'Rank' transformation.

Montgomery [24] states that the ordinary F test, as used above on both the untransformed and the transformed observations, can be applied to the ranks of the observations to give an approximate nonparametric analysis (in other words using a Rank Transformation). This should give a similar answer to the parametric ANOVA if the analysis of variance assumptions for the parametric tests are satisfied. In other words this method may be used to test the independence and normality of the observations, for example. See also Conover [25][26]. The ANOVA table for the rank transformed data is given in Table 7.3.

TABLE 7.3 Analysis of variance table for Rank Transformed Data

Source of Variation	DF	SS	MS	F_0
Days	4	3623.085	905.7713	0.6008
Treatments	10	92850.292	9258.029	6.1586 †
Moulds	15	22614.625	1507.642	5.4500 †
Error	90	24897.0	276.6333	

† Significant at < 1.00 %

It can be seen that the values for F_0 are very similar for both the log transformed (Table 7.2) and the rank "transformed" (Table 7.3) analysis. This provides additional support for the hypothesis that the log transformation has been successful in producing a set of transformed observations which are normally distributed.

In both cases it is clear that there is a highly statistically-significant difference between the treatments nested within the days, and also between the moulds nested

within treatments. There is, on the other hand, no evidence of any variation between the days (ie between crucibles).

It is important to note that this absence of variation between days applies only to the experiment under consideration, where the crucibles were selected from the same suppliers batch, and the same operators and melting conditions were used each day. There may well be variation with suppliers batch, variation with operator, and variation due to interaction between crucible and operator; and it would be highly misleading to attempt to generalise on the basis of this experiment. Similarly, it would be misleading to extrapolate the findings of the experiment to more than one suppliers metal cast, for example.

The next stage in the analysis is to determine which pairs of treatments differ. This is achieved by determining the $100(1-\alpha)\%$ confidence intervals for the treatment means. Since there is no statistically significant difference between the days, the responses can be pooled over the five days to produce a better estimate of the treatment means with more degrees of freedom. The confidence intervals are calculated using the formula:

$$C.I. = \bar{y}_i^* \pm t_{\alpha/2,\,N} \cdot [SE(\bar{y}^*)] \qquad \text{.....[7.6]}$$

where N = number of observations in the mean,

$t_{\alpha/2,N}$ = the two tailed $100(1-\alpha)$ percentage point of the t distribution with N degrees of freedom,

and $SE(\bar{y}^*)$ = standard error of $\bar{y}^* = \sqrt{(\sigma^2 / N)}$.

The means, together with the 95 and 99 percent confidence intervals are given in table 7.4.

FIGURE 7.15 95 and 99 percent confidence intervals on the three treatment means. (Log transformed data, pooled over five days.)

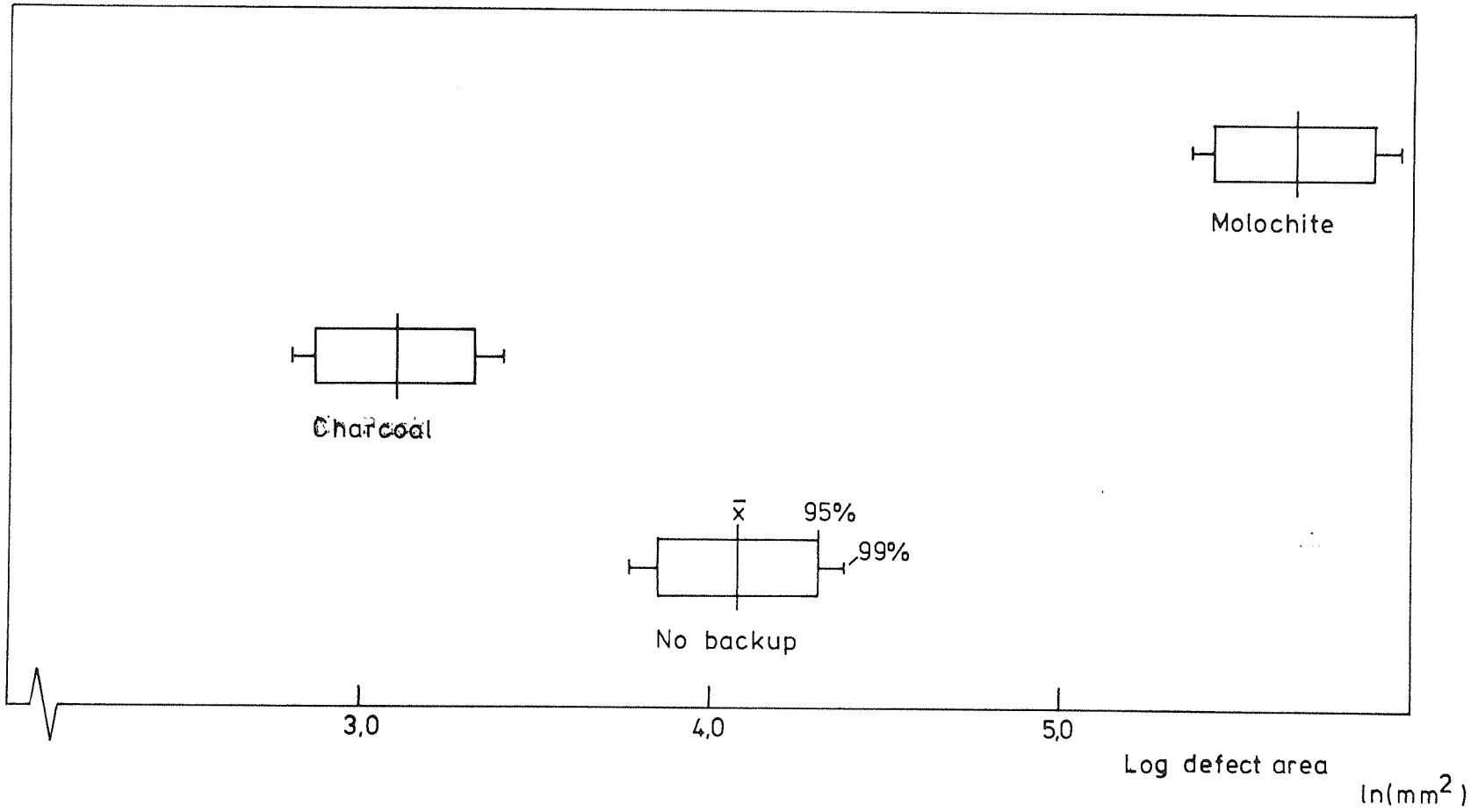

TABLE 7.4 Means and confidence intervals for the three treatments (pooled over all days)

Treatment	Mean	95% C.I.	99% C.I.
No Back-up	4.08	3.85 to 4.31	3.78 to 4.39
Charcoal Back-up	3.11	2.87 to 3.34	2.80 to 3.41
Molochite Back-up	5.66	5.44 to 5.90	5.36 to 5.97

This table, together with the confidence interval plot (Figure 7.15) clearly shows that there is no overlap between any pair of confidence intervals. This means that all three treatments are statistically different. The charcoal backed moulds are statistically less prone to defects than those with no back-up and the Molochite backed moulds more.

The analysis of variance also showed significant variation between moulds within treatments, which is unexpected. In order to try to determine the cause of this unexplained variation, the variation of the mould averages around the treatment averages was plotted against all the measured variables of interest. These "residuals" are given by $\bar{y}^*_{ijk\cdot} - \bar{y}^*_{ij\cdot}$. ($y^*$ indicating the use of transformed data). A list of the variables of interest is given in table 7.5. In no case was there evidence of any systematic tendency or structure in the distribution of these "residuals".

In the absence of any indication of a direct cause for the variation between moulds within treatments it is valuable to investigate whether the variance is different for the three treatments. There are several tests for equality of variance (see Miller[27]; Mason, Gunst, and Hess[28]; Montgomery[29]; and Davies and Goldsmith[30]) – one of the simplest of these is Bartlett's test since the test statistic is compared to the χ^2 distribution and does not require specialised tables.

TABLE 7.5 Variables of interest for the plotting of residuals.

Weight of the assembled wax mould (kg).

Assembly / Dip order (1 to 35).

Ammonia setting cabinet used (R7 or R8).

Autoclave / fire batch number (1, 2, 3, 4, 5, 6 or 7).

Weight of the fired shell (kg).

Average shell thickness (mm).

Preheat time before cast (s).

Time from start of melting to addition of the deoxidant (s).

Time from start of melting to reaching the maximum temperature (s).

Maximum temperature reached (°C).

Time from start of melting removal of deoxidation slag (s).

Time from start of melting to reaching the casting temperature (s).

Time from start of melting to pouring the metal (s).

Time from start of melting to covering the mould (s).

Casting sequence (1 to 30).

Casting sequence within each day (1 to 6).

Metal weight in mould (kg).

Chemical analysis for:-

Carbon, Silicon, Sulphur, Phosphorous, Manganese, Nickel, Chromium, Molybdenum, Vanadium, Aluminium, Copper, Cobalt, Tin, and Lead. (all weight %)

Bartlett's test involves testing $\chi^2_0 = q/c$ against the $\chi^2_{\alpha,a-1}$ distribution, where

$$q = [(N - a)\cdot\ln(S^2_{pool})] - \Sigma_{i=1,a}[(n_i - 1)\cdot\ln(S^2_i)]$$

$$c = 1 + 1/[3\cdot(a - 1)]\cdot\{\Sigma_{i=1,a}(n_i - 1)^{-1} - (N - a)^{-1}\}$$

and where $S^2_{pool} = \{\Sigma_{i=1,a}[(n_i - 1)\cdot S^2_i]\}/(N - a)$

and S^2_i = sample variance of the i^{th} population.

The null hypothesis H_0: $\sigma^2_1 = \sigma^2_2 = \ldots \sigma^2_a$ is rejected if $\chi^2_0 > \chi^2_{\alpha,a-1}$ (Montgomery)[29].

Since there is no significant difference between days, it is permissable to pool the data for each of the three treatments across the five days. The means and variances for the three treatments are calculated as:

$\bar{x}_1 = 4.080632$ $\quad$ $S^2_1 = 1.342518$

$\bar{x}_2 = 3.105255$ $\quad$ $S^2_2 = 1.200729$

$\bar{x}_3 = 5.668178$ $\quad$ $S^2_3 = 0.529608$

(x is used instead of y to emphasise that these data are pooled over the five days)

From the formula, the pooled variance is thus calculated as 1.024285. Hence χ^2_0 is calculated as 8.88 (to 3 significant figures). For (a–1) = 2 degrees of freedom we would expect to get a χ^2_0 equal to or greater than 8.88 with a probability of only 1.18×10^{-2}. Thus there is sufficient evidence to reject the null hypothesis. However, it must be remembered that Bartlett's test, as well as detecting inequality of variance, is also highly sensitive to non-normality. Whilst there is little evidence from the normal probability plot of the log transformed data to invalidate the analysis of variance, the "stepping" observed may be enough to inflate the significance of Bartlett's test. Despite this reservation there is at least some indication that the variation between moulds nested within treatments may result from inequality of variance from treatment to treatment.

7.3 Diagnostics and the analysis of residuals

The process of testing the validity of the linear, normal model for the log transformed data involves plotting the residuals ($y^*_{ijkl} - y^*_{ijk.}$) against the same variables of interest as were investigated whilst studying the variability between moulds (see Table 7.5). In no case was there anything unusual in these plots. Consequently the plots are omitted from the thesis since they are not relevent. What this observation primarily means is that there is no additional variation caused by any of the concomitant variables of interest.

Since the analysis of variance is based on the partition of the sums of squares, it is possible to express the analysis in terms of vector notation [31]. The arithmetic breakup of the data, using vector notation, allows examination of the nested effects for anomolous combinations of values. The arithmetic breakup of the data is given in figure 7.16 This breakup is based on the fact that any individual measured point Y_i (an element of the vector $\mathbf{Y}$) is the sum of the grand average A_i , plus the day effect D_i , plus a treatment effect T_i , plus a mould effect M_i , plus an error (residual) term E_i (where i is the index of the vector). For each vector the sum of squares may be calculated directly, or by using the identity $\mathbf{V}^T\mathbf{V} = \sum V_i^2$ for an $n \times 1$ vector $\mathbf{V}$, where i = 1...n and $\mathbf{V}^T$ is the transpose of $\mathbf{V}$. (In other words when $\mathbf{V}$ is a column vector of dimension $n \times 1$ then $\mathbf{V}^T$ is a line vector of dimension $1 \times n$ such that $\mathbf{V}_{ij} = \mathbf{V}^T_{ji}$). Hence the partition of the sums of squares may also be obtained by this method for checking.

It must be stressed that the data comprises six 120 row vectors (dimension 120×1), which are shown as six 5×24 matrices in figure 7.16 only for convenience of notation (each column of each matrix thus contains the data for one day). The number of decimal places has also been truncated for all the vectors in order to reduce the size of the table. However, all the sums of squares are calculated using five significant figures.

7.4 Preferred location of worst affected castings.

At first sight it appeared that there was some preferred location for the worst castings on a mould, in particular that the severity of defects was greater at one end of the mould than the other, and an analysis was performed to try to confirm this observation. This require testing the null hypothesis, that all locations of the worst casting occur equally, against the alternative hypothesis that at least one location occurs more often than would be expected. The method is to produce a contingency table, and test the calculated value of χ^2 against the expected value of χ^2 for the null hypothesis [32]. For each cell in the table the actual frequency, y_{ij}, (in the centre of the cell) is compared with the expected frequency, $\hat{\eta}_{ij}$, (top right) to give a contribution to the total χ^2 for the table (top left) using the formula $(y_{ij} - \hat{\eta}_{ij})^2 / \hat{\eta}_{ij}$

The contingency table for the locations of castings on moulds is as follows:

1.633 7.5	0.30 7.5	Total
4	9	13
0.333 7.5	0.033 7.5	
10	7	17
Total 14	15	30

Total $\chi^2 = 2.3$

The degrees of freedom for a χ^2 contingency table are given by $(r - 1)(c - 1)$, where r is the number of rows and c is the number of columns. Hence a 2 x 2 contingency table has only one degree of freedom.

For one degree of freedom we would expect to get a total χ^2 of 2.3 or more 12.9% of the time, so there is little evidence to reject the null hypothesis that there is no preferred location for the worst casting on a mould.

Figure 7.16: Arithmetic break-up of data using vector notation

Y_{ijkl}		$\bar{Y}_{....}$		$(\bar{Y}_{i...} - \bar{Y}_{....})$		$(\bar{Y}_{ij..} - \bar{Y}_{i...})$		$(\bar{Y}_{ijk.} - \bar{Y}_{ij..})$		$(\bar{Y}_{ijkl} - \bar{Y}_{ijk.})$
4.26 3.47 5.87 4.64 3.62		4.26 4.26 4.26 4.26 4.26		.033 .127 .186 .112 -.46		-.28 -.37 .248 .284 -.78		.730 -.80 .763 -.79 -.05		-.49 .250 .410 .776 .649
5.38 3.01 5.82 2.22 3.49		4.26 4.26 4.26 4.26 4.26		.033 .127 .186 .112 -.46		-.28 -.37 .248 .284 -.78		.730 -.80 .763 -.79 -.05		.641 -.21 .362 -1.6 .514
4.56 3.06 4.58 3.71 1.79		4.26 4.26 4.26 4.26 4.26		.033 .127 .186 .112 -.46		-.28 -.37 .248 .284 -.78		.730 -.80 .763 -.79 -.05		-.18 -.16 -.87 -.16 -1.2
4.77 3.33 5.56 4.90 3.00		4.26 4.26 4.26 4.26 4.26		.033 .127 .186 .112 -.46		-.28 -.37 .248 .284 -.78		.730 -.80 .763 -.79 -.05		.024 .117 .100 1.03 .021
2.82 4.89 4.11 5.18 1.95		4.26 4.26 4.26 4.26 4.26		.033 .127 .186 .112 -.46		-.28 -.37 .248 .284 -.78		-.73 .801 -.76 .787 .048		-.46 .070 .184 -.26 -1.1
4.08 4.91 3.12 6.21 4.09		4.26 4.26 4.26 4.26 4.26		.033 .127 .186 .112 -.46		-.28 -.37 .248 .284 -.78		-.73 .801 -.76 .787 .048		.795 .090 -.81 .770 1.02
3.65 4.42 4.89 5.51 4.46		4.26 4.26 4.26 4.26 4.26		.033 .127 .186 .112 -.46		-.28 -.37 .248 .284 -.78		-.73 .801 -.76 .787 .048		.368 -.40 .957 .071 1.39
2.58 5.06 3.60 4.86 1.79		4.26 4.26 4.26 4.26 4.26		.033 .127 .186 .112 -.46		-.28 -.37 .248 .284 -.78		-.73 .801 -.76 .787 .048		-.70 .239 -.33 -.58 -1.3
4.51 4.68 3.16 4.03 1.89		4.26 4.26 4.26 4.26 4.26		.033 .127 .186 .112 -.46		-1.1 -1.1 -1.2 -1.6 -1.2		-.23 .783 .392 .480 -.29		1.51 .606 -.52 .806 -.42
3.08 4.26 3.27 2.89 1.98		4.26 4.26 4.26 4.26 4.26		.033 .127 .186 .112 -.46		-1.1 -1.1 -1.2 -1.6 -1.2		-.23 .783 .392 .480 -.29		.086 .184 -.41 -.34 -.33
1.75 3.61 4.58 3.25 3.50		4.26 4.26 4.26 4.26 4.26		.033 .127 .186 .112 -.46		-1.1 -1.1 -1.2 -1.6 -1.2		-.23 .783 .392 .480 -.29		-1.2 -.47 .908 .020 1.19
2.64 3.76 3.69 2.74 1.87	=	4.26 4.26 4.26 4.26 4.26	+	.033 .127 .186 .112 -.46	+	-1.1 -1.1 -1.2 -1.6 -1.2	+	-.23 .783 .392 .480 -.29	+	-.35 -.32 .015 -.49 -.44
2.94 1.98 2.74 3.28 3.26		4.26 4.26 4.26 4.26 4.26		.033 .127 .186 .112 -.46		-1.1 -1.1 -1.2 -1.6 -1.2		.231 -.78 -.39 -.48 .292		-.51 -.53 -.15 1.01 .365
3.92 2.90 5.17 2.14 2.94		4.26 4.26 4.26 4.26 4.26		.033 .127 .186 .112 -.46		-1.1 -1.1 -1.2 -1.6 -1.2		.231 -.78 -.39 -.48 .292		.462 .391 2.28 -.13 .051
3.99 3.42 1.70 .916 2.35		4.26 4.26 4.26 4.26 4.26		.033 .127 .186 .112 -.46		-1.1 -1.1 -1.2 -1.6 -1.2		.231 -.78 -.39 -.48 .292		.534 .905 -1.2 -1.4 -.54
2.97 1.75 1.95 2.74 3.02		4.26 4.26 4.26 4.26 4.26		.033 .127 .186 .112 -.46		-1.1 -1.1 -1.2 -1.6 -1.2		.231 -.78 -.39 -.48 .292		-.48 -.76 -.94 .472 .127
6.29 5.81 4.44 6.23 6.09		4.26 4.26 4.26 4.26 4.26		.033 .127 .186 .112 -.46		1.35 1.46 .916 1.34 1.98		.164 .508 -.72 .423 .737		.488 -.54 -.20 .095 -.43
5.54 6.13 3.92 5.61 6.60		4.26 4.26 4.26 4.26 4.26		.033 .127 .186 .112 -.46		1.35 1.46 .916 1.34 1.98		.164 .508 -.72 .423 .737		-.27 -.22 -.72 -.53 .079
5.50 7.04 4.72 5.63 6.78		4.26 4.26 4.26 4.26 4.26		.033 .127 .186 .112 -.46		1.35 1.46 .916 1.34 1.98		.164 .508 -.72 .423 .737		-.30 .688 .079 -.50 .258
5.89 6.43 5.49 7.07 6.61		4.26 4.26 4.26 4.26 4.26		.033 .127 .186 .112 -.46		1.35 1.46 .916 1.34 1.98		.164 .508 -.72 .423 .737		.082 .075 .845 .932 .093
5.45 4.90 6.19 5.20 5.18		4.26 4.26 4.26 4.26 4.26		.033 .127 .186 .112 -.46		1.35 1.46 .916 1.34 1.98		-.16 -.51 .718 -.42 -.74		-.02 -.44 .109 -.08 .133
6.01 6.10 6.92 5.24 5.08		4.26 4.26 4.26 4.26 4.26		.033 .127 .186 .112 -.46		1.35 1.46 .916 1.34 1.98		-.16 -.51 .718 -.42 -.74		.530 .766 .835 -.04 .035
4.88 5.41 5.96 5.60 4.96		4.26 4.26 4.26 4.26 4.26		.033 .127 .186 .112 -.46		1.35 1.46 .916 1.34 1.98		-.16 -.51 .718 -.42 -.74		-.60 .073 -.12 .316 -.09
5.57 4.94 5.26 5.10 4.96		4.26 4.26 4.26 4.26 4.26		.033 .127 .186 .112 -.46		1.35 1.46 .916 1.34 1.98		-.16 -.51 .718 -.42 -.74		.090 -.40 -.82 -.19 -.08

Vector	$\vec{Y}$	=	$\vec{A}$	+	$\vec{D}$	+	$\vec{T}$	+	$\vec{M}$	+	$\vec{R}$
Sums of Squares	2426.7768	=	2177.4105	+	6.5746	+	153.7865	+	40.2943	+	48.7109
	S_{TOTAL}	=	S_{MEAN}	+	S_{DAYS}	+	$S_{TREATS.}$	+	$S_{MOUSE/S}$	+	S_{ERROR}
Degrees of Freedom	120	=	1	+	4	+	10	+	15	+	90

7.5 Summary

1. The untransformed experimental observations appear to be distributed lognormally.

2. There is a statistically significant difference between moulds with no backup, moulds with a charcoal backup after casting, and moulds backed-up with Molochite after casting. The use of a charcoal backup is found to ameliorate the formation of defects, and the use of Molochite is observed to exacerbate the formation of defects with respect to moulds with no backup.

3.There appears to be a statistically significant difference between moulds nested within treatments. Given the absence of any observed correlation between the mould effects and concomitant variables of interest (and a significant result from Bartlett's test) it seems likely that this difference is a result of non-constant variance between the treatments.

4. There is little statistical evidence to support the hypothesis of a preferred location for the worst affected castings on a mould.

8. DISCUSSION

8.1 THE "GROUP 9" DEFECT

As a result of the preliminary investigations mainly based on metallographic examination, and an appreciation of the metallography of castings based on reading and discussion with experts in the field, four hypotheses were developed each of which could provide an explanation for the formation of a certain type of defect observed in low allow steels - the so called "group 9" defects. These four hypotheses are outlined below.

a). Entrapment Mechanism

The reaction between oxidised metal and shell material forms a low melting point slag as the metal is poured into the mould (Fig 8.1). The slag is incorporated into the molten metal by turbulence, and is then swept along the solidification front to the preferred location.

b). Suction mechanism

Molten slag is produced by a reaction between the ceramic mould and metal oxide, at the interface between shell and metal. In "hot spots", molten metal remains surface connected until a late stage in the solidification process. Subsequent shrinkage of molten metal inside the casting may then suck slag from the surface into intergranular or interdendritic gaps (Fig 8.2).

c). Tearing mechanism

Molten slag forms by a reaction between the ceramic and metal oxide at the interface between shell and metal. Defects could then arise due to the molten slag being sucked into hot tears as they are formed (Fig 8.3).

d). Oxidation mechanism

The formation of defects which begin as a result of internal oxidation on the grain boundary sites (Fig 8.4). Following diffusion of oxygen from the surface of the metal. The intrusion of shell material into some of the defects would occur after breakthrough of the growing grain boundary oxides to the surface.

FIGURE 8.1 The 'entrapment' mechanism (schematic)

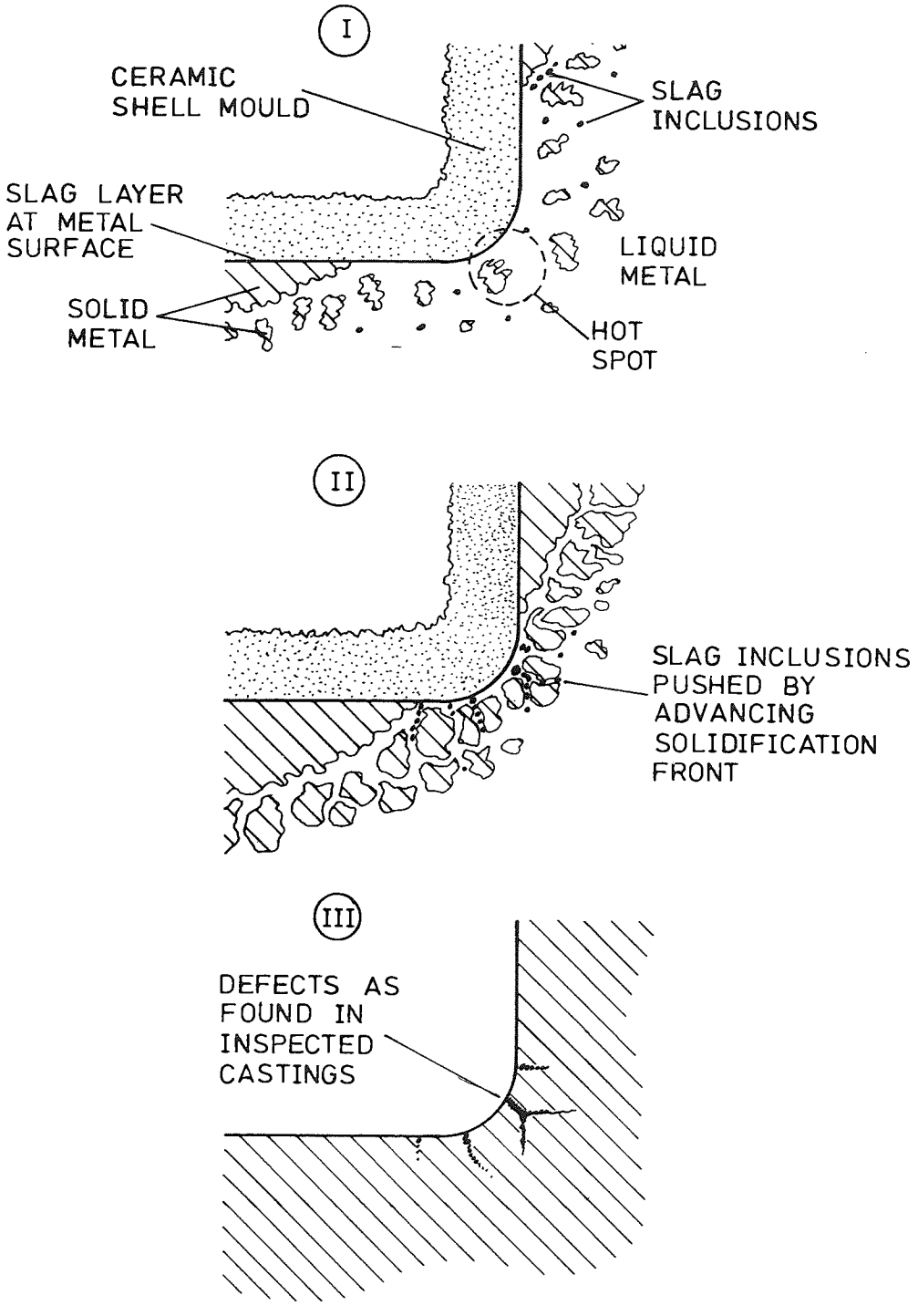

FIGURE 8.2 The 'suction' mechanism (schematic)

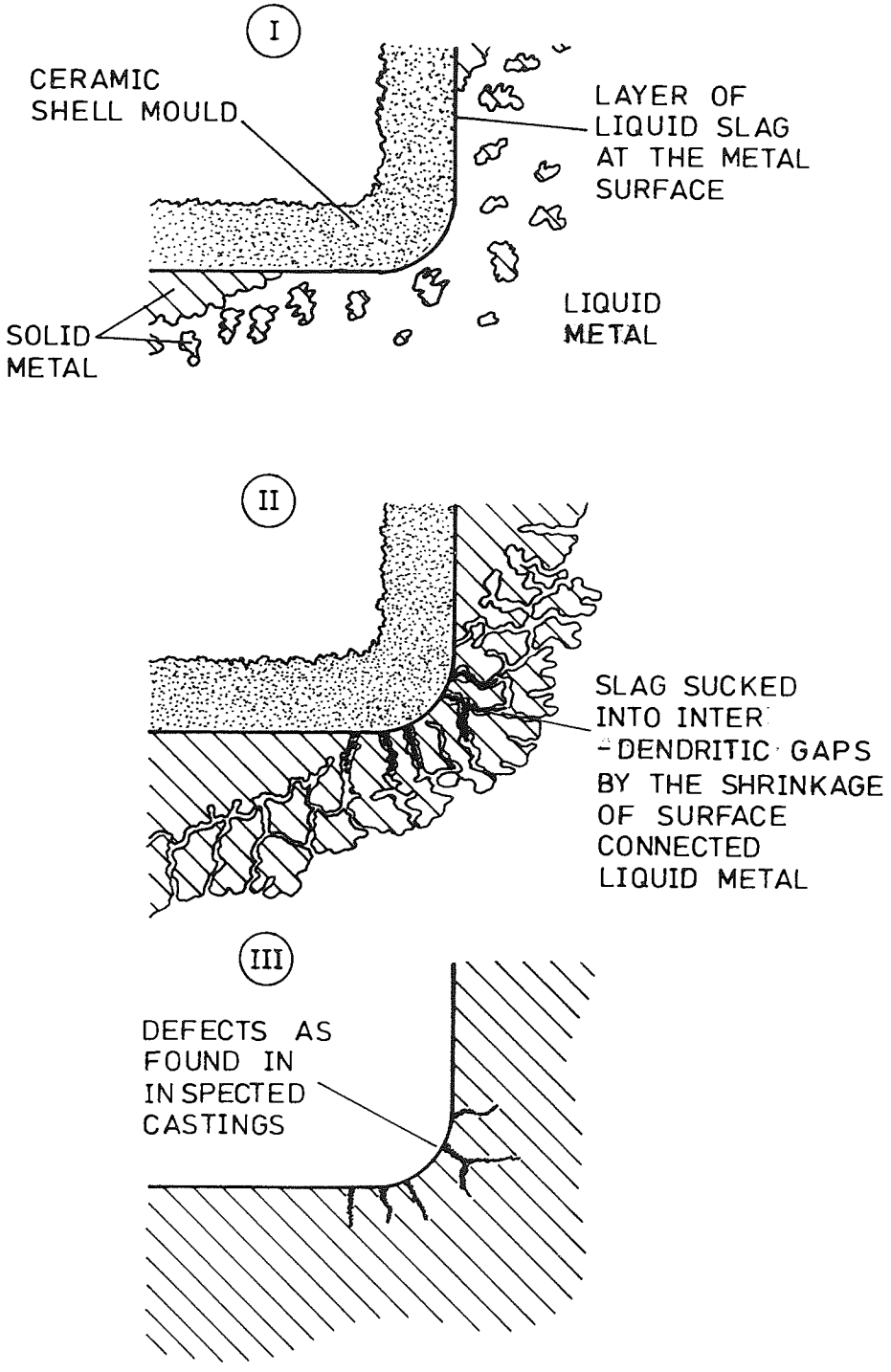

FIGURE 8.3 The 'hot tearing' mechanism (schematic)

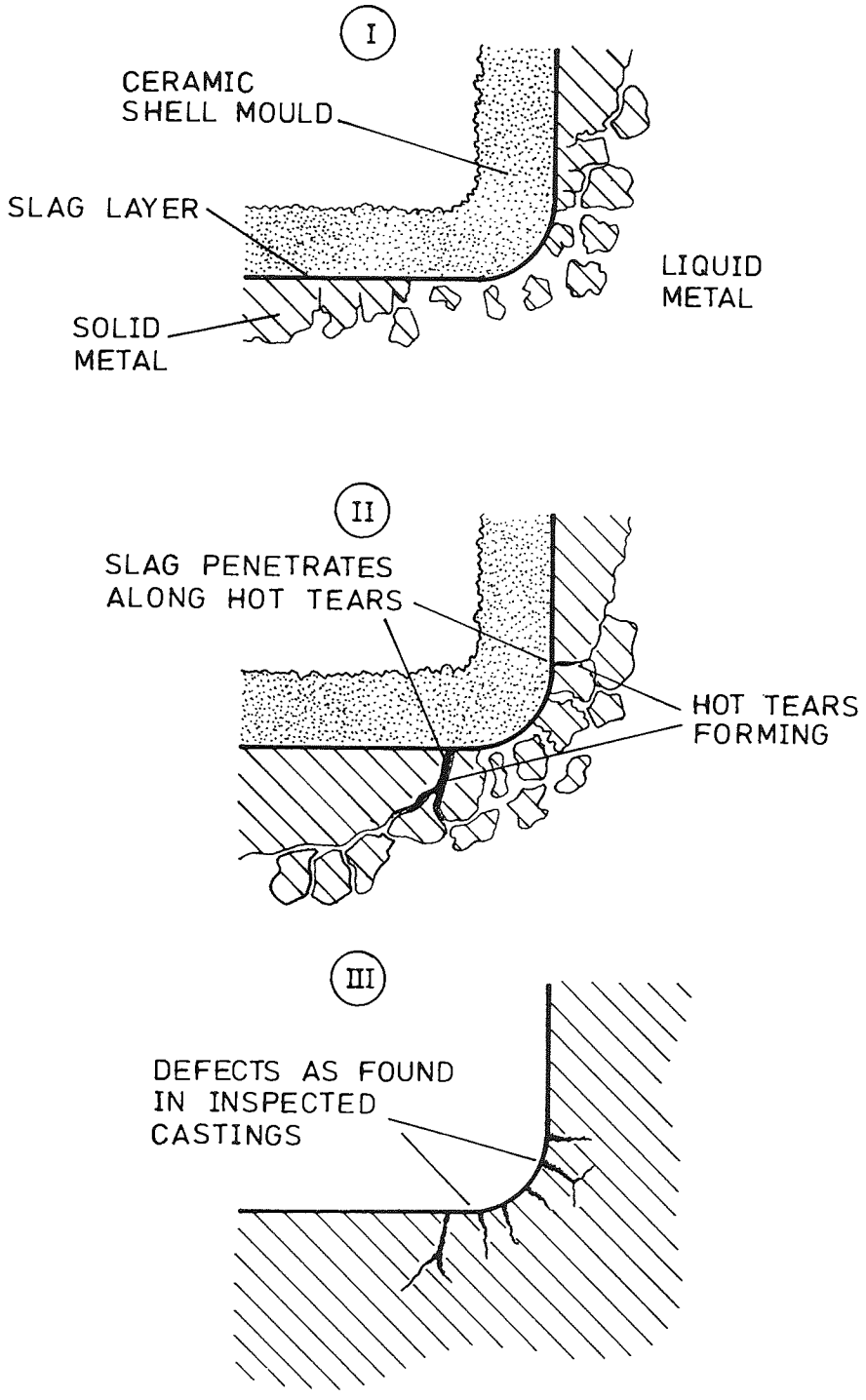

FIGURE 8.4 The oxidation mechanism (schematic)

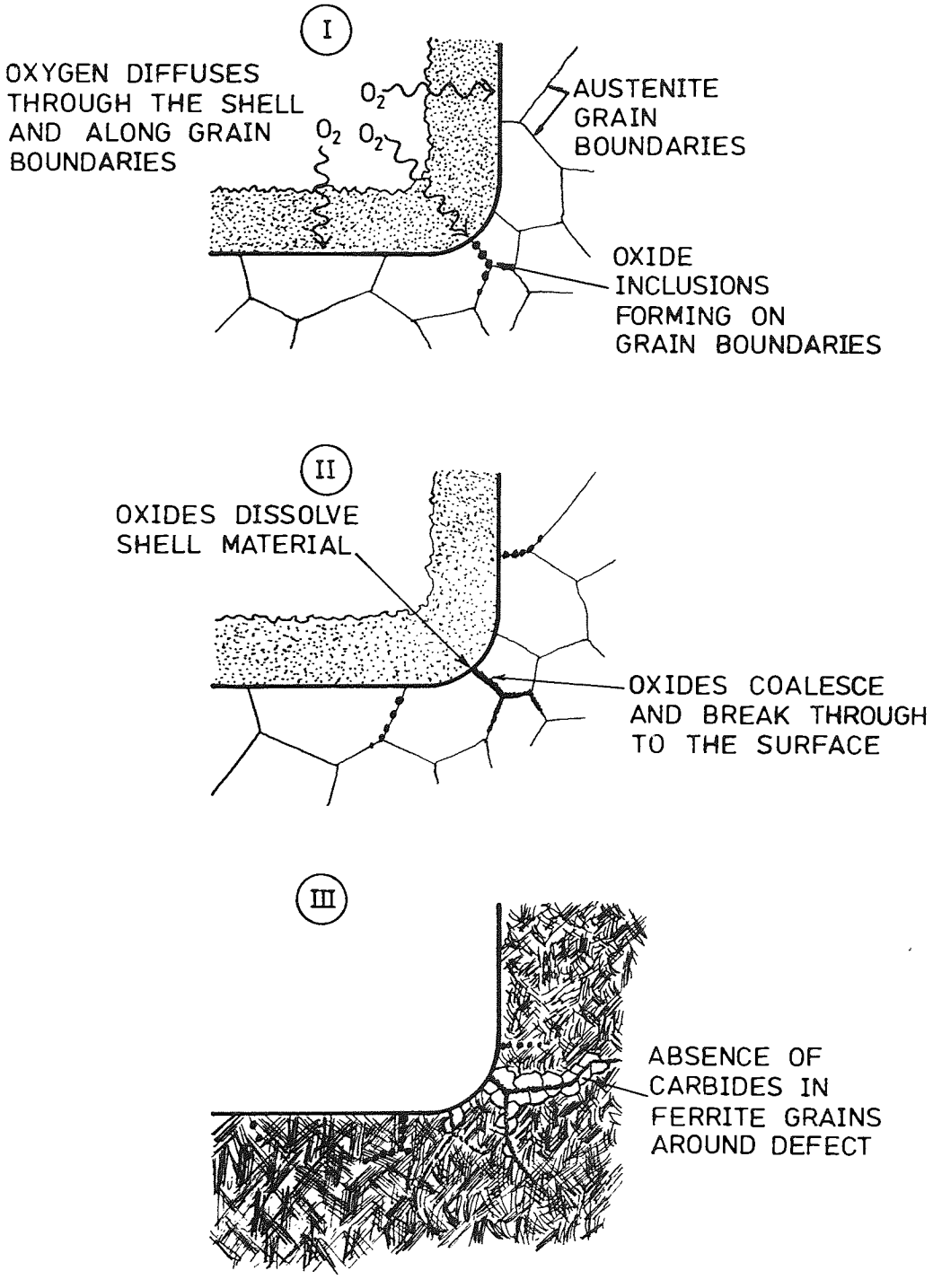

8.1.1 The "Entrapment" Mechanism

A mechanism based on the formation and entrapment of slag or other exogenous inclusions (mechanism 1) would be expected to involve some or all of the following events;

1. Erosion of refractory by metal stream.
2. Reaction of oxidising metal with refractory.
3. Inclusion and entrapment of oxides.
4. Coalescence of inclusions by collision.
5. Pushing or sweeping of inclusions to final locations.
6. Solidification of the metal.
7. Breakthrough of largest inclusions to the surface of the casting.
8. Solidification of included slag.

Erosion of refractory.

The erosion of mould refractory is patently a function of the way the molten metal flows into the mould and is fundamentally affected by factors such as pouring method and speed, refractory surface finish and composition, and the method of feeding and running.

Metal mould reactions

For this method of defect formation to operate, the reaction of refractory oxides with metal oxides must occur whilst the metal is in a molten or semi-molten state and therefore above its solidus temperature. The reactions will be of the form:

⟨Solid metal oxide⟩ + ⟨Solid refractory⟩ = {Liquid slag}

The states of the reacting components make it highly unlikely that reactions would occur within the melt with any eroded refractory, although reaction could occur with metal oxide at the surface as erosion happened. The most likely reaction mechanism, however, involves the formation of metal oxides at the metal surface, followed by reaction with the ceramic shell primary coat. Refractory eroded during pouring would remain unreacted unless it came into contact with metal oxide at the surface of the casting.

Entrapment of inclusions

Inclusions formed at the metal/mould interface will tend to remain there unless removed. It must be assumed for this theory that inclusions are swept into the melt by turbulence resulting from thermal convection in the mass of molten metal. Immediately after pouring there may also be residual turbulence from the filling of the mould.

Whilst the metal is liquid, the inclusions will tend to rise rapidly through the denser metal. However, as the metal begins to solidify, more and more inclusions will become trapped in the forming dendrite mesh.

Coalescence of inclusions by collision.

Coalescence of inclusions can occur by collision of separate inclusions moving through the melt. Immediately after pouring, whilst the molten metal temperatures are still high, inclusions will rise through the melt in a manner defined by Stokes' law. Collisions between inclusions will occur due to different rising velocities (Stokes' law shows that larger particles will rise faster), and also as a result of liquid shear caused by convection currents. Flemings[33] reports experiments to show that, at temperatures of

around 1600°C, silica particles in steel will coalesce rapidly after collision to form a single spherical particle. On the other hand alumina inclusions will collide and adhere to form interconnected clusters, with negligible coalescence.

Later, when the solidification is more advanced, inclusions will collide as a result of interdendritic flow of molten metal, the pushing of inclusions ahead of the growing dendrites, and flotation. At these lower temperatures it is possible for silica inclusions to only partially coalesce, resulting in the formation of multimembered inclusions [34] [35].

Pushing of inclusions

Flemings [36] and Davies [37] both report the pushing of inclusions by growing dendrites. Below a certain critical velocity of the solidification front, inclusions will be pushed by the advancing solid if the sum of the inclusion-liquid and solid-liquid interface energies is lower than the interface energy between the inclusion and the solid metal. This results in an increase in surface energy as the separation between inclusion and solidification decreases, and hence an equilibrium separation is maintained. Uhlman et al. [38] have studied "pushing" of particles in various organic liquids and found that for particles under 15μm in "size" the critical velocity was in the range of 0.2 to 20 $\mu m \cdot s^{-1}$. This was found to be a function of particle material but not of particle size.

Flemings [39] states that inclusions in metals are pushed, because the rate of thickening of dendrite arms in solidifying alloys is much slower than the critical velocities. In particular, silica primary inclusions are known to be pushed by growing dendrites in steel. Myers and Flemings [34] have studied

silica inclusions in iron-copper alloys, and have shown that in addition to being pushed, silica inclusions can collide with one another to form multimembered inclusions, as alumina inclusions do at higher temperatures. The movement of inclusions through interdendritic spaces is thought to be due partly to this dendrite pushing.

Solidification of the metal

During the initial stages of solidification it is likely that, for the particular casting geometries under consideration, certain areas of the casting will solidify "progressively", whilst "extensive" freezing will occur at hot spots. The transition between extensive and progressive freezing modes is governed by the relative magnitude of the freezing range of the alloy and the temperature gradient across the metal mould interface. For an alloy having a freezing range ΔT_{fr} and a temperature range from the liquid interface to the outside of the casting $\delta_l T$, the condition of progressive freezing is;

$$(\Delta T_{fr} / \delta_l T) << 1, \qquad \text{.....[8.1]}$$

so that the freezing range of the alloy is much less than the temperature gradient across the solidifying zone. The condition for extensive freezing is thus;

$$(\Delta T_{fr} / \delta_l T) >> 1, \qquad \text{.....[8.2]}$$

where the temperature gradient is much larger than the solidification range of the alloy. When the freezing range of the alloy and the temperature gradient across the interface are of approximately the same magnitude, no clearly defined laws can be observed[40].

This latter case is likely to exist if both progressive and extensive freezing can occur in different parts of the same casting. As freezing proceeds the

FIGURE 8.5 Illustrating the difference between progressive and extensive freezing.

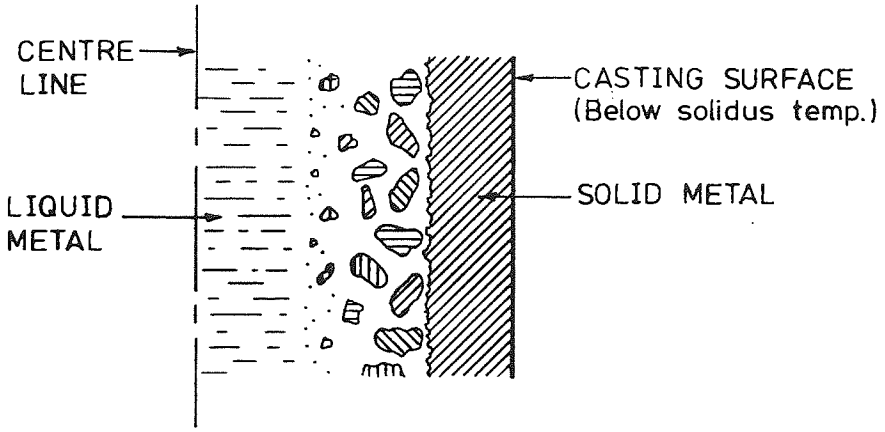

A) Section through casting undergoing progressive solidification

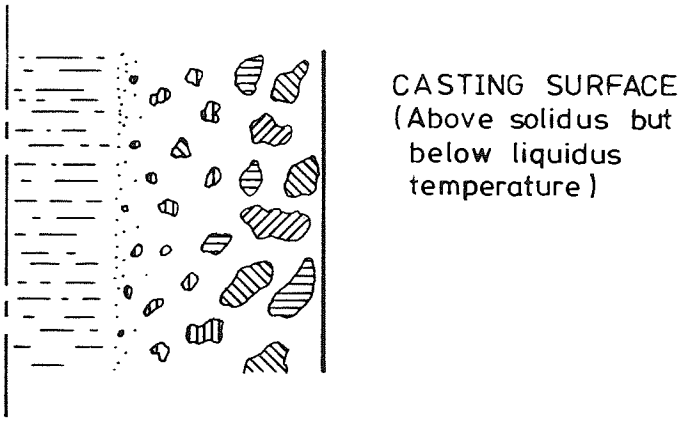

B) Section through casting undergoing extensive solidification

solidification front will therefore move parallel to the casting surface (into the extensive regions), as well as normal to the surface into the centre of the casting. This movement along the metal mould interface will push inclusions ahead of the solidification front to the "hot spots" in the casting (usually at reentrant angles or corners).

Breakthrough to the casting surface.

The final solidification of the metal brings to an end any further movement of included material by pushing. Contraction of the metal on further cooling may cause cracks to develop from the included material due to differential thermal contraction. However, the slag formed by the reaction between metal oxides and ceramic will remain liquid for some time after final solidification of the metal and may therefore flow into such cracks as they form. This will lead to breakthrough of the defects to the surface of the casting. Further break-through due to contraction cracking may also occur after solidification of the slag. However, the shrinkage of the slag on solidification will reduce the maximum stress levels which may afterwards be built up by contraction of the metal.

A critique of the "entrapment" mechanism

The entrapment mechanism is a feasible theory to explain the formation of defects having morphologies similar to those found in low alloy steel castings. There are, however, fundamental anomalies which arise from other observations. Energy dispersive X-ray analysis of defect composition (see chapter 5) has shown that only those defects which are surface connected contain zirconium, which is an indicator of the inclusion of ceramic shell material. Sub-surface defects having the

characteristic "moniliform" shape are found to contain primarily iron and chromium. The composition of the sub-surface defects does not, of itself, invalidate the hypothetical mechanism since it is possible that the moniliform inclusions could have been formed by a separate mechanism. However, the apparent absence of any sub-surface defects containing shell material does provide strong evidence to contradict the hypothesis. It is highly unlikely that all included slag material could be swept to one or two final locations without at least some inclusions being left behind, trapped in the dendrite mesh. Also, some surface-connected zirconium-containing defects retain traces of the moniliform structure.

The evidence from the statistical experiment discussed in chapters 6 and 7 is less conclusive here, but it is sufficient to further undermine the hypothesis that defects are caused by entrapment and "pushing" of slag. The finding that a charcoal backup reduces the severity of these defects is compatible with the theory, in that the production of a reducing atmosphere will prevent oxidation of the metal and, hence, formation of slag. However, the increased severity of defects in castings with a molochite grit backup is harder to explain. If the application of cold molochite grit immediately after casting prevents the formation of extensive freezing zones in a casting, then there should be no mechanism by which included slag can be swept, parallel to the casting surface, to the preferred locations on surfaces forming reentrant corners. This is because when freezing is exclusively progressive, the solidification front travels from the outside of the casting to the inside, and not along the casting surface.

The reason that the statistical evidence is less than conclusive in this case results from doubts about the validity of the assumption that the application of a molochite chill prevents extensive freezing. After the application of the back-up, the molochite would be expected to heat up and eventually act as an insulating layer around the

mould (by reducing the temperature gradient). This would then slow the cooling of the mould. It has been assumed that, for a thin walled casting, the initial chill would be enough to prevent extensive freezing so that the surface metal would be completely solid before the backup began to act as an insulator. However, insufficient time was available to test this assumption experimentally.

8.1.2. The "Suction" Mechanism

The formation of defects by a "suction" mechanism is dependent on the following events:

1. Oxidation of the metal surface, leading to:-
2. Formation of liquid slag.
3. Suction of liquid slag into interdendritic gaps.

Many of the other events discussed in the previous section would also occur, but these are not fundamental to the validity of this mechanism.

Oxidation of the metal surface and formation of liquid slag.

It is axiomatic to this mechanism that metal oxides should be formed whilst the metal is, at least partly, still liquid. At these temperatures, oxidation would be expected to be very rapid; the only kinetic constraints would be diffusion of oxygen through the ceramic shell mould and through the layer of oxide as it forms. An additional consideration is the increased solubility (by a factor of at least 20) of oxygen in liquid steel compared with solid steel [41] [42]. This will naturally affect the equilibrium between atomic oxygen dissolved in the steel and oxygen in the form of metal oxides.

Solution of the mould primary coat by oxides to form slag would also be expected to be rapid because of the high temperatures.

Suction of liquid slag into interdendritic gaps

The force required to suck surface oxides into interdendritic gaps is a result of the shrinkage of the molten metal within the mould cavity. This metal must, of course, remain surface connected.

The effect of changes in the volume of residual internal liquid on the surface of castings is well known from the phenomenon of "tin sweat", where hydrogen evolution causes expansion and forces tin enriched liquid out to the surface of tin-bronze castings.

Campbell [43][44][45][46] has discussed in some depth the formation of contraction pressures in steels and other alloys. The pressures generated in isolated liquid pockets are reported to be sufficient to cause plastic deformation of the solid metal in some cases, and cause internal shrinkage cavities by assisting the nucleation of pores. More pertinently, Campbell also states that, if liquid metal remains interdendritically surface connected, internal contraction of liquid metal can explain the formation of "blow holes" – without recourse to theories based on metal-mould reactions and gas evolution. Campbell believes that blow-holes result from air being sucked into the interdendritic gaps from the surface. It does not require a significant extension to the theory to suggest that if liquid slag of sufficient fluidity is present as a layer at the surface of the casting, that would be sucked into the interdendritic gaps instead.

A critique of the "suction" hypothesis

As was the case with the hypothesis based on entrapment of slag inclusions, the main objections to the "suction" theory stem from the different compositions observed by SEM analysis. A mechanism based on suction of slag into interdendritic spaces would be expected to result in defects having the characteristic morphology of those spaces (Fig 8.6). As has been noted, the majority of the defects observed in many low alloy steel investment castings do, indeed, have such a "moniliform" structure. Unfortunately however, it is precisely those defects

having this morphology which have been found to contain no evidence of zirconium, an indicator of shell material and hence slag. These defects also appear not to be surface connected, although they could be surface connected in planes other than that of the metallographic section. Those defects containing shell material are invariably surface connected and have a distinctly different morphology.

The experimental evidence from the use of different back-up materials is also significant. The formation of defects by this mechanism would be expected to be acutely dependent on the presence of extensive freezing on some part of the casting. However, the formation of slag at the surface would not be so critical since "blow-holes" would still be expected to form, whether or not they were filled with slag. No evidence of blow-holes was found in any of the castings. For this hypothesis to be valid, therefore, the reduction in defects found as a result of backing moulds in charcoal would have to be a result of promoting progressive freezing at the expense of extensive freezing. If this is so then an even greater improvement would be expected following the use of cold molochite, which would give an even greater initial chill than charcoal. In fact, the use of a molochite back-up has been shown to exacerbate the defects.

FIGURE 8.6 Illustrating the morphology of slag, sucked into interdendritic spaces (schematic)

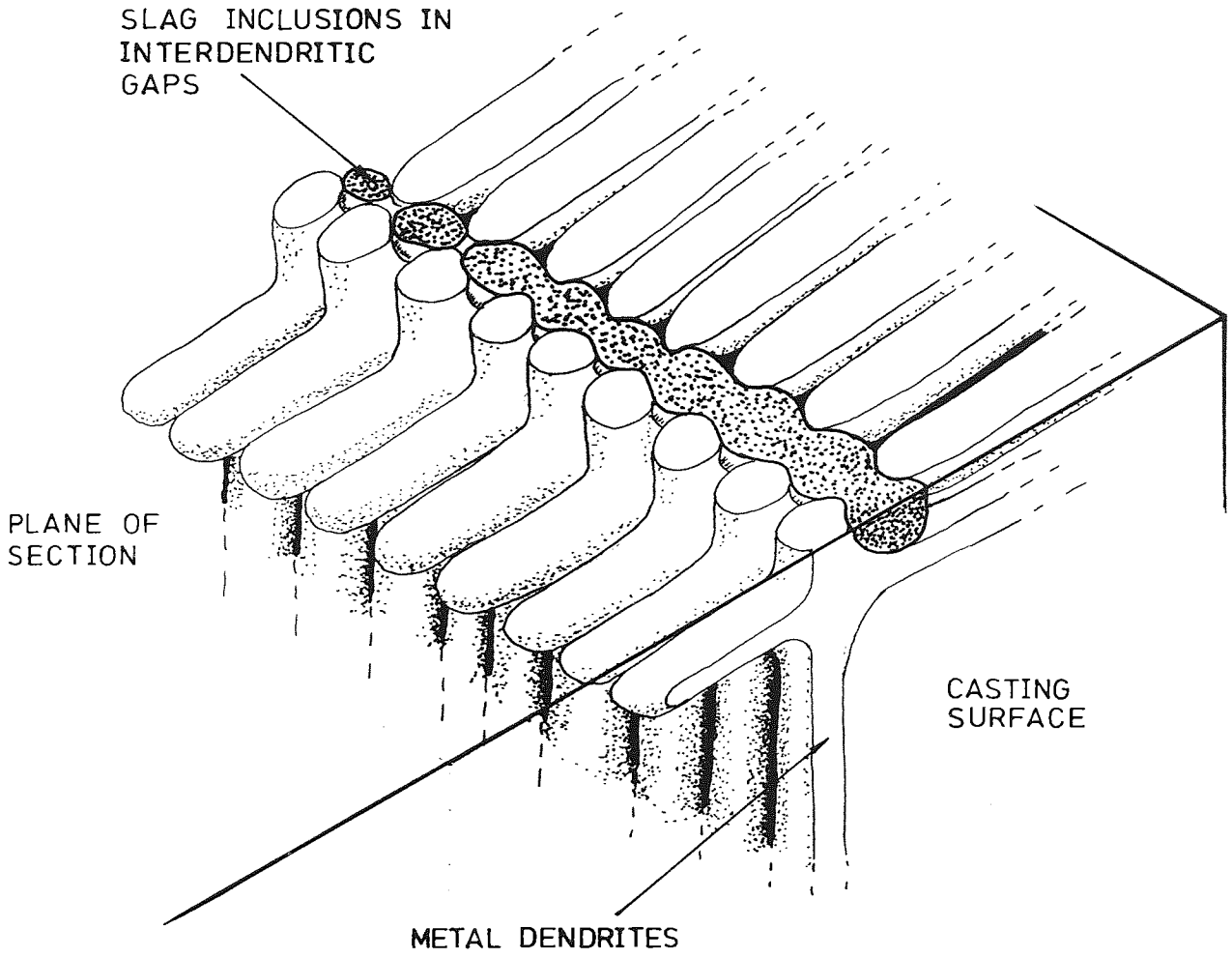

8.1.3 The "Tearing" Mechanism

Hot tearing, hot shortness, and liquid metal embrittlement all involve fissuring, or material separation under the combined effects of stress and a liquid phase. Whilst hot shortness and liquid metal embrittlement occur just above the liquidus as a result of externally applied stress, hot tears are formed during solidification with stresses resulting from contraction of the metal.

In the context of a potential mechanism for the defects under consideration, it would be expected that the following events would play a part:

1. Oxidation of metal at the mould surface,
2. Solution of mould primary coat to form a surface slag layer,
3. Formation of partial interdendritic/intercrystalline films of liquid metal,
4. Formation of tensile stresses, and
5. Suction of surface slag into hot tears as they are formed.

Oxidation of metal and formation of slag

The formation of a liquid slag at the surface of the casting results from metal oxides dissolving the zircon primary coat of the mould. As before, it is necessary for the formation of liquid slag to take place before the metal is fully solid.

Formation of hot tears

In general, hot tears form when thin films of liquid metal partially separate the grains of a solidifying alloy. At the same time enough solid must connect the grains to allow tensile stress to build up sufficient to rupture these solid-solid 'bridges'.

The formation of liquid films has been discussed by a number of authors. One mechanism relates to segregation of alloying constituents to produce smaller and smaller quantities of a low melting point liquid which are eventually trapped between the growing solid grains. If the remaining liquid wets the solid metal so that the dihedral angle is at a minimum, the trapped liquid will take the form of thin films partially separating the solid grains[47].

Another method by which hot tears can form occurs when both extensive and progressive freezing modes occur together in one casting. This situation can occur when 'hot spots' are present due to the geometry of the casting or when chills are used[48]. Wide freezing range alloys will tend to freeze extensively in the hot spots and progressively elsewhere. However, as solidification proceeds, the progressive region will tend to extend into the area of the hot spot so that the solidification front travels along the metal mould interface. This mechanism can be better visualised by consideration of the movement of solidus and liquidus isotherms with time (Figure 8.7). In the transition region between progressive and extensive freezing, there will be a point where the volume fraction of liquid is low enough to permit bridging of solid material. If the tensile stresses due to solidification contraction are sufficiently high, hot tears will develop in the transition zone between the fully frozen and semi solid regions.

Suction of liquid slag into hot tears

The theory of defect formation requires that, as the hot tears open, the liquid slag present at the surface is pulled into the crack, either by capillarity or by suction. Some work has been published discussing the wetting of ceramics

by liquid metals, but no references could be found which discussed the wetting of solid metals by liquid slags.

A critique of the 'hot-tearing' mechanism

For a defect formation mechanism based on hot tearing – as discussed above – to be credible, it is necessary to show that both hot tearing and the formation of liquid slags at the casting surface are consistent with the experimental evidence. One major failing in the hypothesis is the observation that the use of a molochite back-up immediately after casting exacerbates the defects. For a mechanism of defect formation dependent upon hot-tearing it would be expected that the reverse would be the case, since the application of a chill effectively increases the temperature gradient at the metal mould interface and hence promotes progressive solidification. It is also true that the observed variation in chemical composition between defects is anomalous. All defects would be expected to contain shell material since all the incorporated material sucked in from the surface would be metal-oxide/refractory slag. However, this is in fact only true of those defects which are visibly surface connected in the plane of metallographic section section. This is valid for surface connected defects which are 'moniliform' as well as those having a more 'crack-like' morphology. As in those other mechanisms relying on the incorporation of liquid slag from the surface, there is no explanation for the different microstructure around the defect.

FIGURE 8.7 Solidification isotherms in a low-alloy steel casting (schematic)

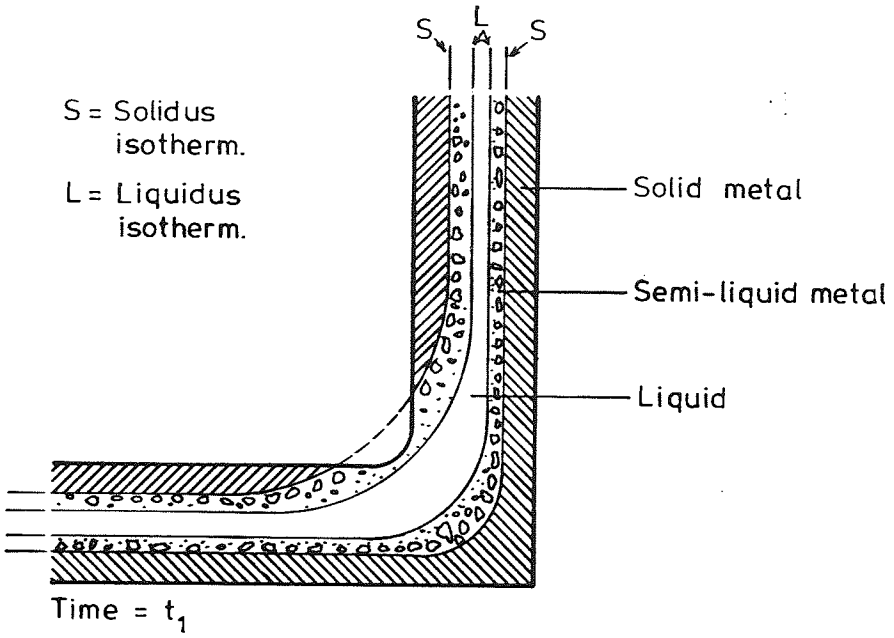

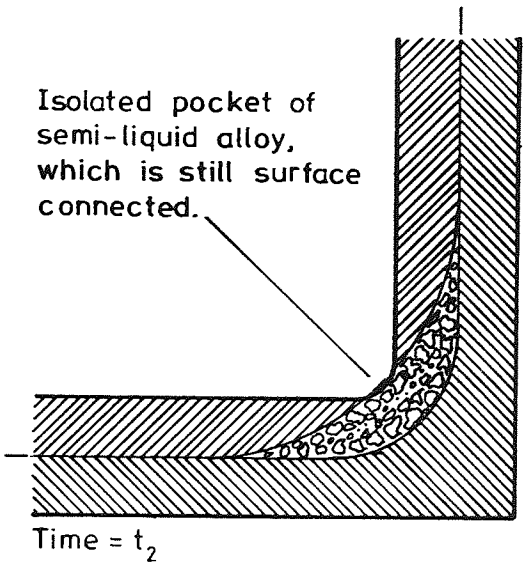

8.1.4. The Oxidation Mechanism

The formation of defects by grain boundary oxidation is substantially different from the other three hypotheses in that defects form after the solidification of the alloy.

The 'oxidation' mechanism is dependent on the following events:

1. Solidification of the metal,
2. Diffusion of oxygen into the grain boundaries,
3. Nucleation of oxides on grain boundaries,
4. Growth of oxides and depletion of chromium,
5. Impingement of the oxides,
6. Breakthrough of some oxides to the surface,
7. Solution of primary coat by surface connected oxides.

Solidification of metal and diffusion of oxygen

The diffusion of oxygen into the metal to form defects is thought to occur primarily along the grain boundaries, as this is where the oxides are observed. Volume internal oxidation of an alloying element occurs when the volume diffusion of oxygen into the alloy is faster than the diffusion of the oxidising element to the surface. In the same way grain boundary internal oxidation would be expected to occur when only the grain boundary diffusion rate of oxygen into the alloy is faster than the volume diffusion rate of the oxidising alloy element. It is generally accepted that grain boundary diffusion would be faster than volume diffusion, as the activation energy for grain boundary diffusion is lower than for volume diffusion (Brophy, Rose & Wulff)[49]. However, Brophy et al. also state that grain boundary diffusion is only significant at low temperatures (when the

difference between the two diffusion rates is greatest), since the grain boundaries only represent a relatively small fraction of the total volume.

Nucleation of oxides at grain boundaries

General mechanisms of surface oxidation of Fe-Cr alloys at 1000°C have been studied by Moreau [50] and by Rahmel [51]. Moreau found that alloys containing more than 15 wt % Cr were protected from oxidation at this temperature by the formation of $FeCr_2O_4$. Those alloys containing less than 15 % Cr formed multilayered oxides: a layer consisting of a mixture of 'FeO' and $FeCr_2O_4$ formed adjacent to the metal, followed by a layer of Fe_3O_4 with Cr^{3+} in octahedral sites; the outermost layer was of Fe_2O_3. The presence of oxides of iron in each layer permit the transport of oxygen through the oxide film to the reacting interface.

Rahmal gives a general regime for the formation of surface oxides at high temperature for all alloys Fe-X, including Fe-Cr, where the concentration of X is not too high. This involves the formation adjacent to the metal of a two phase layer 'FeO'+Fe_yX_zO, followed by a layer of Wüstite – 'FeO'. Next to this is a layer of Magnatite – Fe_3O_4 – followed by an external layer of Haematite – Fe_2O_3. Rahmal states that the source of oxygen for the formation of the two phase layer is from the dissociation of Wüstite at the boundary between the two-phase layer and 'FeO'.

Kubachewski and Alcock[52] have studied the thermodynamics of the oxidation reactions of Cr steels. They showed that Cr_2O_3 will always be the first product of oxidation of iron-chromium alloys containing more than 1.5 wt. % Cr and which are oxidised below 1400K (1127°C). Below this temperature the formation of $FeCr_2O_4$ must be the result of a secondary

reaction between 'FeO' and Cr_2O_3.

Whilst no experimental work was performed, it is assumed that the grain boundary oxides are formed on the austenite grain boundaries in a similar way.

Growth of oxides and depletion of chromium

Following nucleation, the grain boundary oxides will continue to grow whilst the temperature is high enough for oxidation to take place and for oxygen to diffuse into the grain boundaries.

Since Cr_2O_3 is the first product of oxidation it is to be expected that the metal around the oxidation site would become depleted in chromium as it diffuses to the reaction site.

Impingement of the oxides

As the oxides which have nucleated along the grain boundaries grow, they will eventually come into contact with each other. At this point they will resemble strings of beads, although as growth continues the oxides will eventually form a continuous film along the grain boundaries.

Breakthrough of the oxides to the surface

At those locations where the growth of oxides has been the fastest, or the most prolonged, the oxides will eventually achieve sufficient volume to act as a 'wedge' in the contracting metal. This will cause a crack to develop between the end of the oxide and the casting surface, which will be exacerbated as the casting cools and contracts further.

Dissolution of the primary coat

As the oxide inclusions break through to the surface of the casting they will come into contact either with the primary coat of the mould, or with a layer of slag which may have formed at the interface between the metal and the mould. It is at this point in the formation of the defects that shell material is

introduced into the defects. This may occur due to dissolution of the primary coat by the grain boundary oxides, or by incorporation of the slag layer present at the surface. Since the presence of zirconium results in a low melting point slag of high fluidity, it would be expected that shell material would penetrate along the grain boundaries.

Critique of the 'oxidation' mechanism

The various observations and evidence from designed experiments provide broad support for the theory that 'group 9' defects are formed as a result of internal, or grain boundary, oxidation of the metal.

A. Metallographic observations.

The difference in composition between defects is not at variance with the oxidation hypothesis, since the composition of the defects would be expected to change as break-through to the surface occurs and the metal oxides dissolve the shell primary coat. The morphology of the defects is explained by the nucleation, growth and impingement mechanism by which they are created.

The other notable observation is the distinctive microstructure along the defect, as shown in Plates 5.4, 5.5, and 5.6. It has already been noted that those hypotheses which involve the incorporation of surface slag, by one means or another, do not provide an adequate explanation for this phenomenon. However, the microstructure of these alloys (in the as cast condition) is in general a ferrite matrix containing chromium or iron-chromium carbides. Since the oxides forming on the prior austenite grain boundaries are initially Cr_2O_3, this will lead to depletion of the matrix with respect to chromium in these regions. Hence, when the metal temperature

passes the austenite-ferrite transition temperature, the regions around the oxides will transform to ferrite which will not contain the carbides present in the rest of the matrix.

It was noted that the defects are most severe in preferred locations on the casting surface. These areas are those which would be expected to form 'hot spots' due to reduced cooling rates, and it is anticipated that the defects are more prevalent in these areas simply because the retarded cooling allows more time for diffusion and for the growth of the defects.

B. Results of the designed experiment

The observation that the use of a charcoal back-up after casting reduces the incidence of defects in low alloy steel castings is not at variance with any of the proposed hypotheses. However, the observed increase in defects with the application of cold molochite grit to the mould after casting is inconsistent with those hypotheses requiring defects to be formed above the liquidus of the metal. This is because, for all of these mechanisms, defect formation would be expected to be ameliorated by the application of an initial chill.

In the case of the oxidation mechanism, however, defects would be formed at lower temperatures by diffusion of oxygen along the prior austenite grain boundaries. The initial chill caused by application of the cold molochite is therefore less important than the longer term effect of retention of heat once the molochite has reached relative thermal equilibrium with the hot mould.

8.1.5 Implications for the reduction of scrap

Subject to further investigation, it seems most likely that the linear defects are formed by a mechanism of grain boundary oxidation of, initially, chromium. The

grain boundary oxides then grow, some of them eventually breaking through to the surface where they dissolve the shell primary coat. This results in the penetration of shell material along the prior austenite grain boundaries.

These findings imply that the only potential method of ameliorating these defects must involve the prevention of grain boundary oxidation, by the use of reducing or inert atmospheres during or after casting. Modification of the shell chemistry, whilst potentially preventing the incorporation of shell refractory into those defects which break through to the surface, would be expected to have little effect on the overall severity of the problem. It is unlikely that attempts to prevent the defects using kinetic methods (ie more rapid cooling of the preferred locations) are practical since chills are effective for only a limited initial period, and alteration of the casting geometry is not allowed.

8.2 Other defects of interest

Of the other defects investigated in the context of this work, most have been sufficiently discussed in the relevant sections of this thesis which deal with the preliminary work to assess the various defects in terms of their impact on profitability, and their scientific interest.

One defect which is worthy of further comment in the light of the preceding discussion of the 'group 9' problem, is the defect formed on martensitic stainless steels and known as 'black-spot'. Careful observation of the photomicrograph reproduced as Plate 4.2 will reveal lines of oxide inclusions extending from the base of the defect into the metal. In structure these are very similar to the ('group 9') defects found in low alloy steel castings. This similarity suggests that the 'black spot' defects are also formed by a process of internal or grain boundary oxidation followed by solution of the shell primary coat. In fact, such a mechanism is the only way to explain the observation that the defects are lenticular in shape, thus penetrating into the metal as well as into the shell. (This can otherwise only be explained by assuming that the defects are formed whilst the metal is still liquid.)

A hypothetical mechanism can thus be developed as follows:

Following solidification, oxygen diffuses into the metal surface and along the grain boundaries. This oxygen originates from pores and microcracks in the ceramic shell, hence localising the defects.

Oxides nucleate and grow internally below the metal surface. As previously discussed, the first oxide to form is Cr_2O_3, with more complex iron-chromium oxides forming later as the chromium in the alloy is depleted.

As the oxides grow they expand, breaking through to the surface. At this point, the oxides begin to dissolve the primary coat of the shell mould, forming a low

melting point slag containing zirconium. This then results in a lenticular defect containing metal oxides, slag, untransformed shell material, and metal.

In fact, this author carried out an investigation for Deritend Precision Castings (P.N.Whateley 1988)[53] which provides additional support for this hypothesis. The investigation involved an assessment of some methods of reducing the incidence of defects in 17-4 PH austenitic stainless alloy castings for the French aerospace market. Moulds which were backed with charcoal grit after casting were examined and microsections made of test bars exhibiting the 'black spot' defect. It was noticeable that, although the defects appeared to be severe on an initial examination, metallographic investigation showed the defects to be much less developed than those previously observed for the current work. An optical photomicrograph of a typical defect found on a 17-4 PH casting is reproduced from the report in plate 8.1. SEM X-ray maps for iron and chromium, also from this source, are reproduced as plates 8.2 and 8.3. Since it is safe to assume that the charcoal back-up has retarded the formation of the defect, these defects must be very like the early stages of formation of the defects discussed in chapter 4 of this work. The 17-4 PH observations therefore provide considerable support for the theory that the so called 'black spot' defects are a result of internal oxidation of the chromium in the alloy, which in the case of the defects observed earlier is followed by break-through to the surface and reaction with the mould primary coat.

In terms of action recommended for the reduction of scrap, the same problems occur here as with the low alloy steel defects discussed earlier in this chapter. Alteration of the chemistry of the shell may have some effect on preventing the reaction between the metal oxides and the shell material, but will have no effect on

the formation of the internal oxides themselves. The internal oxidation can only be stopped by preventing or reducing the supply of oxygen to the casting. This is usually achieved by the provision of a reducing or inert atmosphere both during and after casting.

This author has also reported[53] that 17-4 PH alloy cast in vacuum is not prone to this type of defect, even though moulds are removed from the furnace immediately after casting. This suggests at first sight that nucleation of the oxides is more critical to the formation of 'black spot' than is their subsequent growth, and is worthy of further investigation.

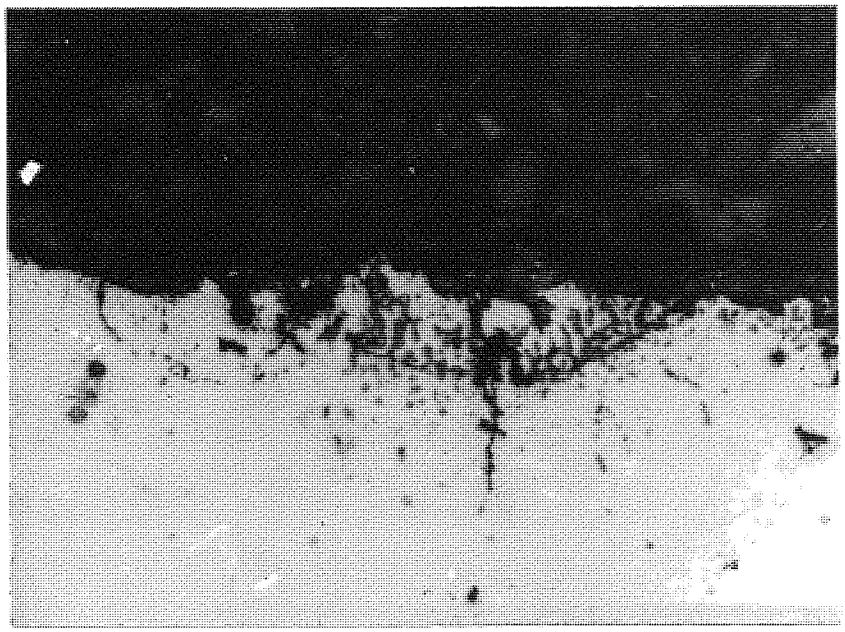

PLATE 8.1:
Optical micrograph of a defect observed on the surface of a 17-4 PH alloy casting. Magnification × 336

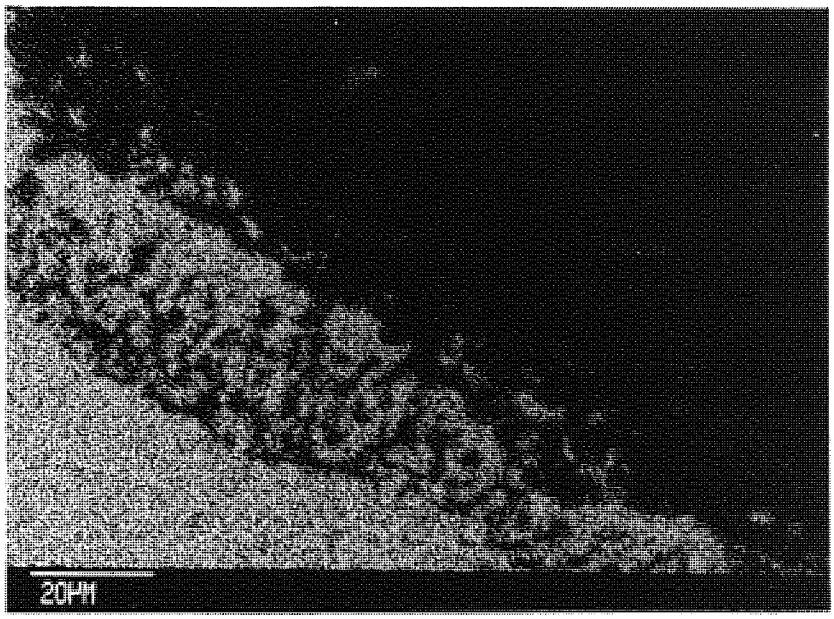

PLATE 8.2:
Fe X-ray map of a defect similar to that in plate 8.1. The metal surface runs from upper left to lower right in this image with the metal at the bottom. (Magnification as marked)

PLATE 8.3:
Cr X-ray map of the same area as plate 8.2. The metal surface runs from upper left to lower right in this image with the metal at the bottom. (Magnification as marked)

9. FURTHER WORK

The statistical analysis has provided a useful addition to the metallographic and other studies performed on low alloy steel ("group 9") defects. However, even this has only been sufficient to establish a "most likely" hypothesis of grain boundary oxidation followed by solution of zircon in the shell primary coat. In order to provide further understanding of the formation of these defects considerable further work is required. Without this work sufficient understanding will not be available to fully prevent the formation of the defects.

1. Research into the mechanisms, kinetics and thermodynamics of oxide formation in chromium containing alloy steels. The early stages of oxidation at very high temperatures, in particular, are little understood. This work should study a range of chromium contents from plain steel up to the types of alloys affected by 'black-spot', in order to establish any similarities between the mechanisms of formation of the two types of defects. If the mechanisms are found to be fundamentally the same, then a study of the transition point in terms of chromium content, between "group 9" and "black-spot" defect morphologies, will provide additional information about the underlying mechanism.

   Fundamental to the study of high temperature oxidation in the context of defect formation is an investigation of the relative diffusion characteristics of oxygen and the alloying elements in the steel. This is important since the defects appear to be formed by a nucleation and growth mechanism and the restriction of the supply of oxidation to the incipient oxide inclusions is likely to provide the most effective method of interfering with the defect formation.

2. Since the metal is cast into a ceramic shell mould, the influence of the mould properties on defect formation in both low alloy and stainless steels must be further studied. Mould defects such as microcracks and pores, as well as the inherent permeability of the mould itself, would all be expected to have an effect on the supply of oxygen to the metal.

   The thermal properties of the shell material may also affect the formation of the defects since their extent will be dependent on the length of the diffusion and reaction times.

   The chemical properties of the primary coat are of interest because it is this material which reacts with oxidised metal to form a low melting point slag. Studies into the thermodynamics and kinetics of these reactions may result in modifications leading to amelioration of the defects.

3. All the alloys affected by this class of defect are melted and cast in air. Inevitably, oxygen will remain dissolved in the melt despite the use of deoxidants. The nucleation and growth of grain boundary oxides and the consequent defects would be expected to be dependent on a critical level of dissolved oxygen, resulting both from diffusion from the metal surface and carried over from oxygen present in the melt. A study of the levels of dissolved oxygen carried over in the molten metal as a function of deoxidation and melting practice is therefore essential for an understanding of the formation of defects.

4. The chemistry of slag formation is relevant only with respect to those defects which are surface connected. However, it is these defects which are observed as defects during routine examination of commercial castings and which lead to the generation of scrap.

5. The statistical analysis, by its nature, was limited to certain variables of interest. Whilst several other variables were measured for the purpose of model diagnostics, other potentially interesting variables were kept constant in order to restrict the size of the experiment to a manageable (and affordable) size. Factors which should be studied in order to obtain a more general assessment of the problem include:

i) the effect of variation between batches of metal from the same and from different metal suppliers;

ii) the effect of variation between different suppliers batches of crucibles;

iii) the effect of differences in the condition of the crucible used (such as the number and composition of previous melts);

iv) the effect of differences between the working practices of different operators, especially with regard to metal melting; and

v) the effect of variations in the shell properties and the method of producing shells.

10. CONCLUSIONS

1. Many of the sources of defective castings result from faulty working practices.

2. Inaccurate assembly of wax moulds can result in shrinkage cavities in castings and the erosion of shell by the molten metal stream. This, latter, can result in shell inclusions in castings.

3 Moulds can become contaminated by extraneous material, especially flakes of shell material, due to poor cleanliness of work areas.

4. Rigid adherence to foundry procedures was found to be especially important. Inconsistent deoxidation and casting temperatures cause variation in mechanical properties, as well as inclusions. Repeated use of crucibles can cause inclusions and cross-contamination between melts.

5. The specific defects observed on austenitic stainless steel castings were found to result from inefficient, or often unnecessary, deoxidation with calcium-aluminium alloy. This led to residual oxides being carried over in the melt during pouring.

6. Statistical analysis of a designed experiment performed on low alloy steel castings has shown that, for the particular constraints and conditions under which the experiment was performed, there is a statistically significant difference between the severity of defects on moulds cast normally, those treated with a charcoal back-up immediately after casting, and those treated with a molochite grit backup.

7. The response variable (of defect area) was found to be distributed lognormally, making a log transformation of the original data necessary. This was confirmed by the use of non-parametric methods.

8. Many variables such as shell weights, alloy chemical composition etc., which were not directly controlled in the experiment were measured concomitantly. Within the range of variation, none of these factors appeared to have an effect on the severity of the low alloy steel defects.

9. Defects were found to be ameliorated by the use of charcoal and exacerbated by the use of molochite, with respect to the control conditions. For the log transformed data the treatment effects were determined as follows. (Units are all $\ln[mm^2]$).

No back up: Mean = 4.08; 99% confidence interval from 3.78 to 4.39.

Charcoal: Mean = 3.11; 99% confidence interval from 2.80 to 3.41.

Molochite: Mean = 5.66; 99% confidence interval from 5.36 to 5.97.

10. Although further work is deemed necessary to clarify the situation, there is some evidence to suggest that both the 'black-spot' defects on martensitic stainless steels, and the characteristic defects observed on low-alloy 'group 9' steels are caused by internal or grain boundary oxidation of the hot metal. In both cases the metal oxides so formed may also reach the surface and react with the refractory primary coat to form a slag.

11. REFERENCES

1: P. R. Taylor: "Lost wax casting - a short illustrated review:" Metals and Materials: **2**,(11), 705-710. (Nov. 1986).

2: R. Kiessling and N. Lange, "Non-metallic inclusions in steel", 2ed. (London: The Metals Society), 1978, p. II-3.

3: R. Kiessling and N. Lange, "Non-metallic inclusions in steel", 2ed. (London: The Metals Society), 1978, pp. II-27 *et seq.*

4: D. L. Sponseller and R. A. Flinn: Trans. AIME, 1964, **230**, pp 876-88.

5: C. E. Sims and C. W. Briggs: "A primer on deoxidation": J. of Metals, Dec. 1959, pp 815-22.

6: F. J. Shortsleeve and D. C. Hilty: "Calcium in iron and steel": *Boron, Calcium, Columbium, and Zirconium in iron and steel.* Alloys of iron new monograph series. (New York and London: John Wiley) 1957.

7: J. S. Taylor: "Prevention of fusion ('spotted- dick') on high chromium steel": 7th annual conf. inv. cast., (British Investment Casters Technical Association, Edgbaston, Birmingham), 1965.

8: V. S. Larin and V. A. Vasil'ev: "Surface defects on stainless steel castings and their production": Russian castings production. July 1969, (7), pp342-3.

(*cont.*)

REFERENCES (*cont.*).

9: Kazuhiro Matsuno and Schinichi Ohama: "Pitting defects in high Cr steels and countermeasure", Ishikawajima Harima Eng. Rev. **21**, (4), pp328-34, (1981).

10: P. W. Wright: "Reactions of zircon refractories with molten steel", J. Austr. Ceram. S., **20**, (2), pp 47-50, (1984).

11: R. L. Shultz and A. Muan: "Phase equilibria in the system MnO – 'FeO' – ZrO_2 – SiO_2.", J. Am. Ceram. S., **54**, (10), pp 504-10, (Oct. 1971).

12: D. R. Muzyka and G. A. Colligen: "Metal-refractory reaction studies in the iron – chromium –silica system", Cast Met. Res. J., **3**, (2), pp 80-89, (1967).

13: D. R. Muzyka and G. A. Colligen: "Kinetics of metal-refractory reactions in the Fe – Cr –SiO_2 system", Cast Met. Res. J., **4**, (2), pp 86-94, (1968).

14: M. Myers and M. C. Flemings, "Behaviour of silica inclusions in a partially solidified iron base alloy", Met. Trans., **3**, (8), pp 2225-34., (Aug. 1972).

15: G.J.Davies, "Solidification and Casting" (London: Applied Science Publishers) 1973.

16: L. Coudurier, D. W. Hopkins, and I. Wilkominsky, "Fundamentals of metallurgical processes", 2ed. (Oxford: Pergamon Press), Fig. 87, p 240.

(*cont.*)

17: T. S. Jones, Shigeyuki Kimura, and Arnulf Muan: "Phase relationships in the system $FeO - Fe_2O_3 - ZrO_2 - SiO_2$", J. Am. Ceram. S., **50**, (3), pp 137-142, (March 1967).

18: R. McCallum and W. Lang: "Development of a technique for assessing ceramic shell performance under simulated casting thermal conditions", Proc. 17th Ann. BICTA Conf., Stratford-upon-Avon. (1983).

19: D.C.Montgomery: "Design and Analysis of Experiments", 2ed. (New York: John Wiley) 1984, pp 250-4.

20: C.Daniel: "Application of Statistics to Industrial Experimentation", (New York: John Wiley) 1976, p 72.

21: C.Daniel: ibid., p76.

22: R.G.Miller, Jr: "Beyond ANOVA, Basics of Applied Statistics", (New York: John Wiley) 1986, pp 10-12.

23: G.E.P.Box, W.G.Hunter, and J.S.Hunter: "Statistics for Experimenters", (New York: John Wiley) 1978, pp 218-9.

24: D.C.Montgomery: "Design and Analysis of Experiments", 2ed. (New York: John Wiley) 1984, p 118.

(*cont.*)

REFERENCES (*cont.*).

25: W.J.Conover, "Practical Nonparametric Statistics", 2ed. (New York: John Wiley) 1980 p337

26: W.J.Conover, ibid. pp 229-37

27: R.G.Miller, Jr: "Beyond ANOVA, Basics of Applied Statistics", (New York: John Wiley) 1986, pp 260-3.

28: R.L.Mason, R.F.Gunst, and J.L.Hess: "Statistical Design and Analysis of Experiments", (New York: John Wiley) 1989, p 295.

29: D.C.Montgomery: "Design and Analysis of Experiments", 2ed. (New York: John Wiley) 1984, p 92.

30: O.L.Davies and P.L.Goldsmith (eds.) "Statistical Methods in Research and Production", 4ed. (Harlow: Longman), p173

31: G.E.P.Box, W.G.Hunter, and J.S.Hunter: "Statistics for Experimenters", (New York: John Wiley) 1978, pp 197 *et seq.*

32: G.E.P.Box, W.G.Hunter, and J.S.Hunter: ibid. pp 145.

33: M.C.Flemings, "Solidification Processing", (New York: McGraw-Hill) 1974, p196.

(*cont.*)

34: M.Myers and M.C.Flemings, "Behaviour of silica inclusions in a partially solidified iron base alloy", Met. Trans., **3**, (8), pp 2225-34., (Aug. 1972).

35: M.C.Flemings, "Solidification Processing", (New York: McGraw-Hill) 1974, p197.

36: M.C.Flemings, ibid. p198.

37: G.J.Davies, "Solidification and Casting" (London: Applied Science Publishers) 1973, p 89.

38: D.R.Uhlman, B.Chalmers, and K.A.Jackson, "Interaction Between Particles and a Solid-Liquid Interface", J. Appl. Phys. **35**, (10), pp 2986-93. (October 1964).

39: M.C.Flemings, "Solidification Processing", (New York: McGraw-Hill) 1974, p199.

40: A.I.Veinik, "Thermodynamics for the Foundryman", (London: Maclaren and Sons) 1968, pp 15-18.

41: E.A.Brandes, ed. "Smithalls Metals Reference Book" 6ed. (London: Butterworths) 1983, §12 - p19.

(*cont.*)

42: J.H.Swisher and E.T.Turkdogan, "Solubility, Permeability, and Diffusivity of Oxygen in Solid Iron" Trans. Met. Soc. AIME, **239**, (4), pp426-31, (April 1967).

43: J.Campbell, "Shrinkage Pressure in Casings (The solidification of a Metal Sphere)", Trans. Met. Soc AIME, **239**, (2), pp138-42, (February 1967).

44: J.Campbell, "Hydrostatic Tensions in Solidifying Materials", Trans. Met. Soc. AIME, **242**, (2), pp264-71, (February 1968).

45: J.Campbell, "Pore Nucleation in Solidifying Metals" in *The Solidification of Metals,* Iron and Steel Institute Publication **110**, 1968, pp18-26.

46: J.Campbell, "On the origin of porosity in long freezing-range alloys", J. Inst. Brit. Foundrymen, **62**, (4), 147-158, (April 1969).

47: J.H.Rogerson and J.C.Borland, "Effect of Shapes of Intergranular Liquid on the Hot Cracking of Welds and Castings", Trans. Met. Soc. AIME, **227**, (2), pp2-7, (February 1963).

48: R.W.Ruddle, "The Solidification of Castings", (London: The Institute of Metals), 1957, p198.

(*cont.*)

49: J.H.Brophy, R.M.Rose, and J.Wulff, "The Structure and Properties of Materials, Vol. II, Thermodynamics of Structure", (New York: John Wiley), 1964, p83.

50: J.Moreau, "Étude du méchanisme de l'oxydation des alliages binaires fer-chrome aux températures élevées", Comptes rendus, **236**, (1), pp 85-87, (Jan. 1953).

51: A.Rahmel, "Zum Bildungsmechanismus zweiphasiger Oxydschichten auf Eisenlegierungen bei hohen Temperaturen", Zeitschrift für Elektrochemie, **66**, (4), pp 363-7.

52: O.Kubaschewski and C.B.Alcock, "Metallurgical Thermochemistry" 5ed, (Oxford: Pergamon Press) 1983, pp254-7.

53: P.N.Whateley, "Defects in 17-4 PH Alloy Investment Castings", (Deritend Precision Castings) 1988, Unpublished Report.

54: D.C.Montgomery: "Design and Analysis of Experiments", 2ed. (New York: John Wiley) 1984, pp250-3.

12. APPENDIX

Rules for Expected Mean Squares

Formulae for the expected mean squares are required in order to form the F-test statistic for hypothesis testing. The test statistic is a ratio of mean squares, chosen so that the expected value of the numerator mean square differs from the expected value of the denominator mean square only by the fixed factor or variance component under test

A method for the formation of mean squares is proposed by Montgomery [54] and is quoted below, using the nested design discussed in chapter 7 as illustration.

*"**RULE 1** Each effect has either a variance component (random effect) or a fixed factor (random effect) associated with it. ... A variance component has Greek letters as subscripts to identify the particular random effect. ... A fixed effect is always represented by the sum of squares of the model components associated with that factor divided by its degrees of freedom"*

*"**RULE 2 EXPECTED MEAN SQUARES.** To obtain the expected mean squares, prepare the following table. There is a row for each model component (mean square), and a column for each subscript. Over each subscript write the number of levels of the factor associated with that subscript, and whether the factor is fixed (F) or random (R). Replicates are always considered random.*

***(b)** In each row, write 1 if one of the dead subscripts (i.e. those in brackets) in the row component matches the subscript in the column"*

Factor	R a i	F b j	R c k	R n l
α_i				
$T_{j(i)}$	1			
$\beta_{k(ij)}$	1	1		
$e_{l(ijk)}$	1	1	1	

*"**(b)** In each row, if any of the subscripts on the row component match the subscript in the column, write 0 if the column is headed by a fixed factor and 1 if the column is headed by a random factor."*

Factor	R a i	F b j	R c k	R n l
α_i	1			
$T_{j(i)}$	1	0		
$\beta_{k(ij)}$	1	1	1	
$e_{l(ijk)}$	1	1	1	1

*"**(c)** In the remaining empty row positions, write the number of levels shown above the column heading."*

Factor	R a i	F b j	R c k	R n l
α_i	1	b	c	n
$T_{j(i)}$	1	0	c	n
$\beta_{k(ij)}$	1	1	1	n
$e_{l(ijk)}$	1	1	1	1

*"**(d)** To obtain the expected mean square for any model component, first cover all columns headed by a live (i.e. not in brackets) subscript on that component. Then, in each row that contains at least the same subscripts as those on the component being considered, take the product of the visible numbers and multiply by the appropriate fixed or random factor from Rule 1. The sum of these quantities is the expected mean square of the model component being considered."*

To find $E(MS_T)$, for example, cover column j. The product of the visible numbers in the rows that contain at least subscripts i and j are cn (row 2), n (row 3), and 1 (row 4). Note that j is missing in row 1. Therefore the expected mean square is

$$E(MS_T) = \sigma^2_e + n\sigma^2_\beta + c\,n\left[\sum\sum T_{j(i)} / a\,(b-1)\right]$$

The complete table of expected mean squares for the model in question is given in Table 12.1

TABLE 12.1 Table of Expected Mean Squares

	R	F	R	R	
	a	b	c	n	
Factor	i	j	k	l	Expected Mean Squares
α_i	1	b	c	n	$E(MS_\alpha) = \sigma^2_e + n\sigma^2_\beta + bcn\sigma^2_\alpha$
$T_{j(i)}$	1	0	c	n	$E(MS_T) = \sigma^2_e + n\sigma^2_\beta + c\,n\left[\sum\sum T_{j(i)} / a\,(b-1)\right]$
$\beta_{k(ij)}$	1	1	1	n	$E(MS_\beta) = \sigma^2_e + n\sigma^2_\beta$
$e_{l(ijk)}$	1	1	1	1	$E(MS_e) = \sigma^2_e$